

**IZMIR KATIP CELEBI UNIVERSITY
GRADUATE SCHOOL OF NATURAL AND APPLIED
SCIENCES**

**EFFECT OF PARTICLE SIZE DISTRIBUTION MODALITY OF
CaCO₃ ON SEALING WIDE FRACTURES USING SEPIOLITE
MUDS**

**M.Sc. THESIS
Meltem TEZCAN**

Department of Energy Engineering

Thesis Advisor: Asst. Prof. Dr. Ali Ettehad

Co-advisor: Assoc. Prof. Dr. Gürşat Altun

JUNE 2020

**IZMIR KATIP CELEBI UNIVERSITY
GRADUATE SCHOOL OF NATURAL AND APPLIED
SCIENCES**

**EFFECT OF PARTICLE SIZE DISTRIBUTION MODALITY OF
CaCO₃ ON SEALING WIDE FRACTURES USING SEPIOLITE
MUDS**

M.Sc. THESIS

Meltem TEZCAN

(Y170208005)

0000-0003-1544-9938

Department of Energy Engineering

Thesis Advisor: Asst. Prof. Dr. Ali Ettehadi

Co-advisor: Assoc. Prof. Dr. Gürşat Altun

JUNE 2020

**İZMİR KATİP ÇELEBİ ÜNİVERSİTESİ
FEN BİLİMLERİ ENSTİTÜSÜ**

**CaCO₃ PARÇACIK BOYUT DAĞILIM MODALİTESİNİN
SEPIYOLİT ÇAMURLARI KULLANILARAK GENİŞ
ÇATLAKLARIN TIKANMASINA ETKİSİ**

YÜKSEK LİSANS TEZİ

Meltem TEZCAN

(Y170208005)

0000-0003-1544-9938

Enerji Mühendisliği Ana Bilim Dalı

Tez Danışmanı: Dr.Öğr.Üyesi Ali Ettehadı

Eş Danışman: Doç. Dr. Gürşat Altun

HAZİRAN 2020

Meltem TEZCAN, a M.Sc. student of **IKCU Graduate School of Natural and Applied Sciences**, successfully defended the thesis entitled “**EFFECT OF PARTICLE SIZE DISTRIBUTION MODALITY OF CaCO₃ ON SEALING WIDE FRACTURES USING SEPIOLITE MUDS**”, which she prepared after fulfilling the requirements specified in the associated legislations, before the jury whose signatures are below.

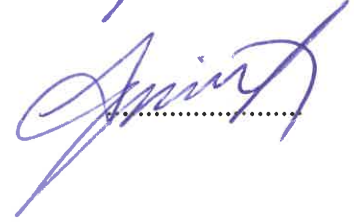
Thesis Advisor :

Asst. Prof. Dr. Ali Ettehadı
Izmir Katip Celebi University



Thesis Co-advisor:

Assoc. Prof. Dr. Gürşat Altun
Istanbul Technical University



Jury Members :

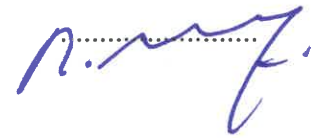
Prof. Dr. İbrahim Kocabaş
Izmir Katip Celebi University



Asst. Prof. Dr. M. Hakan Özyurtkan
Istanbul Technical University



Prof. Dr. Niyazi Aksoy
Dokuz Eylul University



Date of Defense : 26.06.2020

To my family

FOREWORD

First and foremost, I would like to thank my advisor, Asst. Prof. Dr. Ali ETTEHADİ, for his encouragement, guidance, support, and patience during my MSc study. He had given useful criticism and assistance during all stages of this study. It was a great honor working with him. I also would like to thank Assoc. Prof. Dr. Gürşat ALTUN from Petroleum and Natural Gas Engineering Department at Istanbul Technical University for sharing his valuable knowledge with us and supported us during every stage of this study. A special thanks to my best friends Nilay İNCE and Merve BARDAK for their support and encouragement throughout my study. At last but not least, I would like to say my grateful thanks to my family for their support and patience during my study.

This thesis was supported by Izmir Katip Celebi University, Coordination Office of Scientific Research Projects. (IKCU-ÖNP-MUM-0001) and Scientific and Technological Research Council of Turkey (TUBITAK-217M723 & TUBITAK-119M084). A special thanks to the Petroleum and Natural Gas Engineering Department of ITU for providing Pore Plugging Apparatus (PPA). In addition, I would like to thank NİTAŞ and KAYEN SONDAJ companies for their support in purchasing materials and chemicals during the project.

June 2020

Meltem TEZCAN

TABLE OF CONTENTS

	<u>Page</u>
FOREWORD	vi
TABLE OF CONTENTS	vii
LIST OF TABLES	ix
LIST OF FIGURES	x
ABBREVIATIONS	xii
ABSTRACT	xiii
ÖZET	xiv
1. INTRODUCTION	15
2. STATEMENT OF PROBLEM	18
3. LITERATURE REVIEW	19
3.1 Properties and Usage of Sepiolite Clay	19
3.2 Uses of Sepiolite Clay as Drilling Mud	21
3.3 Lost Circulation General Overview	22
3.3.1 Lost Circulation Material (LCM)	24
3.3.2 LCM Treatments	25
3.3.2.1 Corrective LCM Treatments	26
3.3.2.2 Preventive LCM Treatments	26
3.4 Plugging and Sealing Theories	27
3.4.1 Pore Plugging Theories	27
3.4.2 Fracture Sealing Models	31
3.5 Recent Experimental Studies	37
4. METHODS AND MATERIALS	39
4.1 Permeability Plugging Apparatus (PPA).....	44
4.2 Fann Model 35SA Viscometer	47
4.3 Aging Cells.....	47
4.4 Roller Oven	48
4.5 Multi Mixer	49
4.6 Discovery Hybrid Rheometer (DHR-II).....	50
5. RESULTS AND DISCUSSION	51
5.1 Rheological Properties of Sepiolite Mud	51
5.2 Effect of Unimodal CaCO ₃ Particle Size Distribution on Sealing Time and Fluid Loss.....	56
5.3 Effect of Bimodal and Trimodal CaCO ₃ Particle Size Distribution on Sealing Time and Fluid Loss.....	63
5.4 Optical Microscope Analysis	66
5.4.1 Optical Microscope Analysis for All Discs	66
5.4.2 Optical Microscope Analysis of the Effect of Unimodal, Bimodal, Trimodal Particle Size Distribution	70
5.5 Plugging Effect of LCM Geometries	71

5.5.1 Particle Size Distribution Analysis of LCMs-Circularity	71
5.5.2 Effect of LCM Geometries (Shape).....	73
5.5.3 LCM Particles Concentration and Its Effect on Plugging.....	75
CONCLUSIONS	77
RECOMMENDATIONS	79
REFERENCES	80
APPENDIX – A: XRF and XRD Results for Sepiolite Clay	88
APPENDIX – B: XRD Results for Wyoming Bentonite Clay	90
APPENDIX – C: Unimodal Particle Size Distribution for All Discs.....	91
APPENDIX – D: Bimodal Particle Size Distribution for All Discs	107
APPENDIX – E: Trimodal Particle Size Distribution for All Discs.....	110
APPENDIX – F: Preliminary Experiments to Determine LCM Optimum Size Distribution	112
APPENDIX – G: Effect of Bentonite Clay on Fracture Plugging	125
APPENDIX – H: Effect of Sepiolite and Bentonite Clay Blend on Fracture Plugging	130
CURRICULUM VITAE.....	132

LIST OF TABLES

	<u>Page</u>
Table 3.1 The summary of pore plugging theories' selection criteria.....	30
Table 3.2 Summary for the proposed loss circulation and borehole strengthening models in fractured formation.....	37
Table 4.1 Compositions of sepiolite mud systems.....	39
Table 4.2 Bimodal and trimodal compositions of the CaCO ₃ particles sizes.....	43
Table 5.1 Sepiolite fluid system properties as measured accordance with API standards.....	52
Table 5.2 Slotted discs specifications.....	56
Table 5.3 Total concentration of each LCM to formulate unimodal blends.....	57
Table 5.4 LCM size and concentration values for 3048 disc (Blend#1).....	66
Table 5.5 LCM size and concentration values for 2540 disc (Blend#3).....	67
Table 5.6 LCM size and concentration values for 2032 disc (Blend#4).....	68
Table 5.7 LCM size and concentration values for 1524 disc (Blend#5).....	68
Table 5.8 LCM size and concentration values for 1016 disc (Blend#6).....	69
Table F.1 Preliminary experiments to determine LCM optimum size distribution Blend# D1-D10.....	113
Table F.2 Preliminary experiments to determine LCM optimum size distribution Blend# D11-D20.....	115
Table G.1 LCM size and concentration values for 1524 μm disc-1.....	125
Table G.2 LCM size and concentration values for 1524 μm disc-2.....	126
Table G.3 LCM size and concentration values for 2032 μm disc-1.....	126
Table G.4 LCM size and concentration values for 2032 μm disc-2.....	127
Table G.5 LCM size and concentration values for 2540 μm disc-1.....	128
Table G.6 LCM size and concentration values for 2540 μm disc-2.....	129
Table H.1 LCM size and concentration values for 2540 μm disc.....	130
Table H.2 Effect of clay type on fracture sealing time and fluid loss.....	131

LIST OF FIGURES

	<u>Page</u>
Figure 3.1 The structure of sepiolite clay.....	19
Figure 3.2 SEM images of sepiolite clay with different scales as a) 10 μ m b) 1 μ m c) 100nm.....	20
Figure 3.3 The common usages of sepiolite clay.....	20
Figure 3.4 Classification of lost circulation zones	23
Figure 3.5 Lost circulation materials (LCMs).....	24
Figure 3.6 Pore plugging mechanism.....	28
Figure 3.7 Expression of fracture mouth and fracture tip	31
Figure 3.8 Schematic of a) Fracture Plugging b) Fracture Bridging c) Fracture Filling Procedures	32
Figure 3.9 The stress caging process.....	33
Figure 3.10 The Fracture Closure Stress (FCS) model process	34
Figure 3.11 a) Fracture propagation mechanism using WBM b) Fracture propagation mechanism using OBM/SBMs.....	35
Figure 5.1 Rheological properties of sepiolite fresh water fluid sample (DHR II)....	53
Figure 5.2 Thixotropy of sepiolite fresh water fluid (DHR II).	54
Figure 5.3 Sepiolite fresh water fluid–structure break down and build up (DHR II)....	55
Figure 5.4 Frequency sweep of sepiolite mud (DHR II).....	55
Figure 5.5 Fracture sealing time vs. pump pressure (508 μ m fracture disc)- Unimodal.....	58
Figure 5.6 Fracture sealing time vs. pump pressure (1016 μ m fracture disc)- Unimodal.....	60
Figure 5.7 Fracture sealing time vs. pump pressure (1524 μ m fracture disc)- Unimodal.....	61
Figure 5.8 Fracture sealing time vs. pump pressure (2032 μ m fracture disc)- Unimodal.....	62
Figure 5.9 Fracture sealing time vs. pump pressure (2540, 3048 μ m fracture disc)- Unimodal.....	63
Figure 5.10 Effect of bimodal CaCO ₃ particle sizes distribution on plugging evaluation parameters.....	64
Figure 5.11 Effect of trimodal particle size distribution of CaCO ₃ on fracture plugging performance	64
Figure 5.12 Effect of unimodal, bimodal and trimodal particle size distribution of CaCO ₃ a) 1524 μ m, b) 2032 μ m, c) 2540 μ m d) 3048 μ m fractured discs.	65
Figure 5.13 Optical Microscope Analysis for 3048 μ m disc (Blend#1): a) general view, b) top view and c) side view of formed mud cake.. ..	66
Figure 5.14 Optical Microscope Analysis for 2540 μ m disc (Blend#3): a) general view, b) top view and c) side view of formed mud cake.. ..	67

Figure 5.15 Optical Microscope Analysis for 2032 μm disc (Blend#4): a) general view, b) top view and c) side view of formed mud cake..	68
Figure 5.16 Optical Microscope Analysis for 1524 μm disc (Blend#5): a) general view and b-c) top view of formed mud cake.....	69
Figure 5.17 Optical Microscope Analysis for 1016 μm disc (Blend#6): a) general view and b-c) top view of formed mud cake.....	69
Figure 5.18 Formed seal of bimodal PSD in 2540 μm fracture: a) formed seal under fractured disc b) Optical microscopic image of formed seal.	70
Figure 5.19 Sealing efficiency of a) unimodal, b) bimodal, and c) trimodal CaCO_3 particle sizes distribution through 3048 μm microns fracture disc.	71
Figure 5.20 Particle Size Distribution Analysis of LCMs-Circularity using Image-J	72
Figure 5.21 Optical microscopy images of coarse CaCO_3 particles a) well sorted, high spherical b) poor sorted, low spherical	73
Figure 5.22 Sphericity and Roundness Chart	74
Figure 5.23 Effect of LCM Geometries on fracture sealing integrity.	74
Figure 5.24 Optical microscopy images of trimodal blends seal containing a1, a2) non-homogeneous low spherical b1, b2) homogeneous high spherical coarse CaCO_3 particles.	75
Figure 5.25 Concentration of CaCO_3 particles in formed seal.....	76

ABBREVIATIONS

DHR-II	: Discovery Hybrid Rheometer
PPA	: Pore Plugging Apparatus
LCM	: Loss Circulation Material
PSD	: Particle Size Distribution
PV	: Plastic Viscosity
YP	: Yield Point
GS	: Gel Strength
NPT	: Non-Productive Time
TVD	: True Vertical Depth
IPT	: Ideal Packing Theory
FCS	: Fracture Closure Stress
FPR	: Fracture Propagation Resistance
FG	: Fracture Gradient
WBS	: Borehole Strengthening
WBM	: Water Based Mud
OBM	: Oil Based Mud
SBM	: Synthetic Based Mud
PDF	: Probability Density Function

EFFECT OF PARTICLE SIZE DISTRIBUTION MODALITY OF CaCO₃ ON SEALING WIDE FRACTURES USING SEPIOLITE MUDS

ABSTRACT

Lost circulation is defined as the invasion of naturally fractured and unconsolidated formations by the drilling fluid. Preventing loss circulation is a highly challenging problem while drilling a well. High loss circulation results in cost increase and well instability problems along with the contamination of productive formations. Lost circulation materials (LCMs) are used to prevent partial or total losses through pore throat and fractures. Special LCM treatments may be applied in the case of severe losses for wide fractures. However, the outcomes of all these efforts have not been leading to provide a valid theory or protocol particularly in early time wide fracture sealing.

This experimental study attempts to investigate the contribution of LCM sizes and concentrations, unimodal, bimodal, and trimodal LCM particle size distributions (PSD) and LCM combination quantity on the early time wide fracture sealing. The fracture sealing time was analyzed using sepiolite mud prepared by taking into consideration the API standard. In order to evaluate the rheological properties of sepiolite mud as carrier fluid, the steady shear flow, thixotropy loop, and oscillatory dynamic shear tests were performed with Discovery Hybrid Rheometer (DHR-II). The set of seventeen sieves (75 μ m-3360 μ m) was used to grain size analysis of CaCO₃ as LCM. In addition, six slotted disks of varying fracture diameters (508 μ m-3048 μ m) and lengths were examined for the effect of sixteen different LCM sizes on the fracture sealing time. The wide range of sieve sets made a significant contribution to examine the effect of unimodal, bimodal, and trimodal PSD, combination, and concentration of LCM for minimizing fracture sealing time. Using an optical microscope the sealing efficiency of LCM sizes and concentrations was visually examined. The PPA results demonstrate that the early fracture sealing time varies depending on the combination, concentration, particle size distribution, and particle shape of LCMs. In addition, it has been shown that as the size of the fracture increases, the amount of LCM usage increases to improve plugging performance. To efficiently seal fractures and reduce fracture sealing time, the fine, medium, and coarse LCMs should be used with optimum concentrations.

Keywords: Fracture plugging, Wide fractures, Early plugging time, Sepiolite mud, Bimodal and trimodal particle size distribution.

CaCO₃ PARÇACIK BOYUT DAĞILIM MODALİTESİNİN SEPIYOLİT ÇAMURLARI KULLANILARAK GENİŞ ÇATLAKLARIN TIKANMASINA ETKİSİ

ÖZET

Kayıp sirkülasyon, sondaj akışkanının doğal olarak oluşmuş çatlaklı formasyonlara ve konsolide olmamış çatlak formasyonlara (unconsolidated fractured formations) nüfuz etmesi olarak tanımlanmaktadır. Kayıp sirkülasyonunun önlenmesi, sondaj operasyonları sırasında oldukça önemli bir problemdir. Yüksek kayıp sirkülasyonu, kontamine edici oluşumların yanı sıra maliyet artışına ve kuyu stabilitesi (well instability) sorunlarına yol açmaktadır. Kayıp sirkülasyon malzemeleri (LCM), gözeneklerde ve çatlaklarda oluşan kısmi veya toplam kayıp sirkülasyonu önlemek için kullanılmaktadır. Geniş çatlaklarda ciddi kayıplar olması durumunda özel LCM kombinasyonları uygulanabilmektedir. Bununla birlikte, literatürde çatlakların erken tıkanması ile ilgili geçerli bir teori veya protokol bulunmamaktadır.

Bu deneysel tez çalışmasında, LCM boyutları ve konsantrasyonları, tek modlu (unimodal), iki modlu (bimodal) ve üç modlu (trimodal) LCM parçacık boyutu dağılımlarının (PSD) ve LCM kombinasyon miktarının erken zamandaki geniş çatlak tıkanmasına etkisi araştırılmıştır. Çatlak tıkanma zamanı, API standartları dikkate alınarak hazırlanan sepiyolit bazlı çamur kullanılarak analiz edilmiştir. Sepiyolit bazlı çamurunun reolojik özelliklerini incelemek amacıyla Discovery Hybrid Rheometer (DHR-II) ile sabit kayma, tiksotropi döngü ve osilasyonlu dinamik kayma testleri yapılmıştır. CaCO₃ tanecik boyutu analizinde elde edilen on yedi elek seti (75µm-3360µm) LCM olarak kullanılmıştır. Ayrıca, değişen çatlak boyutlarına (508µm-3048µm) ve uzunluklara sahip altı yarık disk, on altı farklı LCM boyutunun çatlak tıkanma zamanına etkisi incelenmiştir. Geniş aralıkta elek setinin kullanılması, tek modlu, ikimodlu ve üç modlu PSD, kombinasyon ve LCM konsantrasyonunun çatlak tıkanma zamanına etkisini incelemek için önemli bir katkıda bulunmuştur. Optik mikroskop analizi ile LCM boyutları ve konsantrasyonlarının çatlak tıkanma etkinliği görsel olarak incelenmiştir. PPA sonuçları, erken çatlak tıkanma zamanının LCM'lerin kombinasyonuna, konsantrasyonuna, parçacık boyut dağılımına ve parçacık şekline bağlı olarak değiştiğini göstermektedir. Ek olarak, çatlak boyutu arttıkça, tıkanma performansını arttırmak için kullanılan LCM miktarının arttığı gözlemlenmiştir. Çatlakları etkili bir şekilde tıkanmak ve çatlak tıkanma zamanını azaltmak amacıyla ince, orta ve iri LCM'ler optimum konsantrasyonlarda kullanılmalıdır.

Anahtar kelimeler: Çatlak tıkanma, Geniş çatlaklar, Erken tıkanma süresi, Sepiyolit çamuru, İki modlu ve üç modlu parçacık boyutu dağılımı

1. INTRODUCTION

In conventional drilling process, high permeable and naturally fractured depleted or low-pressure zones contribute to the phenomena called lost circulation which is the invasion of permeable or fractured formations by the drilling fluid. The formations are classified in which lost circulation may occur as; cavernous formations, highly permeable (unconsolidated) formations, natural and induced fractures [1]. The lost circulation is one of the most vital drilling problems that increase well costs and risking for operators and scaring them to pose greater issues in the future [2]. Statistical study in the Gulf of Mexico (GOM) region indicates that 44% of total drilling non-productive time (NPT) results from borehole instability issues in the form of stuck pipe, borehole collapse, sloughing shales and lost circulation which covers 24-27% of the GOM operator's drilling budgets [3]. It was also reported that operators in the GOM were forced to spend USD \$1 billion annually to combat severe lost circulation, stuck pipe, collapsed hole, well control issues, and other difficulties on the unstable borehole. It was also stated that the borehole instability, lost circulation and well control are the three big reasons why subsurface NTP occurs [4].

Preventive and corrective methods have been developed for lost circulation problems. The purpose of the preventive method is to prevent the lost circulation problem by plugging the fractures with the particles added into the drilling mud. Unlike the preventive method, the corrective method can be applied after the lost circulation take places. In the corrective method, the control additives are added to the drilling mud in order to control the lost circulation. Although several lost circulation preventive methods are available, using lost circulation material (LCM) as a preventive method has recently been used in terms of reducing the time and cost. It is very effective to seal unconsolidated permeable formations.

Several models such as the ideal packing theory [5], Abrams median particle size rule [6], average particle size theory [7], and Vickers method [8] clarify the

significance of particle size distribution in pore and fracture plugging using LCM. Newhouse (1991) performed the analysis of production zones and reported that the PPA is an important apparatus for evaluating drilling fluid plugging capability [9]. The PPA experiments have been carried out by applying upward pressure using various permeable ceramic discs with different pore sizes [10]. Pilehvari and Nyshadham (2002) have experimentally tested the efficiency of twenty-four different LCMs on three different drilling fluids [11].

Most of the theoretical and experimental laboratory studies revealed critical theoretical insights and practical methods [11–17]. However, the wide fracture (fracture width $\geq 1000 \mu\text{m}$ or 1mm) plugging mechanism using LCMs is not understood in detail. It might be due to the lack of sensible experiment equipment, wide ranges of LCM particle sizes, precise measure of sealing time, and detailed visual evaluation of the LCMs particle positions through the fractured formations. The deficiencies regarding them were detected in the light of the studies related to pore and fracture plugging [17–22].

Recent studies indicate that there is an impact of different parameters on the sealing capability of conventional and unconventional LCMs at high pressures and temperatures. Alsaba et al. (2014, 2016) examined the plugging performance of LCMs using a series of tapered slots with a maximum fracture width of 2000 μm . The results demonstrate that unconventional LCM is capable of plugging 5 mm fracture widths, but the conventional ones are inadequate [23,24].

In this experimental study, the plugging mechanisms and factors affecting fracture plugging was investigated. The fractures are represented through slotted discs having a fracture diameter of 508, 1016, 1524, 2032, 2540, and 3048 μm . Most importantly, this study aimed to investigate the wide fractures (fracture width $\geq 1000 \mu\text{m}$ or 1mm) plugging efficiency in detail. In addition, this study is an attempt to find the optimum LCM sizes and concentrations to provide efficient wide fracture plugging in terms of unimodal, bimodal, and trimodal particle size distribution. Computer-controlled precise pressure transmitter connected to experimental setup enables to record and observe pump pressure variations versus sealing time. The elapsed time which involves pressure oscillations until pump pressure is stabilized proves fracture

sealing time. The optical microscope made a significant contribution to understanding the importance of the selection of LCM sizes and concentrations. In addition, dry mud cakes obtained from PPA tests were diluted with distilled water to observe the distribution and amount of particles effective in fracture plugging. Throughout the study, all experiments on fracture plugging were carried out using sepiolite mud as a carrier fluid of LCMs. Meanwhile, the rheological properties of sepiolite have been analyzed in detail.

2. STATEMENT OF PROBLEM

The main purpose of this thesis is to investigate the plugging performance of LCMs on fractures and particularly wide fractures (fracture width $\geq 1000 \mu\text{m}$ or 1mm) using sepiolite mud as a carrier fluid of LCMs.

The main purposes can be divided into the following sub-purposes;

- Investigate the sepiolite mud's rheological properties and effectiveness on fracture plugging.
- Examine the LCM features (size, concentration, geometry and PSD of LCMs) impact on fracture plugging efficiency.
- Determine the importance of LCM modality (unimodal, bimodal and trimodal) on various fracture sizes.
- Achieve the early plugging time with the least amount of LCMs on different fracture sizes.

As these objectives are accomplished, it is aimed to solve the lost circulation problems at the earliest time and with the most effective method during drilling operations.

3. LITERATURE REVIEW

The main purpose of this part is to review the properties and applications of sepiolite clay, lost circulation phenomena, pore plugging and fracture sealing methods and recent experimental studies to identify the existing ideas and limitations.

3.1 Properties and Usage of Sepiolite Clay

Sepiolite is a sedimentary clay-mineral that occurs naturally. The most important features of this clay are being non-swelling, light, porous, and it has a wide surface area. The sepiolite's individual particles have a needle-like appearance, as opposed to other clays. The porous and large surface area of the sepiolite clay and the particle shape structure cause extraordinary absorption ability. Also, the colloidal properties of sepiolite clay improve this clay's usage areas and make it an important material. Sepiolite is not a porous phyllosilicate, in contrast to other clays. It can be described as a quincunx of talc-type layers, which are divided by parallel channels in the framework. This chain-like structure creates needle-like particles like other clays, rather than plate-like particles. Figure 3.1 demonstrates the structure of sepiolite clay.

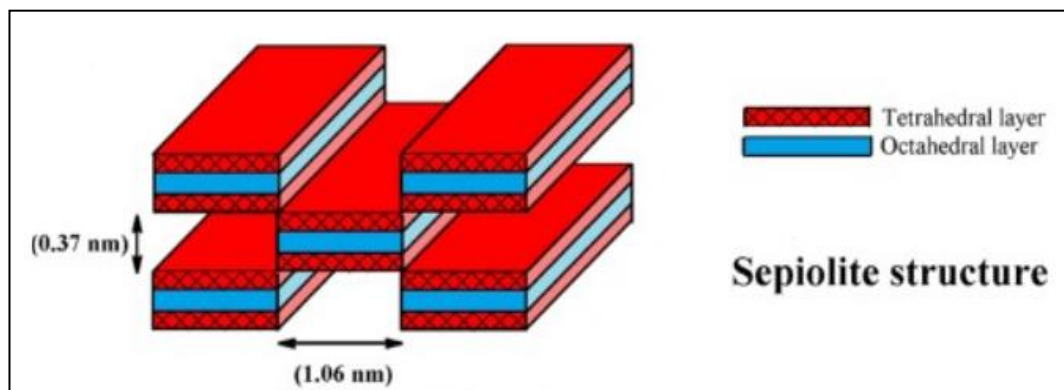


Figure 3.1 The structure of sepiolite clay [20].

Sepiolite has the largest surface area (approximately 300 m²/g) of all clay minerals. In addition, the hydrophilic property is further clarified by the high density of silanol groups (-SiOH) in this clay. The cation exchange capacity is very low since the silicate lattice of the sepiolite clay does not have a remarkable negative charge.

The sepiolite clay's high surface area and porous structure affect its remarkable adsorption and adsorbent properties. This clay can also absorb approximately its own weight and other liquids. Sepiolite clay does not swell and its granules do not

crumble even when saturated with liquids. Colloidal degrees of sepiolite clay can be mixed in water or other liquids using high shear mixers. It forms a network of uniformly intermeshed elongated particles until distributed in the liquid, which is preserved by physical intervention and hydrogen bonding and traps the liquid, thereby increasing the suspension viscosity. Even in systems with high salt concentrations, this structure is stable, conditions which cause the flocculation of other clay suspensions (such as bentonite). The SEM images of sepiolite clay with different scales are shown in Figure 3.2.

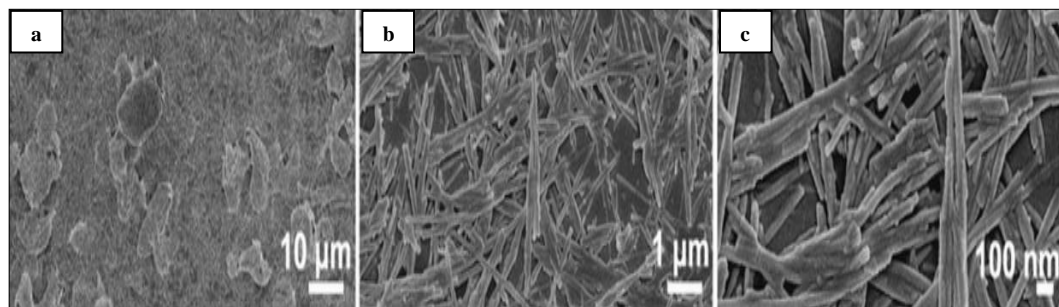


Figure 3.2 SEM images of sepiolite clay with different scales as a) 10 μ m b) 1 μ m c) 100nm [21].

The random sepiolite particle network retains coarser particles in the liquid avoiding their gravitational settling and acting as a suspending force. In addition to that, sepiolite enables its suspensions with pseudoplastic and thixotropic properties which makes it a valuable material for improving the processability, application, or handling of the end product in multiple applications.

Sepiolite clay, which has the above-mentioned properties, has a wide application area from the areas of pet litters to the rheological additives for organic systems. Figure 3.3 shows the common usage of sepiolite clays.

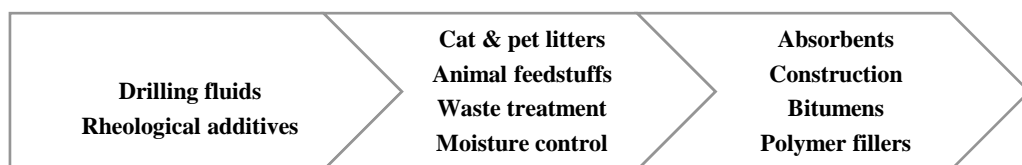


Figure 3.3 The common usages of sepiolite clay [22].

3.2 Uses of Sepiolite Clay as Drilling Mud

Formulation of drilling mud using sepiolite clay was investigated for the first time by Carney and Meyer (1976) [1]. Several researchers have carried out studies to formulate a water-based mud system that can be used in both high temperature and high salinity conditions [23–30]. The common aim of these studies is to obtain minimum cost by providing suitable viscosity and filtration conditions of all drilling muds prepared with sepiolite clay.

Carney and Meyer (1976) conducted experimental studies to obtain sepiolite-based drilling mud that can withstand ultra-high temperatures. In addition, the rheological properties of sepiolite muds exposed to temperatures up to 800 °F were investigated in their studies. As a result of rheological investigations, it was observed that some changes were observed after the sepiolite was exposed to temperatures up to 800 °F, but there was no change in its basic structure [1].

Experimental studies of Carney and Guven (1980) show that sepiolite-based drilling muds without additives retain their structure up to 300 °F and behave more preferable than bentonite and attapulgite clay under the same conditions [23]. In studies conducted by Güven et al. (1988), sepiolite clay at higher temperatures was observed to perform better rheological properties when used with saponite. Furthermore, sepiolite begins to turn into smectite at 300 °F and this reaction is completed at 500 °F. These smectites formed in sepiolite drilling mud increase viscosity and improve filtration losses due to their morphological structure. Consequently, after adding some additives to sepiolite-based muds, it has been observed that these muds exhibit better rheological and water loss properties and have been experimentally proven to be used in harsh environments [26].

Under room conditions, sepiolite mud was compared with bentonite and attapulgite muds [2]. In addition, the experimental results showed that sepiolite mud provides preferable rheological and filtration properties under different salinity conditions. Altun et al. (2005) experimental studies demonstrated that sepiolite-based muds provides better viscosity and filtration properties with increased mixing speed and mixing time and decreased particle size [3]. Although sepiolite-based mud has poor filtration properties, some experimental studies have proven that the filtration

properties of sepiolite-based mud can be controlled relatively cheap using commercial additives [31].

Recent studies demonstrate that sepiolite mud can be used as drilling mud in both high temperature and high salinity conditions [32–35]. Using a thermal rheometer, Etehad and Altun (2018) experimentally investigated the rheological properties of sepiolite-based mud at high pressure and high temperature conditions. As a result of rheological characterization, sepiolite-based mud has been observed to be effective in saline conditions [35].

Intensive literature survey carried out by the researcher showed that there are insufficient number of studies regarding the rheological and filtration characteristics of sepiolite muds. Instead, the studies available were mostly focused on investigating the ways of improving properties of main clay such as bentonite, saponite, attapulgite by adding sepiolite as an additive.

3.3 Lost Circulation General Overview

Lost circulation is known as drilling fluid invasion into the formation which is naturally fractured and high permeable depleted zones. It is one of the most significant problems that increase operational costs and create serious issues while drilling [5]. The drilling cost is substantially affected as circulation is continuously lost drilling through weak and highly fractured formations. A quick glance at some published statistical data verifies this fact. Operators in the Gulf of Mexico (GOM) were forced to spend USD \$1 billion annually to combat severe lost circulation, stuck pipe, collapsed hole, well control issues, and other difficulties on unstable borehole [7]. Circulation loss occupied 12.7% of total drilling non-productive time estimated for 2520 gas wells drilled in water depths of 600 ft or less and a total true vertical depth (TVD) of 15,000 ft or less in the GOM [36]. It is also known that lost circulation is considered as one of the most expensive problems which are commonly seen in the field of geothermal drilling caused by high temperature. Around 10% of total well costs in the mature geothermal areas and more than 20% of the costs in exploratory wells and developing fields belong to the lost circulation. Since the cost of drilling a well is about 35-50% of the total capital costs for a typical geothermal

project; therefore, approximately 3.5-10% of the whole cost for a geothermal project can be related to lost circulation [37].

Types of drilled formation have also significant influence on loss circulation rate. Cavernous, vugular, fractured, or unconsolidated formations are the most candidate zones for lost circulations in the case of improper drilling conditions such as high hydrostatic pressure and pressure surges during tripping (Figure 3.4). Totally or partially lost circulation can be occurred depending on the type of formations penetrated and drilling conditions.

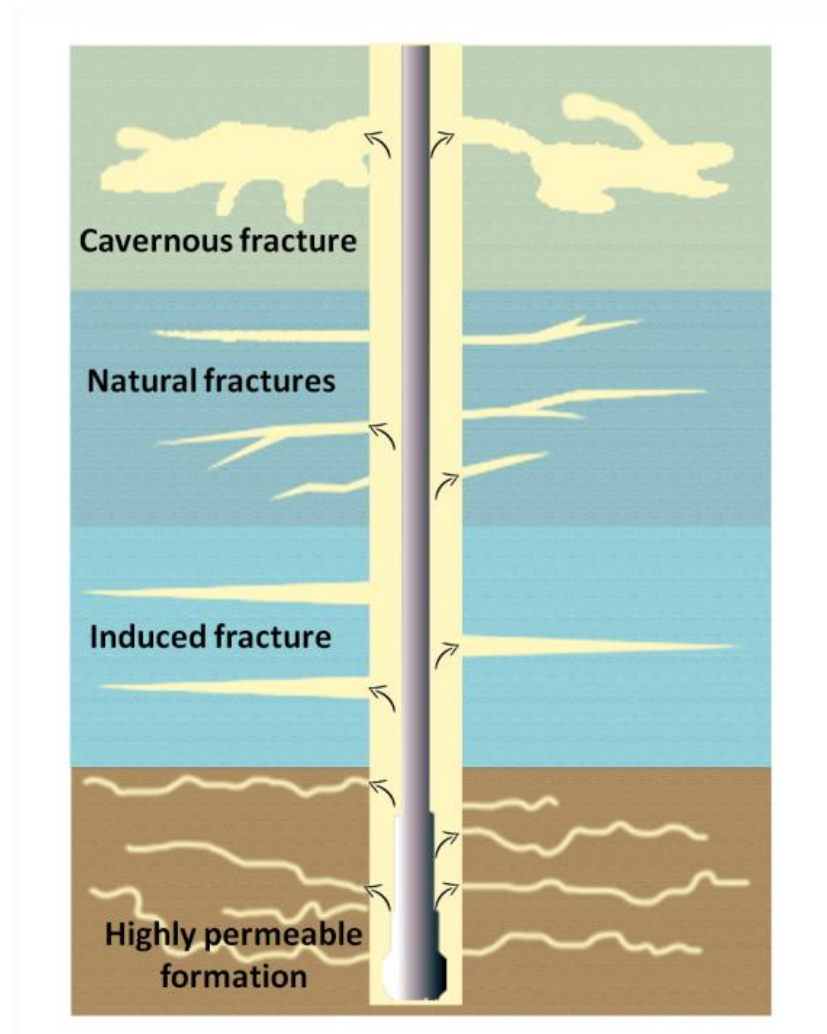


Figure 3.4 Classification of lost circulation zones [37].

For many years operation companies tried to find effective remediations to overcome severe circulation loss as a source of other crucial drilling problems. Four types of comprehensive lost circulation management techniques have been introduced to the drilling industry. Three techniques of them encompass lost circulation prevention

measures including best drilling practices, drilling fluid selection, and using borehole strengthening material. The fourth one concerns the remediation of losses using lost circulation materials [38].

Using lost circulation materials (LCM) as discrete pills have recently been growing up in order to plug pores and fractures. Several LCMs are used in the industry to prevent lost circulation. Oil-soluble resins, fibers acid-soluble particulates, graded salt slurries, high concentrated linear, and cross-linked biopolymers and non-biopolymers are some of these LCMs [39]. Calcium carbonate (CaCO_3) is more often used as bridging agents than others because of their favorable mechanical and chemical properties. Pressure differentials and generated surge/swab pressures in the borehole cannot negatively affect the effectiveness of CaCO_3 pills. It also suggested that calcium carbonates can be used in producing zones due to their acid solubility.

3.3.1 Lost Circulation Material (LCM)

The fundamental purpose of using lost circulation material (LCM) is to struggle with the lost circulation problem. The LCMs are mixed with the drilling mud in order to seal unconsolidated fractured formations (Figure 3.5).



Figure 3.5 Lost circulation materials (LCMs) [40].

It is very effective that LCM should be able to resist the pressure changes and suitable for operation in synthetic, oil, and water-based muds [41]. Howard et al. (1951) made LCM classification in terms of physical properties for the first time. In his classification, there are four types of LCMs as fibrous, lamellated, granular, and dehydratable [5]. White (1956) added a new type of LCMs flaky and mentioned that mixing LCMs can provide effective plugging [42]. According to Alsaba et al. (2014), the LCM can be classified as granular, fibrous, flaky, acid or water-soluble, high fluid loss LCM squeeze, and swellable LCM combinations [43].

The selection of LCM depends on regional availability and most importantly, the cost of the LCM. They can be classified as fibrous, flaked, granular, and a combination of fibrous, flaked, and granular materials. The fibrous LCMs are extensively used in drilling mud to seal losses in more fractured formations. Flaked LCMs act properly to prevent drilling fluid losses in porous formation. Granular materials accumulate in the surface formation and create an impermeable structure to establish sealing. A combination of these three types can be considered depends on the drilled formation type and drilling condition [44].

Although several LCMs are used in the industry to prevent the lost circulation, mechanical and chemical properties of calcium carbonate (CaCO_3) have made it more often used bridging agents than others. Pressure differentials and generated surge and swab pressures in the borehole cannot affect the effectiveness of calcium carbonate pills. It is also suggested to be used in producing zones due to its acid solubility.

3.3.2 LCM Treatments

Based on the time of implementation, there is a common classification for lost circulation treatments. If lost circulation treatments are performed before the occurrence of lost circulation problems, such treatments are called preventive. However, the treatments which are conducted after the occurrence of lost circulation event are called corrective.

3.3.2.1 Corrective LCM Treatments

Any method that is performed after the occurrence of the losses is called corrective solution [18]. In such an approach, the materials of lost circulation mitigation are either continuously added to the lubricating substance or spotted as a concentrated pill in discrete ways so as to prevent the losses.

The physical discrete particles suspended in the drilling fluid which are used to prevent losses are called conventional LCM's. They are often classified into four main types; fibrous, flaky, and granular or a blend of all three [5,42,45]. This classification is based on LCM's appearance or physical properties. The main objectives of using conventional LCM treatments are often to control seepage or partial losses. However, there is no common standard to use conventional LCM treatments to deal with severe losses. In the literature, different solutions have been reported to prevent/mitigate severe losses and can be classified into two main types; LCM solutions and mechanical solutions.

LCM solutions have many types such as cross-linked cement [46–50], concentrated LCM pills [50,51], cement [52], gunk squeezes[13,50–54], chemically activated cross-linked pills, deformable-viscous-cohesive systems[53], nano- composite gel [54], and concentrated sand slurries [55,56].

Mechanical solutions have many aspects such as expandable liners [57–59] and casing drilling [60–62]. The mechanical solutions are often tried after the LCM solution list due to the high cost associated and also the required logistics limitation. Therefore, the first option to be tried is LCM solutions, and then mechanical solutions might be applied. Although such LCM treatments might be successful, the underlying mechanisms are not well understood. This means that this type of LCM solutions might work in one well while it might not work for other wells.

3.3.2.2 Preventive LCM Treatments

The solutions which are applied prior to the occurrence of losses are called preventive treatments. Strengthening the borehole is the main objective of this method [63]. Borehole strengthening can be defined as any practice used to efficiently plug and seal induced fractures during drilling operations by means of enhancing the fracture gradient and widening the operational window [64].

It can be said that the main objective of preventive LCM treatments is to widen the mud weight window through enhancing the fracture gradient. Many researchers experimentally investigated the strengthening effect by means of LCM addition [48,65–67]. It has been documented within the field scale that the application of LCM to drilling fluids could effectively raise fracture gradients compared to previously drilled wells in permeable rocks [68,69]. To understand the mechanisms of such techniques on how to increase the fracture gradient, extensive experimental investigations were conducted. Furthermore, different models have been proposed to explain borehole strengthening phenomena by adding such LCM materials [68,70,71].

3.4 Plugging and Sealing Theories

3.4.1 Pore Plugging Theories

The mechanism of pore plugging using bridging materials was previously investigated by several researchers [8,9,39,44,47,72–82]. Fine particles move into formation and cause to form an internal mud cake during construction of external mud cake. The internal mud cake decreases formation permeability by plugging pore throats of borehole wall. These fine particles can be placed so deeply in formation so that it is not easy to remove them. Therefore, quick building of the external mud cake and minimizing the internal mud cake are highly preferable [83]. This can be performed using lost circulation materials (LCMs), which plug formation pores or fracture throats, form a filter cake, and reduce filtrate flux into formation (Figure 3.6).

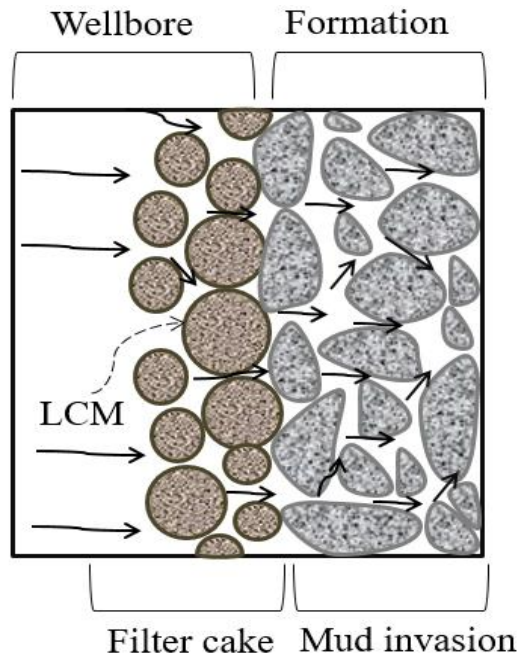


Figure 3.6 Pore plugging mechanism [84].

There have been abundant studies to determine the relationship between loss circulation and particle sizes of LCM used in drilling fluid. In order to determine the optimum particle size distribution (PSD), concentration, size, and shape of the LCMs used in pore plugging applications, several design guidelines were implemented.

Abrams (1977) proposed a rule to estimate the minimum percentage of the fluid volumes invading, non-damaging drill-in fluids [72]. This rule explains that the average particle size of the bridging agent needs to be equal or slightly larger than third of the medium pore size for the targeted formation. For instance, according to this rule, the 50 μm bridging particles should be effective with a good sealing efficiency to the pores with up to around 150 μm in diameter. According to Abrams (1977), the concentration of the bridging solids should be at least 5% of the injected fluids volumes [72]. However, in his calculations, Abrams only considered the particle size that initiates the bridge. In fact, his rule does not provide the optimum size or consider the best packing sequence of the particle size for reducing the fluid invasion and optimizing the sealing efficiency. Based on these guidelines, the fluid design needs to contain a wide range of particles sizes in order to provide a wide range of bridging capabilities.

The full range particle size distribution needed to seal all voids which included the ones are made by the bridging agents efficiently is called Ideal Packing Theory (IPT) [9]. IPT determines LCM for the desired formation characteristics or the optimum particle size distribution of bridging material by graphical approach. With the help of the $D^{1/2}$ rule bridging agents which are the ones a wide range of commercially available are plotted on the same graph. This rule states that the ideal packing occurs when the percent of cumulative volume vs. the $D^{1/2}$ forms a straight-line relationship where $D^{1/2}$ is square root of the particle diameter [85]. In the line of formation information optimum target line must be plotted on the same graph with the optimum bridging agent distribution curve. The worst-case probability regarding the largest dominant pore size or fracture width is the first step of the design process. Thin section analyses enable us to get pore sizing data which is used as the preferred method. To determine the optimum target line, instead of utilizing pore sizing data, when the cases are not available, the formation permeability information can be used. In 2000, Dick et al. adapted the ideal packaging theory to the drilling industry [9]. They carried out a study about using bridging materials to decrease filtration loss through formation. The plugging ability of water and oil based muds was investigated using Pore Plugging Apparatus (PPA) under high pressure and high temperature conditions through ceramic discs with different pore sizes. As results of this study, they figured out the optimum particle size distribution of introduced bridging materials. A study was conducted by Newhouse (1991) about production zones [79]. This study reported that the PPA is an effective apparatus to determine and develop the plugging efficiency of drilling fluids. PPA was used by Davis et al. (1991) through using several ceramic discs which have different pore sizes to simulate the formations with upward pressure flow application [75]. Another proposal stated that bridging materials PSD can be matched with the pore size to reduce the fluid accessibility into permeable formations [76]. Other researchers investigated the plugging ability of two samples from oil based mud containing different LCM particle sizes [81]. Their study specified the critical impact of particle sizes on plugging performance. According to their findings, the drilling mud should be consisted of an additive with a wide range of particle sizes for effective pore plugging. The maximum particle size should be the same with the size of pore or

fracture to plug them efficiently based on their conclusions. Cargnel and Luzardo (1999) developed “average particle size theory” which was previously suggested by Abrams (1977) [74]. When the LCM particle sizes are between 1/7 and 1/3 of the average pore throat, it could provide better plugging [74]. Pilehvari et al. (2002) experimentally studied the performance of 24 different LCMs and seepage control material (SCM) on three different drilling fluids [8]. They also used PPA to perform plugging tests. In their study, the optimum particle sizes to plug the pores were also determined. Samuel et al. (2003) presented a study to introduce the development and the first field application of a new solid-free non-damaging viscoelastic surfactant based fluid loss pill (VES-PILL) [39]. Their experimental studies revealed that such kind of pills could be used up to 190°C (375°F). Vickers et al. (2006), influenced by Abrams' studies, introduced “Vickers Criteria” to determine PSD standards of LCM blends [82]. Table 3.1 summarized different studies reported in the literature with different selection criteria investigating the plugging theory.

Table 3.1 The summary of pore plugging theories' selection criteria.

Authors	Method	Selection Criteria
1930-Andreasen & Andersen	Ideal Package Theory	Power law relationship between particle size & cumulative volume
1977-Abrams	Abrams Rule	1/3 of formation average pore size \leq D50
1996-Smith et al. 1998-Hands et al.	D90 Rule	Formation pore size = D90
1999-Cargnel & Luzardo	Average particle size Theory	Particle sizes are between 1/7 and 1/3 of average pore throat, provides better plugging
2000-Dick et al.	Adapted Ideal Package Theory	Optimum particle size distribution introduced
2006-Vickers et al.	Vickers Method	smallest pore throat < D10 1/7 of mean pore throat = D25 1/3 largest pore throat \leq D50 2/3 largest pore throat \leq D75 largest pore throat = D90

The current bridging theories and selection criteria are valid for pore plugging. Most of the formations are naturally fractured or induced fractured as a results of drilling operation. As these fractures have different complex geometries, current theories may not be applicable in fracture plugging. Therefore, the following section extensively explains the fracture plugging theory.

3.4.2 Fracture Sealing Models

To conduct critical studies on fracture plugging mechanisms, the fundamental terms of fractures should be clearly explained. Fracture mouth can be defined as the first portion of the fracture which is close to the borehole. Fracture tip can be explained as the end part of the fracture which so close to the formation matrix (Figure 3.7)

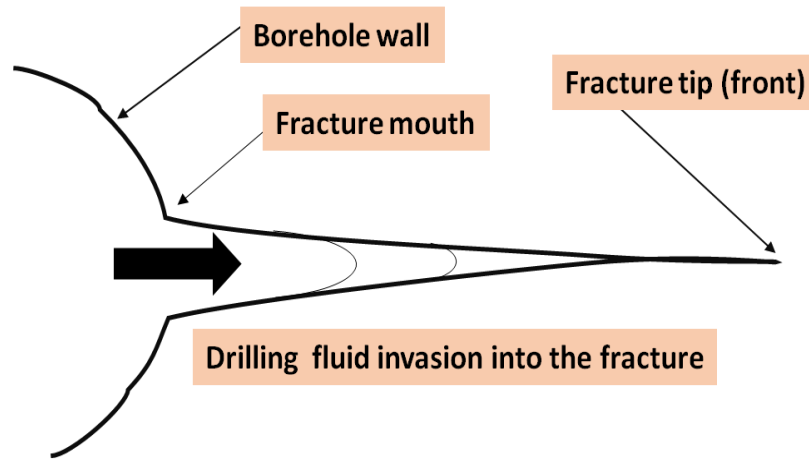


Figure 3.7 Expression of fracture mouth and fracture tip [86].

Fluid-loss treatments in fractured formation can be classified in two main types; low fluid loss and high fluid loss treatment. Among low fluid loss treatment methods, particle base treatment should be designed using wide range of LCMs (coarse, fine and finer). This means that following to formation of coarse-particle framework, finer particles can also be incorporated to reduce the fluid loss in the losses zones which require such a remedy. Although the mechanisms of loss-fluid treatments are so different such as plugging and bridging, the finer particles are so necessary in terms of filling the voids among the coarse particles and producing tight filtercake which results in enhancing the seal and fluid loss control as shown in Figure 3.8. In Figure 3.8, function of LCM in fracture sealing can be clearly observed. Different mechanisms such as plugging, bridging, and filling can happen at the same time with same formation fracture aperture. Fracture plugging occurred as the D90 of the LCM is greater than the aperture of the formation openings (Figure 3.8a). When the aperture is two times greater than the D90 of the LCM particles, fracture bridging will be formed (Figure 3.8b). When the fracture aperture is much more than three time the D90 of the LCM particles only means that fracture is filling (Figure 3.8c) [87].

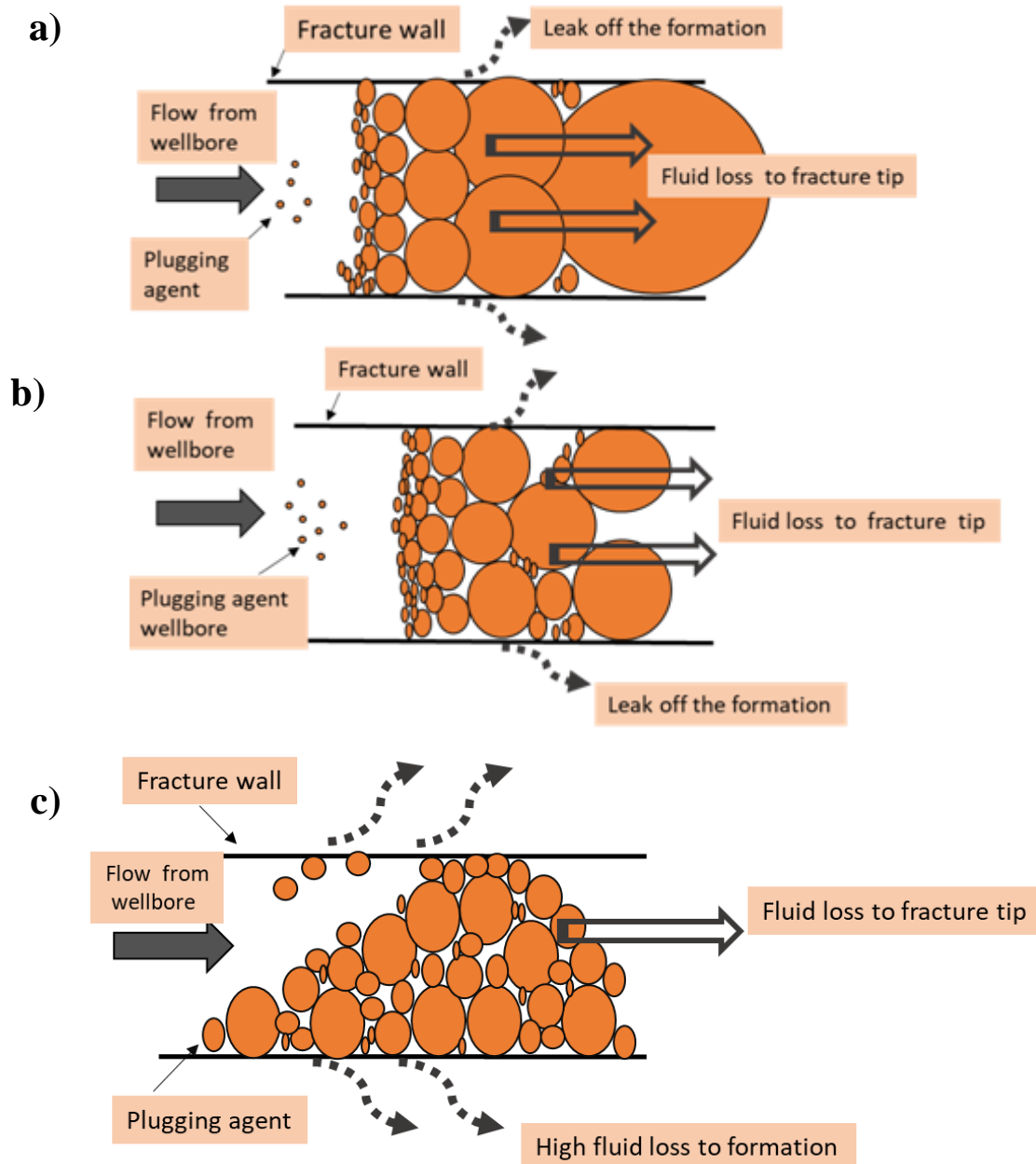


Figure 3.8 Schematic of a) Fracture Plugging b) Fracture Bridging c) Fracture Filling Procedures [87].

Field applications and laboratory studies indicate that the fracture pressure can increase with borehole strengthening operations. Different models have been previously developed to explain the physical mechanism of the borehole strengthening [65,69,70,88–94]. However, there are three common borehole strengthening treatments used in the drilling industry such as stress cage model [70], fracture closure stress model [91] and fracture propagation resistance model [65]. The following section discusses the three most common models in details.

The stress cage model was introduced based on the models of linear elastic fracture mechanics [70]. This model indicates that the hoop stress around the borehole is strengthened by propping the fracture with LCMs. The LCMs should be placed at the fracture mouth for effective fracture sealing purposes. Alberty and Mclean (2004) explained the stress cage model by the following steps: 1) When the fractures were induced on the borehole wall, LCM particles are getting into the fractures, 2) the largest particles firstly plug the fracture mouth area which is basically near the borehole wall, 3) then, smaller LCM particles start filling in the spaces between the larger particles and fracture surfaces before sealing the fracture mouth, 4) The trapped fluids inside the fractures filter into the rock matrix through the fracture surfaces and compressive forces resulting in forming LCM bridges at the fracture mouth, 5) finally, the fracture is bridged near the fracture mouth resulting in increasing the hoop stress that is near the bridge location, which makes the fracture more difficult to open. Figure 3.9 presents the proposal of stress caging process [70].

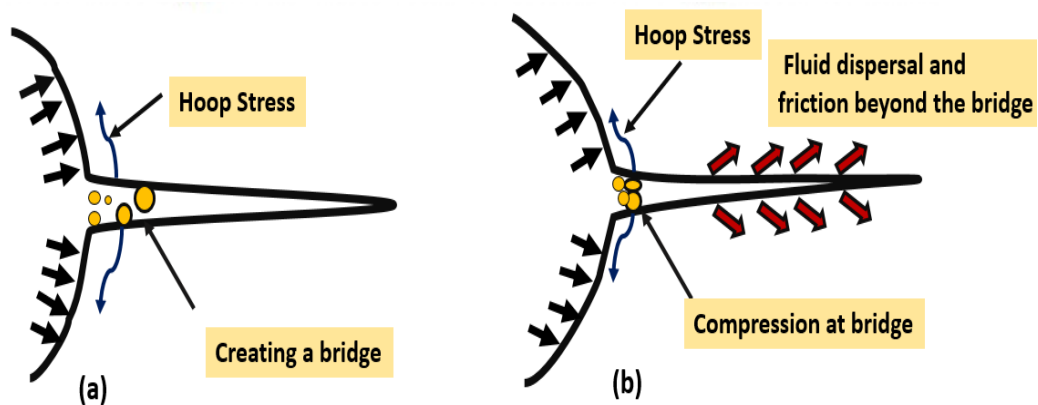


Figure 3.9 The stress caging process [70].

The Fracture Closure Stress (FCS) model was developed to illustrate the reason behind the increase in the fracture gradient (FG) resulted from adding LCMs for loss circulation treatments [91]. The increment in FCS results from widening the fracture and sealing the fracture tip. Therefore, the compression of the adjacent rock produces additional near-borehole hoop stresses. Dupriest (2005) explained this model by proposing the following steps: 1) Fracture on the borehole wall is firstly created and then widened which results in increasing FCS of neighboring rocks, 2) This means that the fractures with larger width would have the larger FCS and vice versa, 3) The LCM particles, which are mixed with drilling fluids, are swapped into the fracture, 4)

Liquid filters out from the pumped drilling slurry to the formation rock, and finally
5) LCM particles are gathered producing an immobile mass in the fracture [91]. The immobile masses have several benefits:

a) They keep the fracture opened.

b) They isolate the fracture tip from the borehole pressure.

c) The immobile mass will keep interacting and developing with filtrate loss. The developed immobile mass is packed back to the borehole wall which resulted in increasing the fracture closure stress and isolating the fracture tip. This process makes the fracture more difficult to open and extend. Figure 3.10 shows the methodology for the proposal of Fracture Closure Stress (FCS) model.

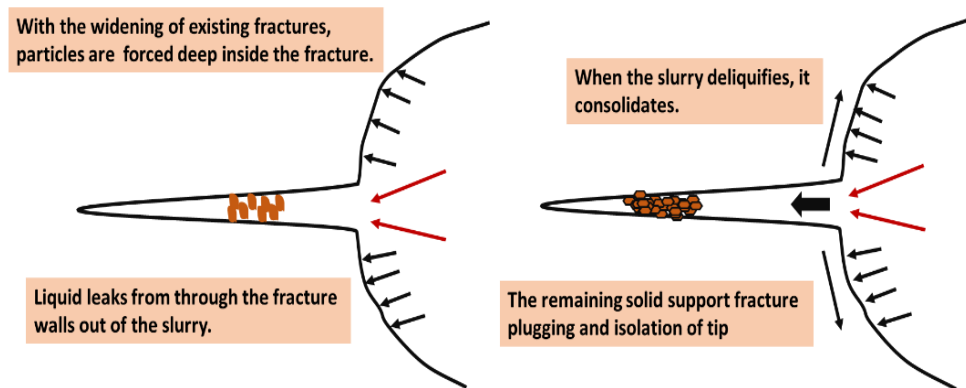


Figure 3.10 The Fracture Closure Stress (FCS) model process [91].

The Fracture propagation resistance (FPR) model was described by Van Oort et al. (2011). Van Oort et al. (2011) used the outcomes of Drilling Engineering Association-13 (DEA-13) experiments [48] to develop their model [71]. This model indicated that the fracture gradient (FG) increases due to the increment in the FPR providing tip insulation with LCM. This model assumes that the accumulated filter cake inside the fracture, which resulted from the fracture propagation and filtrate loss, can seal the fracture tip and prevent the pressure communication between the tip and borehole. Therefore, the resistance for fracture propagation will be so high. To give a better explanation of the fracture propagation resistance model, the variations between fracture-tip screen-out behavior of water based mud (WBM) and oil/synthetic based muds (OBM/SBM) are shown in the Figure 3.11.

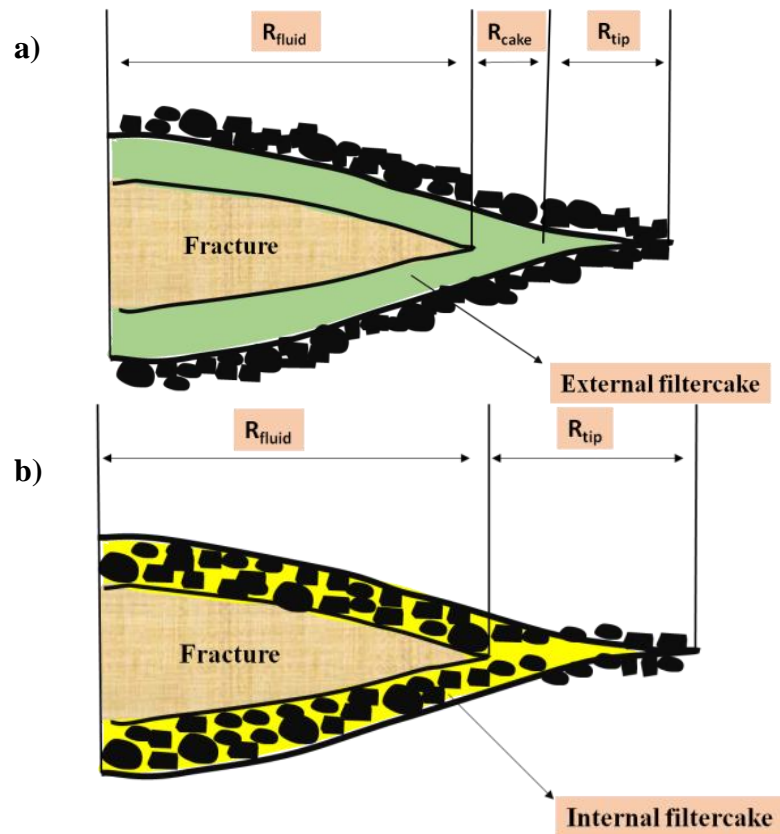


Figure 3.11 a) Fracture propagation mechanism using WBM b) Fracture propagation mechanism using OBM/SBMs [48].

It can be observed that the fracture tip is clearly sealed by the external filter cake by using the WBM (Figure 3.11a). The external filter cake contributes in preventing the effective pressure communication between the drilling fluid and the fracture tip. Hence, the fracture extension is constrained. The radial distance surrounding the borehole that the drilling fluid occupies in the fracture is defined as R_{fluid} . While the thickness at the R_{cake} refers to the filtercake that builds up between the drilling fluid and the beginning of the fracture tip. The length of the filter tip (R_{tip}) should be measured from the end of the R_{cake} to the outer edge. In OBM/SBM systems (Figure 3.11b), the internal filtercake can not prevent the full pressure communication to the tip resulting in facilitating the fracture extension at propagation pressures. The same definition of R_{fluid} and R_{tip} can be used in WBM cases [48].

The other two models has been determined to correlate the change in near-borehole stress to the increase in fracture closure stress. However, the fracture propagation resistance model has been determined to correlate the increment in formation resistance towards fracture propagation.

On the other hand, Van Oort et al. (2011) stated that the fracture propagation pressure could be considerably increased as a result of the borehole strengthening treatments without increased in fracture initiation and reopen pressure [65].

It is known that the three above presented physical models are only qualitatively explaining the mechanisms of the borehole strengthening at a phenomenon based level. However, they do not quantify how much the fracture pressure can be enhanced during the borehole strengthening treatments and how the most important factors can affect the strengthening results. Some analytical models and numerical simulations have been attempted to quantify fracture behaviors and pressure-bearing capacity of the borehole over the last two decades.

Aadnoy and Belayneh (2004) presented the Elastic-Plastic Fracture model in order to explain how the fracture gradient (FG) value can exceed the theoretical value during fracture treatments [71]. Wang et al. (2007) suggested a 2D element-boundary model simulating the borehole strengthening [95]. This model estimates the fracture width and stress distribution near the borehole before and after the fracture bridging. The simulation results indicate that the hoop stress value considerably increased via using the stress cage method. Guo et al. (2011) examined two pre-existing fractures which are symmetrical in the borehole wall using the 2D finite element model to investigate the fracture width distribution. Various in-situ stress and fracture length conditions were studied. However, the model does not give any information regarding the fracture behavior after application of borehole strengthening treatments [92]. Salehi (2012) analyzed the borehole hoop stress hypothesis improvement as fracture sealing technique by means of 3D poro-elastic finite-element model for simulating fracture initiation, propagation and sealing surrounding borehole [64]. The simulation findings conflict with the opinion that suggests fractures sealing would raise the hoop stresses above the ideal condition of the borehole. It was also concluded that the efficient fracture mouth sealing provides hoop stress restoration around borehole. Feng et al. (2015) and Feng and Gray (2016, 2017) developed a 2D finite element model considering the rock porosity by conducting a comprehensive study to strengthen the borehole. This model provides information about fracture width distributions and pore pressure before and after fracture bridging. The results reveal that the hoop stress near the borehole and through fractures considerably increased

by means of fracture bridging with LCM [96]. Different loss circulation and borehole strengthening models in fractured formation have been classified in the literature with fracture types examining the fracture plugging models as shown in Table 3.2.

Table 3.2 Summary for the proposed loss circulation and borehole strengthening models in fractured formation.

Authors	Models	Fracture Type
1992-Fuh et al.	Fracture Pressure Inhibitor	Stationary fracture
2004-Alberty & McLean	Stress Cage	Stationary fracture
2005-Dupriest	Fracture Closure Stress (FCS)	Stationary fracture
2004-Aadnoy & Belayneh	Fracture Healing	Stationary fracture
2007-Wang	2D-Boundary Element Model (BEM)	Stationary fracture
2011-Guo et al.	2D-Finite Element Model (FEM)	Stationary fracture
2011-Van Oort et al.	Fracture Propagation Resistance (FPR)	Stationary fracture
2012-Salehi et al.	Fracture Mouth Sealing	Dynamic frac (pre-defined)
2015-Feng et al.	2D-Finite Element Model (FEM)	Stationary fracture
2016,2017-Feng & Gray	3D-Finite Element Model (FEM)	Dynamic frac (pre-defined)

3.5 Recent Experimental Studies

Alsaba et al. (2014, 2016) conducted a detailed laboratory analysis that examines the effect of various parameters on the sealing impact of conventional and unconventional LCMs under high pressure and temperature conditions. In their study conducted on a set of tapered slots, it has been demonstrated that the unconventional LCM can plug fractures with a width of 5 mm where the conventional LCM is not sufficient [43,97].

Razavi et al. (2016) experimentally investigated the effect of the PSD on the ability of LCM blends to seal fractures. In their study, it was observed that although the one-third rule, ideal packaging theory, and Vickers criteria could provide basic PSD guidelines, it did not properly represent the physics behind the fracture sealing. Therefore, new design curves are introduced for optimum PSD in the borehole strengthening (WBS) experiments. The new design curves methodology was introduced to generate the optimum PSD for LCM blends. Basically, the new design curves stand on the functionality of a log-normal Cumulative Distribution Function (CDF) with Gauss error function. This technique used a bimodal PSD that provides suitable sized fine and coarse particles with enough concentrations in the LCM blend, which is crucial for a successful fracture plugging [98].

In spite of the reported encouraging laboratory experiments and the field applications, the real mechanisms of borehole strengthening treatments are not well understood. Many arguments are still existed in the drilling industry about the mechanisms of the borehole strengthen treatment. However, remedial borehole strengthening operations are still performed on a large scale with a trial-and-error basis. The industry has a lack of understanding of mathematical models to quantitatively describe the treatment process. Some of the phenomena are still not clear, namely, the effect of some parameters as well as the strength and LCM size distribution, the location and mechanical patterns of LCM bridge/plugs, and the anisotropy of field in-situ stresses.

4. METHODS AND MATERIALS

In this study, alternative water based mud clay known as sepiolite obtained from AEM Company near Sivrihisar-Eskişehir district of Turkey was used (commercially known as Turk Taciri Bej). The sepiolite clay as a thermal stable viscosifier can be used in harsh drilling conditions such as high temperatures, due to its favorable rheological properties, less gelling tendency, and effective fluid loss when used with some suitable additives [1,3,28]. Therefore, the plugging time of sepiolite mud in wide fractures has been extensively investigated.

The raw sepiolite clay sample was grinded without physical or chemical treatment and sieved to be less than 74 μm . X-Ray Fluorescence Spectrometry (XRF) and X-Ray Diffraction method (XRD) were used to perform elemental analysis of sepiolite clay. The results obtained are given in detail in the Appendix-A.

In addition, the plugging properties of bentonite clay, which is widely used in geothermal fields, in fractured formations were investigated. The results obtained were compared with sepiolite clay. Moreover, the effect of sepiolite and bentonite clay blend on fracture plugging has been observed. In this study, wyoming bentonite clay supplied from Kayen Drilling Company was used (It is a commercial product known as Aquagel). Also, XRF was used to perform elemental analysis of bentonite clay. The results obtained are given in detail in Appendix-B.

The formulation of sepiolite mud is given in Table 4.1. Mud samples were prepared by adding only 17.5 lb / bbl (50 kg / m^3) of sepiolite clay into 350 ml of pure water.

Table 4.1 Compositions of sepiolite mud systems.

Substance	Quantity (kg/m^3)	
	Unweighted	
	Base Mud	Base Mud with CaCO_3
Sepiolite	50	50
Calcium Carbonate (CaCO_3)	None	unimodal, bimodal, trimodal

API standard procedures were followed throughout the all experimental studies [99]. Couette type viscometer (Fann Model 35SA/SR-12) was used to measure rheological properties such as apparent viscosity, plastic viscosity (PV), yield point (YP) and gel strength (GS).

In addition, the gel structure and thixotropic properties of the sepiolite mud samples were determined using DHR-II. The oscillating amplitude, frequency and dynamic time sweep tests were performed to find the rheological properties (yield point and gelation time) of the sepiolite mud samples. Besides, the thixotropy loop and oscillatory dynamic shear tests were performed to analyze the gel strength and thixotropic properties of sepiolite mud samples [100].

The Pore Plugging Apparatus (PPA) has been modified and used to investigate plugging ability and fluid loss characteristics of the sepiolite mud samples through six slotted disks with different fracture diameters at 1000 psi pressure differential in the upward flow direction. The overall particle size that can be measured with PPA must be smaller than 1000 μm (1 mm or 1000 μm) to prevent plugging the orifice of the bottom cap and the needle valve into the apparatus. This restriction allowed a standard fracture diameter of 1000 μm to be used. To overcome this limitation, the installed needle valve was replaced by a ball valve and a handmade screen was put under the baffle in the receiver portion of the LCM evaluation to prevent particles larger than 1 mm from passing through (Figure 4.1).

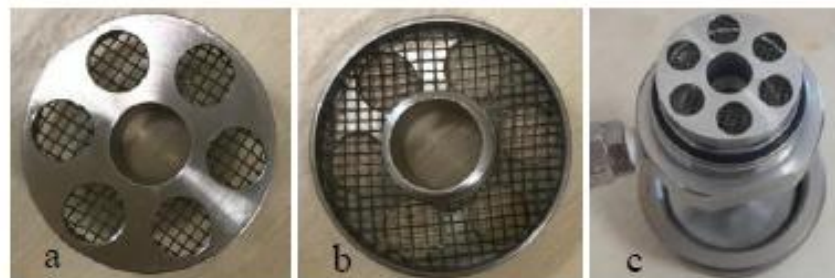


Figure 4.1 Modification of baffle in LCM evaluation receiver used in PPA a) Top view b) Bottom view c) Baffle.

The computer controlled precise pressure transmitter is used to record the pump pressure against the sealing time. The time elapsed by pressure oscillations until the pump pressure is constant is expressed as fracture sealing time. The test results can

be summarized as follows: (A) sealing initiation, (B) sealing development, and (C) pressure stabilization, sealing completion (Figure 4.2). Sealing started at the end of zone A (with 300 psi back pressure) and then the pressure increased with some oscillations (Zone B). Plugging continues until there is a significant pressure increase of up to 1300 psi (1000 psi pressure difference).

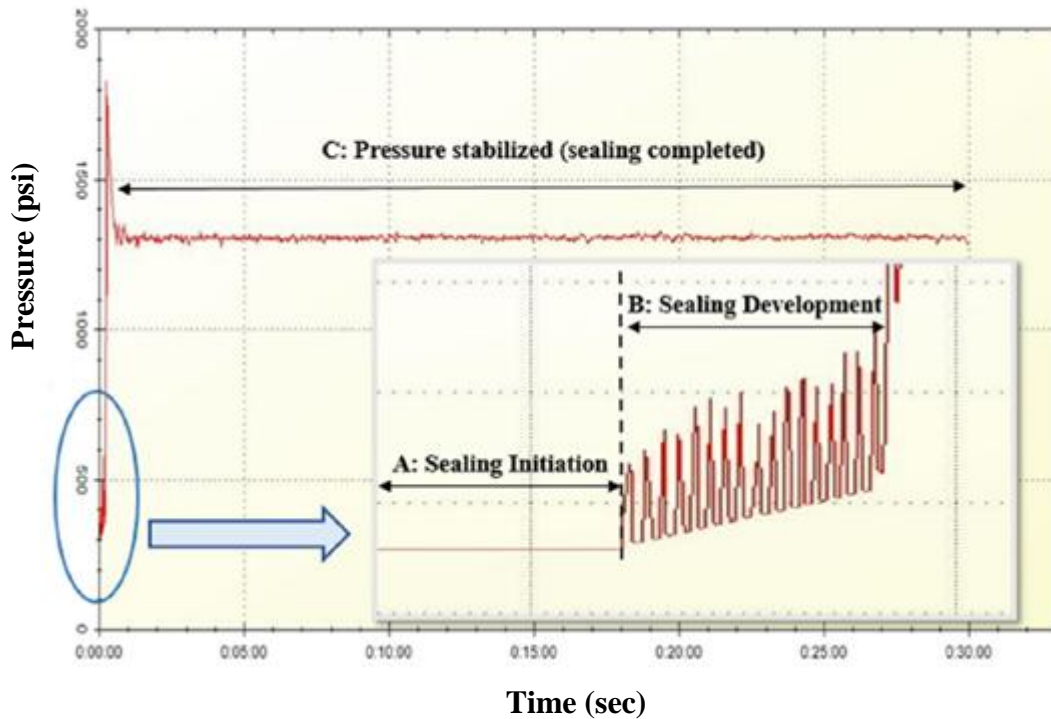


Figure 4.2 Three main regions with differences in pump pressure vs. sealing time results.

There are some limitations in measuring large particle sizes in the laser diffraction technique. Therefore, dry sieve analysis was used to analyze the LCM particle size distribution. A set of sieves (74 μm up to 3360 μm) adjusted to the ASTM-E11 standard was used to achieve 16 different LCM particle size ranges of CaCO_3 (Figure 4.3). However, two sieves (other than ASMT specifications) with a mesh diameter of 2500 and 3000 μm were used to plug the 2540 and 3048 μm fracture discs.



Figure 4.3 Sixteen different CaCO₃ particle sizes.

Utilizing a wide range of CaCO₃ particles on slotted discs enabled to analyze the plugging efficiency of sepiolite mud samples. The wide sieve sets have been used to achieve unimodal, bimodal and trimodal particle size distribution of CaCO₃ particles. In addition, before determining unimodal, bimodal and trimodal combination and LCM amounts, a template was created by conducting preliminary experiments and experiments were continued according to this template. The preliminary test results for each disc are detailed in Appendix-F. The different unimodal CaCO₃ compositions obtained were examined on slotted discs. However, the bimodal and trimodal compositions of the CaCO₃ particles were chosen the same, except for the largest particle size. Table 4.2 shows the bimodal and trimodal compositions of CaCO₃ particles.

Table 4.2 Bimodal and trimodal compositions of the CaCO₃ particles sizes.

Disc fracture diameter (μm)	LCM size interval (μm)		% of Total Concentration		
			Bimodal	Trimodal	Bimodal distribution for 1016 μm disc
3048	Largest particle size (μm)	3000-3360	30	30	
2540		2500-2830			
2032		2000-2380			
1524		1410-1680			
Same LCM sizes for all discs		1180-1410	20	15	-
		1000-1180	15	10	30
		841-1180	-	10	20
		595-841	-	-	15
		500-595	-	10	-
		297-420	-	10	-
		250-297	15	5	-
		149-250	-	-	15
		106-149	10	5	10
	75-106	10	5	10	
Total LCM Conc. (ppb)			40	40	40

The probability density functions (PDF) of the unimodal, bimodal and trimodal distribution of CaCO₃ particles were calculated. Figure 4.4 shows the PDF of the unimodal, bimodal and trimodal distribution selected for the fracture width of 2032 μm.

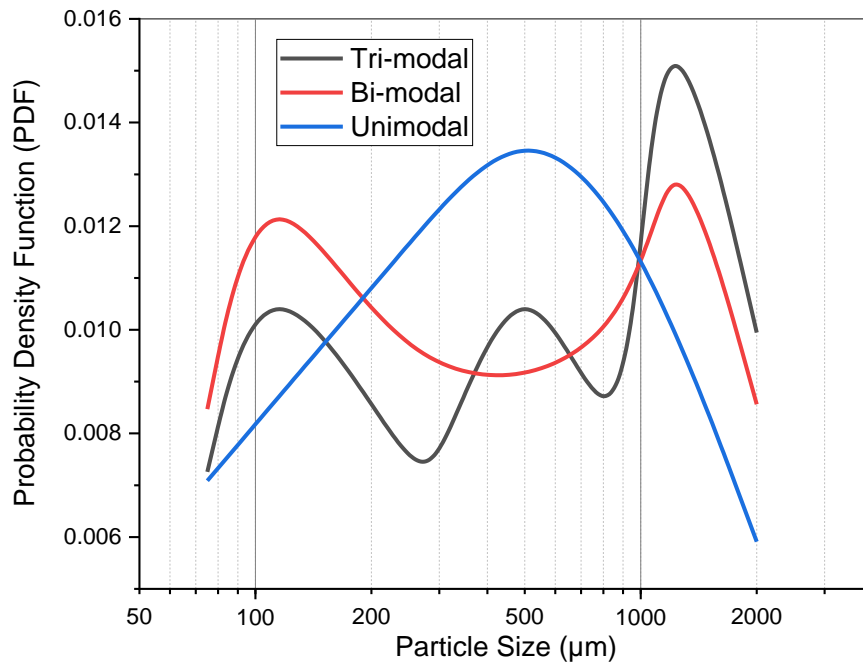


Figure 4.4 Unimodal, bimodal and trimodal distribution for 2032 μm fracture width.

The mud cakes on slotted discs were visually examined using an optical microscope. Thus, the importance of LCM sizes, concentrations and LCM particles in fracture plugging was observed. Dry mud cakes are diluted with distilled water until the sepiolite clay particles swell again. Thus, precipitation of CaCO_3 particles was achieved. In addition, wet sieve analysis was performed using 74 micron sieve to separate the CaCO_3 particles from sepiolite clay less than 74 microns.

The distribution and amount of active CaCO_3 particles in the fracture plugging process were examined based on the results of the wet sieve analysis. When the results of the experiments were evaluated, it was observed that the particles had a more obvious effect in fracture plugging due to the different shapes. Therefore, all experiments with each of the selected LCM combinations were repeated 5 times. Thus, variables such as sealing initiation and sealing development, and total fluid loss were optimized and evaluated.

4.1 Permeability Plugging Apparatus (PPA)

The Permeability Plugging Apparatus (PPA) is an instrument that was introduced to simulate downhole static filtration by operating at high pressure, high temperature conditions that have similar features with well conditions. It has a slotted disc which is used as filter media and is placed above the sample fluid. By intensely simulating the formation structure, the disks give an illustration of the filter cake.

The flotation piston inside the cell enables to transfer of hydraulic pressure to the drilling fluid sample. The top limit of test pressure is 5000 psi (34,474 kPa) while the maximum temperature is 500°F (260°C). Additionally, the pressure for the backpressure receiver can be 750 psi (5171 kPa) at most. Figure 4.5 shows the PPA used in the study. In order to get the plugging time measurement the PPA is connected with a precise pressure transmitter and computer system.



Figure 4.5 Permeability Plugging Apparatus (PPA) and Accessories [101].

The purpose of volume cell (500 ml) which has a movable piston at the bottom to fill the testing fluid. The slotted disc which is used as filtering media is placed at the top of the volume cell. While nitrogen gas is used for the purpose of pressurizing, the pressure is applied from the top of the upside-down receiver which is a must to prevent evaporation at high temperatures. The fluid collector which is positioned at the top of the system is a collection point of the pressure from the downward is applied with hydraulic oil pump and filtrate. The hydraulic pump is illustrated in Figure 4.6. The hydraulic pump which has oil inside can have a maximum of 5000 psi pressure. The oil inside the pump must be monitor in each experiment in the case of decreasing the amount of oil, if so the oil must be filled up till the required level.

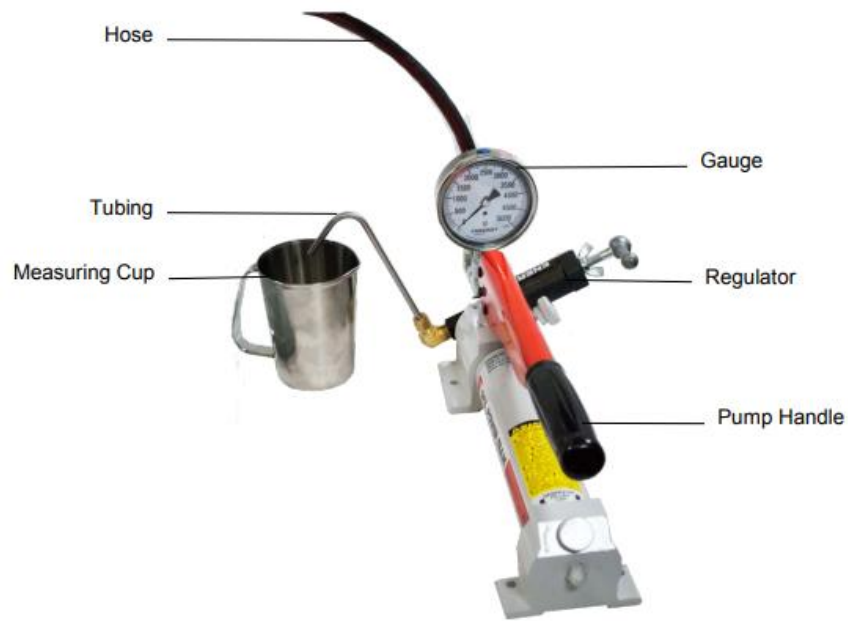


Figure 4.6 Pump Assembly [101].

The fracture diameter of slotted discs are represented as 0.02 in (508 μ), 0.04 in (1016 μ), 0.06 in (1524 μ), 0.08 in (2032 μ), 0.1in (2540 μ) and 0.12 in (3048 μ) in Figure 4.7.

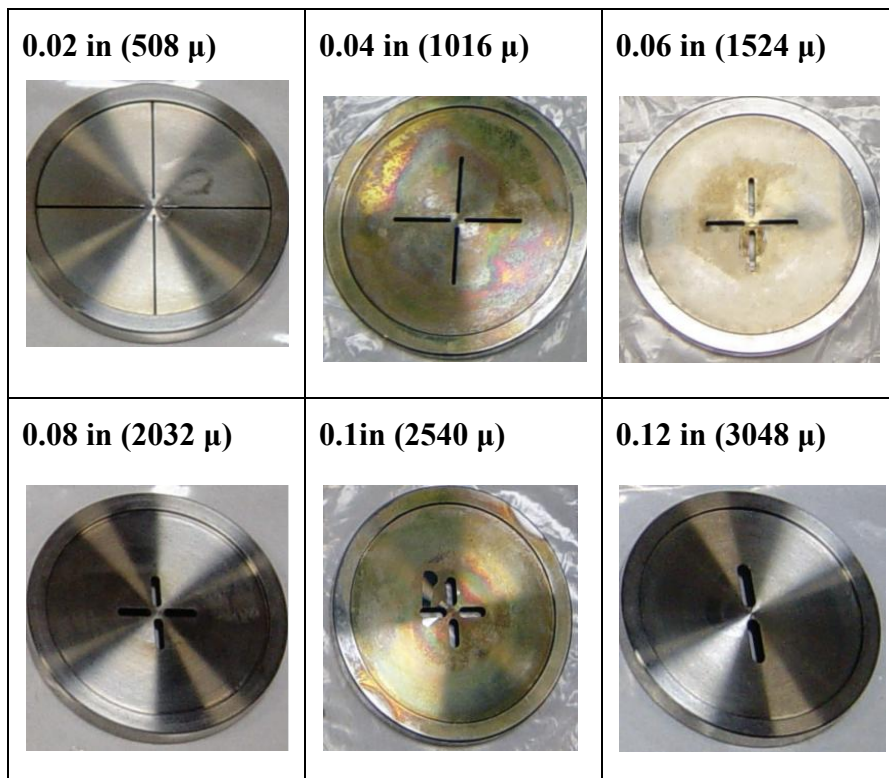


Figure 4.7 Slotted discs [101].

4.2 Fann Model 35SA Viscometer

Fann Model 35 viscometers are measurement direct reading instruments having two major designs, six-speed and twelve-speed, which can be used on either 50 Hz or 60 Hz electrical power. The measurement fluid is in the annular space between the outer cylinder and the bob. While the rotation, at a known velocity, outer cylinder results in a viscous drag exerted by the fluid, the viscosity measurements are made. The deflection of the precision spring is measured by the transmission of torque on the bob which is caused by viscous drag.

Model 35, a Couette viscometer, is used to measure the shear stress caused by a given shear rate and is used to measure viscosity. Alterations in the rotor speed and rotor-bob combination results in changes in the shear rate. To enhance shear stress ranges and allow viscosity measurements in a variety of fluids various torsion springs that can be adopted easily are utilized. The Fann Model 35SA viscometer is demonstrated in Figure 4.8.



Figure 4.8 Fan Model 35SA viscometer [102].

4.3 Aging Cells

In order to get more fully developed rheological and filtration properties of drilling fluid sample which had been experienced a period of shear, drilling fluid aging is done. The time required to have fully developed properties ranges from as being the minimum, several hours (usually 16 hours) to as much as several days. Ambient or elevated temperatures are a range for aging temperatures. Drilling fluid formulations

must create a homogenous fluid that can be provided by using a drilling fluid formulation includes a base liquid and additives that are dissolved or are mechanically dispersed into the liquid. To get a homogenous blend and to starting aging the fluids are mixed or sheared as many as required to. The condition is not a single specific condition for aging; they vary from static to dynamic and from ambient to highly elevated temperatures. Figure 4.9 demonstrates aging cells.



Figure 4.9 Aging cells [103].

4.4 Roller Oven

In order to get more fully developed rheological and filtration properties of drilling fluid sample which had been experienced a period of shear, drilling fluid aging is done. The time required to have fully developed properties ranges from as being the minimum, several hours (usually 16 hours) to as much as several days. Ambient or elevated temperatures are a range for aging temperatures.

To carry the aging process to the next level, Roller Ovens (Figure 4.10) which are perfect to age fluid samples. Samples are heated on moderate heat and rolled by the power-driven by the rollers. However, roller ovens are not necessary to heat the samples since they can be processed without applying static aging. The temperature of the samples which are well insulated is monitored by a digital electronic controller. Distribution of the temperature evenly throughout the oven is ensured by the internal circulation fan.



Figure 4.10 Roller Oven.

4.5 Multi Mixer

The drilling fluid includes solid additives as well as polymers, resins, and soluble salts which are used to get desired rheological properties for the drilling process. The common consensus is on using The Five-Spindle Multi-Mixer Model 9B mixer with No. 9B29X impeller blades (Figure 4.11) as a general purpose mixing of drilling fluids in preparation for laboratory tests of mud materials. A single sine-wave impeller approximately 25 mm in diameter which is mounted flash side up is joined with each spindle. This configuration obliges with the American Petroleum Institute (API) Specification 13A for mixing water-based and oil based drilling fluids.



Figure 4.11 Five-spindle multi-mixer [104].

4.6 Discovery Hybrid Rheometer (DHR-II)

Stress and strain values can be controlled by an instrument called The Discovery Hybrid Rheometer (DHR-II). Real-time strain control at each point of the oscillatory measurement is enabled by Direct Strain Oscillation. On the other hand, materials that are undergoing thermal, chemical, or structural transitions can be conceptualized by rapid data collection which is allowed by Responsive Strain Control. Examination of materials with a non-linear response at very large amplitudes by getting the highest data quality is ensured by highly precise and accurate deformation control (stress or strain).

Figure 4.12 displays the DHR-II used in the study. However, there is an issue caused by the temperature which is the evaporation of the sample. This problem was dealt with the solvent trap at 50 ° C which is shown in Figure 4.13.



Figure 4.12 Discovery Hybrid Rheometer (DHR-II).



Figure 4.13 DHR-II Accessory-Solvent trap [105].

5. RESULTS AND DISCUSSION

5.1 Rheological Properties of Sepiolite Mud

The yield point (YP) and gel strength (GS) are two essential criteria that must be continuously monitored while drilling operations. The yield stress [106,107] and thixotropy [108,109] identify the capacity of muds to suspend when mud is in under static conditions. The gel strength is an indication of how easily the fluid structure avoids the accumulation of solid particles or greatly decreases them. Also, when the gel strength is very progressive, high pump pressure is required to break the gel strength of the mud and start the circulation [110].

Most of the drilling fluids demonstrate thixotropic properties (drilling fluids viscosity increases over time under static conditions). The thixotropic properties of drilling mud characterize the structure reconstruction over time and are essential to the suspension to avoid cuttings from being settled in static conditions. As the drilling fluid is stationary during the PPA experiments, it is necessary to use the high thixotropic and shear thinning fluid system, especially to plug wide fractures with large LCM sizes.

In this study, sepiolite mud shows high thixotropy and appropriate shear thinning index properties. In addition, sepiolite mud has an appropriate yield point (YP) and gel strength (GS) properties. Yield point value is generally known as the dominant mud property that affects circulating friction losses and especially cuttings transport efficiency. Table 5.1 summarizes the suspension particle diameter and viscosity parameters measured by the Fann viscometer. As shown in Table 5.1, as the dial reading temperature value increases, the yield point value decreases and as a result, the maximum particle size diameter that the sepiolite mud can carry decreases. As a conclusion, sepiolite mud has a sufficient carrying capacity that can be used in plugging experiments.

Table 5.1 Sepiolite fluid system properties as measured accordance with API standards.

		Dial reading @24°C	Dial reading @49°C
Rotor speed (rpm)	600	52	37
	300	46	32
	200	43	30
	100	37	26
	6	23	17
	3	23	17
Plastic Viscosity (Cp)		6	5
Yield Point (lb/100ft ²)		40	27
Gel Strength, 10sec./ 1min./ 10min.		22/24/31.	21/22/32.
pH		8.1	8.1
Density (ppg)		8.5	8.5
Apparent Viscosity (Cp)		26	18.5
Suspension particle diameter (in)		0.26	0.18

A rotor speed of 3 rpm is applied to the sepiolite mud using the Fann viscometer. The highest values obtained in the first 10 seconds and 10 minutes are reported as gel strength. In addition, 3 rpm was chosen randomly as the rotor speed. A higher gel force value is obtained if 6 rpm is applied to the mud sample, and a lower gel force value is obtained if 1 rpm is applied. It is therefore important to consider the more realistic thixotropy characterization of the mud sample. Therefore, the rheological properties of sepiolite mud have also been studied using DHR-II.

In this study, constant shear and oscillation dynamic shear tests were carried out using DHR-II in order to characterize the gel structure of the sepiolite mud sample and determine the yield stress and thixotropy index value. Figure 5.1 shows the steady shear rheological properties of the sepiolite fresh water mud sample measured with DHR-II.

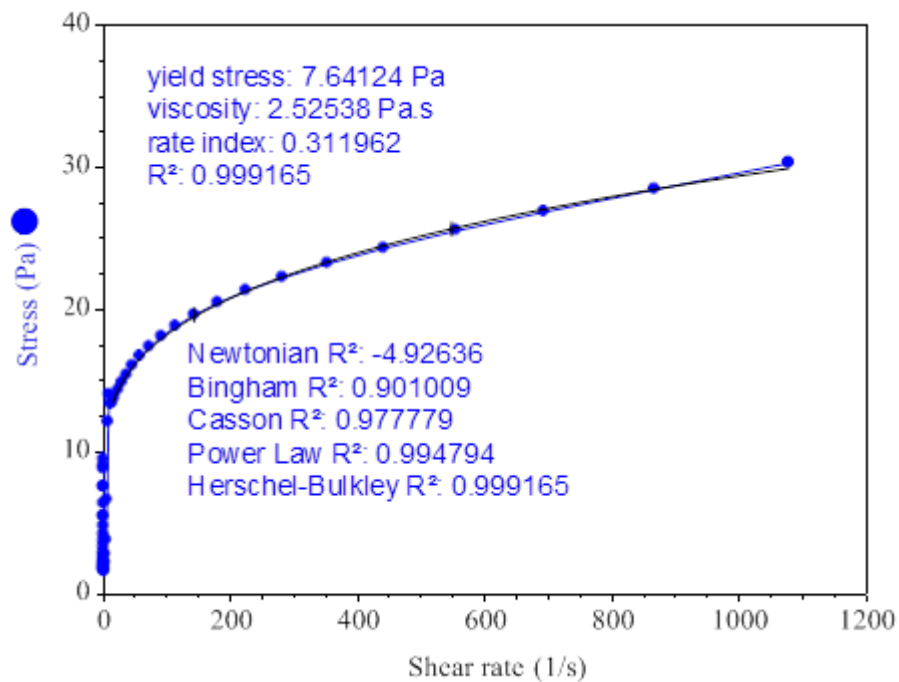


Figure 5.1 Rheological properties of sepiolite fresh water fluid sample (DHR II). The Herschel Bulkley rheological has proved to be the most effective rheological model for sepiolite fresh water mud samples. The "thixotropic loop" test is the simplest test that explains thixotropy. Thixotropic loop tests, the hysteretic response obtained when a material is subjected to a sequence of up and down shear rates, can be used to demonstrate the degree of structural change between the up and down curves. The thixotropy cycle test for sepiolite fresh water mud is given in Figure 5.2. The area within the hysteresis cycle represents the energy consumed in structure degradation, which is an indicator of the degree of thixotropy. As the area obtained increases, more suitable thixotropic properties are observed in the mud sample.

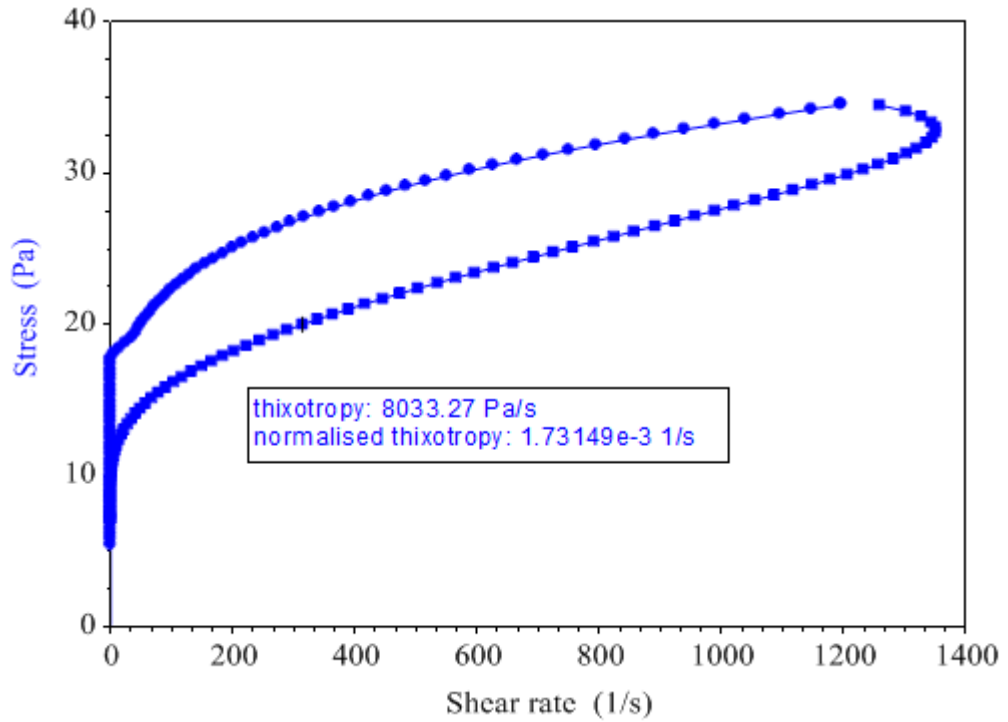


Figure 5.2 Thixotropy of sepiolite fresh water fluid (DHR II).

The behavior of sepiolite fresh water mud as a result of oscillating time sweep test under low and high strain is given in Figure 5.3. With the oscillating time sweep test, the change of the behavior of the mud sample can be observed continuously. The ability of the mud system to reach equilibrium is very important for the performance of the mud sample during the mud circulation. Sepiolite mud shows stable behavior as it has an effective clay-based mud system.

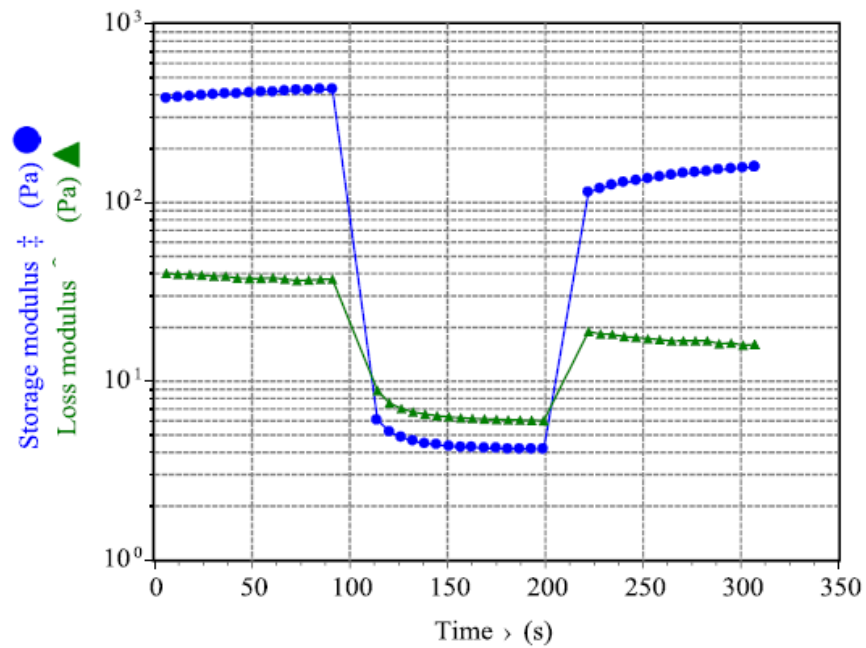


Figure 5.3 Sepiolite fresh water fluid–structure break down and build up (DHR II). The frequency sweep test result for sepiolite mud as shown in Figure 5.4. In the frequency range studied, the storage module (G') is larger than the loss module (G''). This indicates that sepiolite mud has a stable gel structure. The formation of a stable structure is very important to suspend small particles.

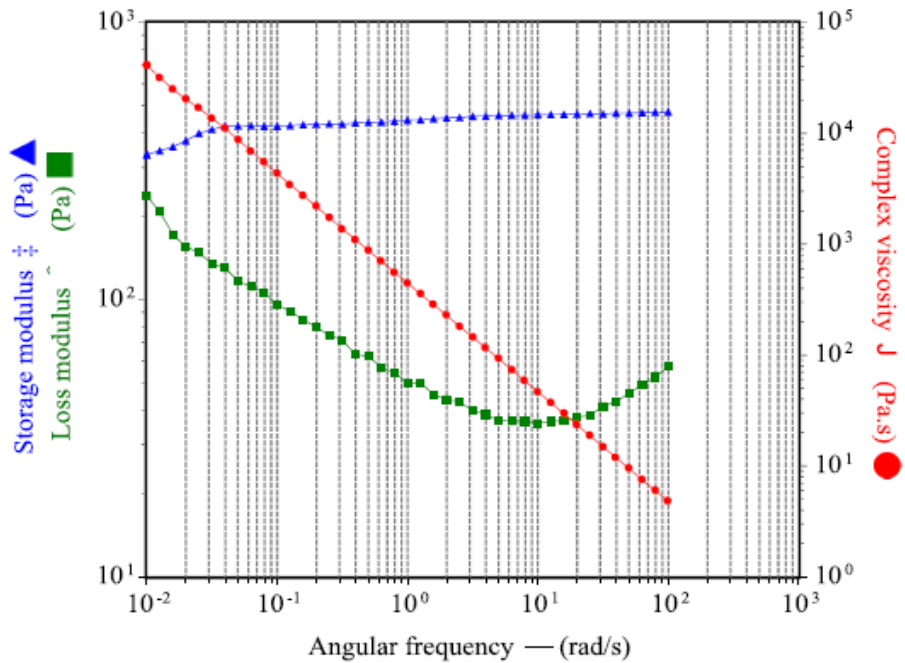


Figure 5.4 Frequency sweep of sepiolite mud (DHR II).

5.2 Effect of Unimodal CaCO₃ Particle Size Distribution on Sealing Time and Fluid Loss

The effect of unimodal CaCO₃ particle size distribution (PSD) on sealing time and amount of fluid loss was investigated on six slotted discs (Table 5.2) with different fracture diameters and lengths using PPA. In addition, the test results are classified in compliance with the diameter of the slotted discs.

Table 5.2 Slotted discs specifications.

Slot Description		
Length (inch)	Width (inch)/ Micrometer	Type
1.000	508 μm (0.02 in.)	Constant Area 4 radial arms
0.531	1016 μm (0.04 in.)	
0.381	1524 μm (0.06 in.)	
0.313	2032 μm (0.08 in.)	
0.279	2540 μm (0.1 in.)	
0.428	3048 μm (0.12 in.)	Constant Area 2 radial arms

Six unimodal CaCO₃ PSD combinations were selected and added to the sepiolite mud to represent fracture sealing by slotted discs with a fracture diameter of 508, 1016, 1524 and 2032 μm. While three unimodal combinations of LCM were designed for 2540 μm discs, one unimodal combination of LCM is used for 3048 μm discs. The percentage of overall concentration of each LCM to formulate each particular LCM blend is shown in Table 5.3. For instance, Blend#4 represents 30% of LCM ranges size of 420–500 μm, 30% of LCM ranges size of 150-355 μm and 40% of LCM ranges size of 0-150 μm. It also represents 28.5 kg / m³ (10 ppb) of CaCO₃, which is used to plug the 508 μm disc.

Table 5.3 Total concentration of each LCM to formulate unimodal blends.

Disc	Fracture Widths (μm)	Blend #	1	2	3	4	5	6	7
508		LCM Size (μm)	% of Total Concentration						
		600-841	-	30	-	-	-	-	-
		500-600	30	-	-	-	-	-	-
		420-500	-	-	30	30	50	70	30
		150-355	-	-	-	30	-	-	70
		0-150	70	70	70	40	50	30	-
		Total LCM Conc. (ppb)	10	10	10	10	10	10	10
		30 min. fluid loss (ml)	17	42	12	9	11	11	-
1016		LCM Size (μm)	% of Total Concentration						
		1000-1180	-	-	-	-	-	40	-
		841-1180	50	30	40	40	40	-	-
		500-600	-	30	-	-	-	-	-
		355-420	-	-	20	-	-	-	-
		150-355	-	-	20	30	30	-	-
		250-300	-	-	-	-	-	30	-
		75-106	-	-	-	-	-	30	-
		0-150	50	40	20	30	30	-	-
		Total LCM Conc. (ppb)	10	10	10	10	20	20	-
	30 min. fluid loss (ml)	-	-	-	45	13	19	-	
1524		LCM Size (μm)	% of Total Concentration						
		1410-1680	50	40	25	57.1	45	40	-
		500-600	25	40	25	14.3	25	20	-
		250-300	-	-	25	14.3	15	20	-
		75-106	25	20	25	14.3	15	20	-
		Total LCM Conc. (ppb)	20	20	20	21	20	20	-
	30 min. fluid loss (ml)	141	82	38	49.5	34	22	-	
2032		LCM Size (μm)	% of Total Concentration						
		2000-2380	20	20	20	30	40	30	-
		1000-1180	20	-	20	20	20	20	-
		841-1000	-	20	-	-	-	-	-
		600-841	20	-	-	-	-	-	-
		500-600	-	20	20	20	20	20	-
		250-300	20	20	20	15	10	15	-
		75-106	20	20	20	15	10	15	-
		Total LCM Conc. (ppb)	20	20	20	20	20	40	-
	30 min. fluid loss (ml)	47	36	30	27	30	25	-	
2540		LCM Size (μm)	% of Total Concentration						
		2500-2830	20	30	30	-	-	-	-
		1000-1180	20	23.3	20	-	-	-	-
		600-841	20	-	-	-	-	-	-
		500-600	-	16.7	20	-	-	-	-
		250-300	20	-	15	-	-	-	-
		106-150	-	16.7	-	-	-	-	-
		75-106	20	13.3	15	-	-	-	-
	Total LCM Conc. (ppb)	20	30	40	-	-	-	-	
	30 min. fluid loss (ml)	-	82	54	-	-	-	-	
3048		LCM Size (μm)	% of Total Concentration						
		3000-3360	30	-	-	-	-	-	-
		1000-1180	20	-	-	-	-	-	-
		500-600	20	-	-	-	-	-	-
		250-300	15	-	-	-	-	-	-
		75-106	15	-	-	-	-	-	-
	Total LCM Conc. (ppb)	40	-	-	-	-	-	-	
	30 min. fluid loss (ml)	19	-	-	-	-	-	-	

Figure 5.5 shows the fracture sealing time against the pump pressure for a 508 μm disc with a total concentration of 28.5 kg/m^3 (10 ppb) CaCO_3 particles.

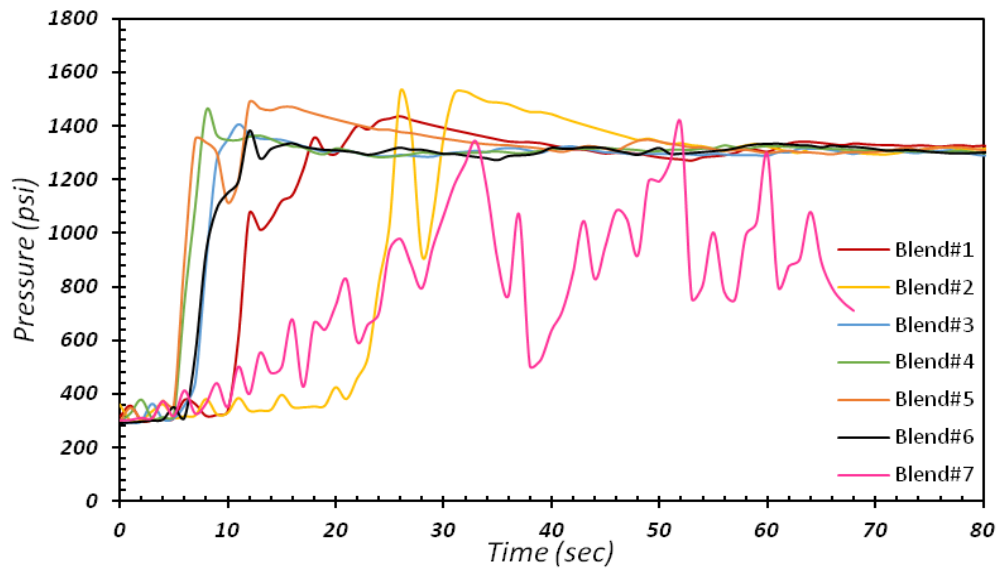


Figure 5.5 Fracture sealing time vs. pump pressure (508 μm fracture disc)-
Unimodal.

According to Table 5.3, it was concluded that more LCM usage is required and the number of LCM size changes should be increased increased due to the increased fracture width. For PPA experiments, three different LCM size are appropriate to plug the 508 μm disc. However, if unimodal LCM particle distribution with a fracture width of 2032 μm or more is used, five different LCM size variations should be used.

When the plugging time results obtained and evaluated, a combination of coarse, medium and fine particles must be present in the sepiolite mud to provide effective fracture plugging. 3 coarse particle ranges (600-841 μm , 500-600 μm , 420-500 μm) and 2 medium (150-355 μm) and fine (0-150 μm) particle ranges were chosen to plug the 508 μm disc. Plugging failed because the Blend#7 did not contain fine particles (in the range of 0-150 μm). In fact, it was observed that the plugging started 10 seconds after starting the test, but the sealing did not occur due to the absence of fine LCM particles. The ranges of coarse and fine particles in Blend#3, 5 and 6 are 420-500 μm and 0-150 μm , respectively. It also provides fluid losses with similar occlusion time (Table 5.3).

For Blend#4, in addition to the coarse and fine particles, medium (150-355 μm) LCM particles are added to optimize fracture plugging. Using coarse particles in Blend#2 to plug the thickness of 600-841 μm , which is larger than the fracture width, causes the plugging time about 4 times later than that of Blend#3, 4, 5 and 6. When the test results were examined, it was confirmed that if the coarse LCM had a size approximately equal to the fracture width, a combination of coarse, medium and fine particles could be used for effective plugging.

Figure 5.6 shows the relationship between pump pressure and plugging time for a 1016 μm disc. For Blend#1 and 2, fracture plugging failed when an amount of 10 ppb CaCO_3 of coarse and fine particles was added. However, when medium particles were added with coarse and fine particles, the plugging started even if it was late (46 sec.). This was observed in blend 3 of coarse (850-1180 μm), 2 kinds of medium (355-420 μm , 150-355 μm) and fine (0-150 μm) range. Although a total of 10 ppb CaCO_3 was used for the 1016 μm disc, plugging started after 21 seconds. However, the plugging developing time was approximately 42 seconds and the plugging was completed after 63 seconds. It was observed that when the appropriate medium particle size for Blend#4 was chosen as 150-355 μm and the amount of fine particles was increased, the plugging time decreased to about 11 seconds and then plugging developing time decreased to 17 seconds. Increasing the total concentration from 10ppb to 20 ppb for the Blend#5 caused a reduction in the plugging initiation time (9 seconds) and the plugging developing time (4 seconds) as well as more effective fracture plugging. Selecting the appropriate LCM particle range provides the most effective fracture plugging. When 1000-1180 μm coarse particle size, 250-300 μm medium particle size and 75-106 μm fine particle size are used, the plugging initiation time and plugging developing time is reduced to 5 seconds. For Blend#6, the plugging development occurred immediately after the plugging initiation and also early effective fracture plugging achieved.

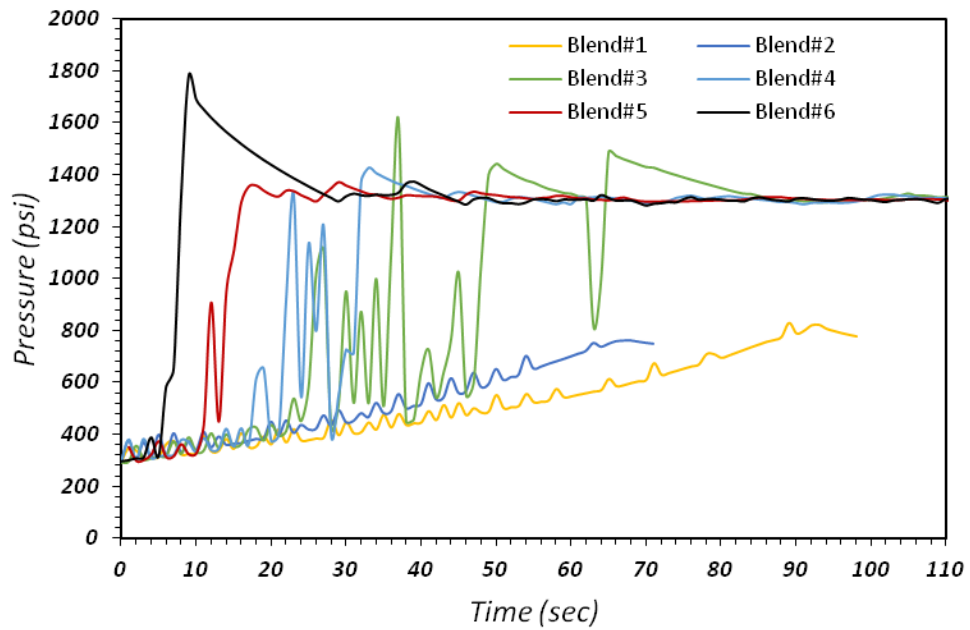


Figure 5.6 Fracture sealing time vs. pump pressure (1016 μm fracture disc)-
Unimodal.

Figure 5.7 shows the relationship between pump pressure and fracture plugging time for a 1524 μm disc. A total of 20 ppb CaCO_3 particles were added to all blends except Blend#4 (18 ppb). For Blend#1, using 10 ppb coarse (1410-1680 μm), 5 ppb medium (500-600 μm) and 5 ppb fine (75-106 μm) particle size will result in delayed fracture plugging (33 sec) and large amounts of fluid loss (141ml). While the amount of medium particles was increased from 5 ppb to 8 ppb in Blend#2, the reduction of coarse and fine particles caused better plugging initiation and developing time. For Blend#3, adding the different medium particle size (250-300) to maintain the total concentration stable significantly reduced the all measured parameters. In order to minimize the measured parameters, different coarse, medium and fine LCM particles with constant total concentration were evaluated using 4, 5, and 6 blends. In spite of the early plugging time (7 secs) in Blend#5, it was observed that Blend#6 was more successful in plugging developing time (14 secs) and fluid losses (22 ml).

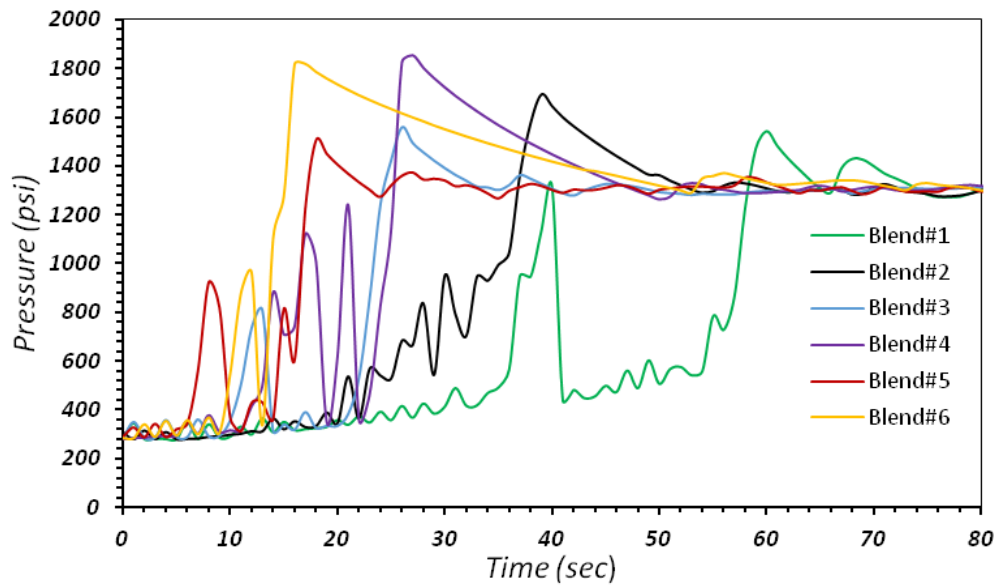


Figure 5.7 Fracture sealing time vs. pump pressure (1524 μm fracture disc)-
Unimodal.

In Figure 5.8, plugging initiation, developing and plugging completed regions in terms of pump pressure are specified for 2032 μm disc. A total of 20 ppb LCM particles were added from Blend#1 to Blend#4. Three different combinations of coarse, medium and fine particles of constant concentration (4 ppb) were chosen from Blend#1, 2 and 3 to investigate effective fracture plugging. For Blend#3, the selection of particles (2000-2380 μm , 1000-1180 μm) much larger than medium (500-600 μm , 250-300 μm) and fine (75-106 μm) particles causes more effective fracture plugging in comparison to Blend#1 and Blend#2. By increasing the amount of coarse and medium particles without changing the total LCM concentration, earlier plugging initiation time (16 and 15 seconds) and rapid plugging developing time (20 and 17 seconds) was achieved in Blend#4 and Blend#5, respectively. When the overall concentration of LCM in Blend#6 was doubled by 20 ppb to 40 ppb, the plugging initiation time, plugging developing time and fluid losses decreased by 70 %, 30%, and 16% respectively.

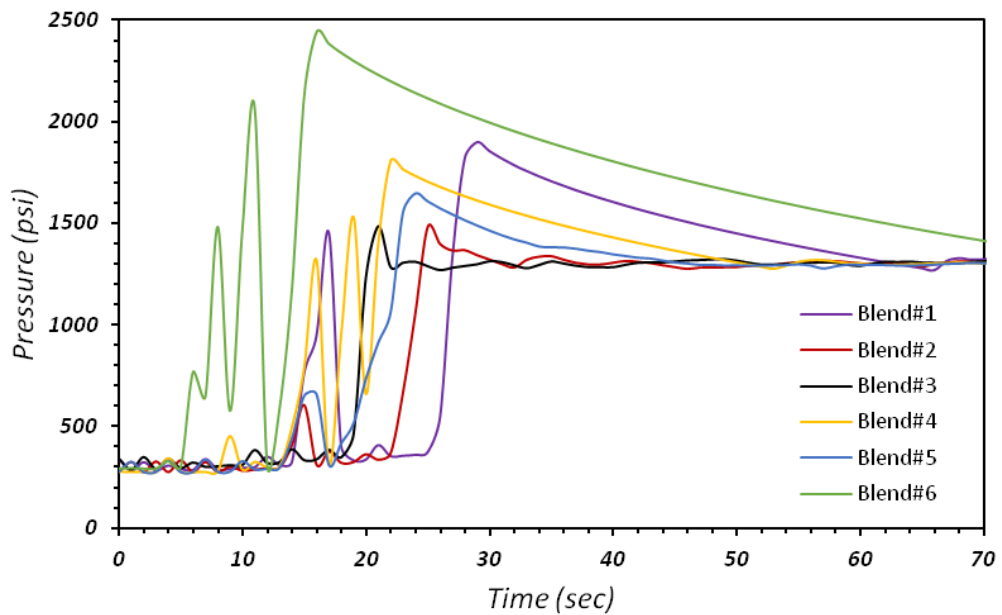


Figure 5.8 Fracture sealing time vs. pump pressure (2032 μm fracture disc)-
Unimodal.

Figure 5.9 demonstrates the plugging initiation time and plugging performance of three LCM blends for the 2540 μm disc and one LCM blend for the 3048 μm disc. Although the plugging started in around 1 min for Blend#1, the medium and fine particle sizes failed in the plugging developing time. Additionally, it has been shown that a very high level of fluid loss is also a problem with plugging fractures. Increasing the total LCM concentration in Blend#2 and Blend#3 from 20 ppb to 30 ppb and 40 ppb was a crucial factor in decreasing plugging and plugging developing time. Adjustment of the LCM concentration to a large amount of coarse, less amount of medium and fine particles increased the effect of increasing total LCM concentration on fracture plugging performance. While the plugging time of Blend#2 and Blend#3 (10 sec) was approximately the same, the plugging occurred earlier in Blend#3 than Blend#2. Consequently, the positive impact of the change in the overall concentration of LCM was detected.

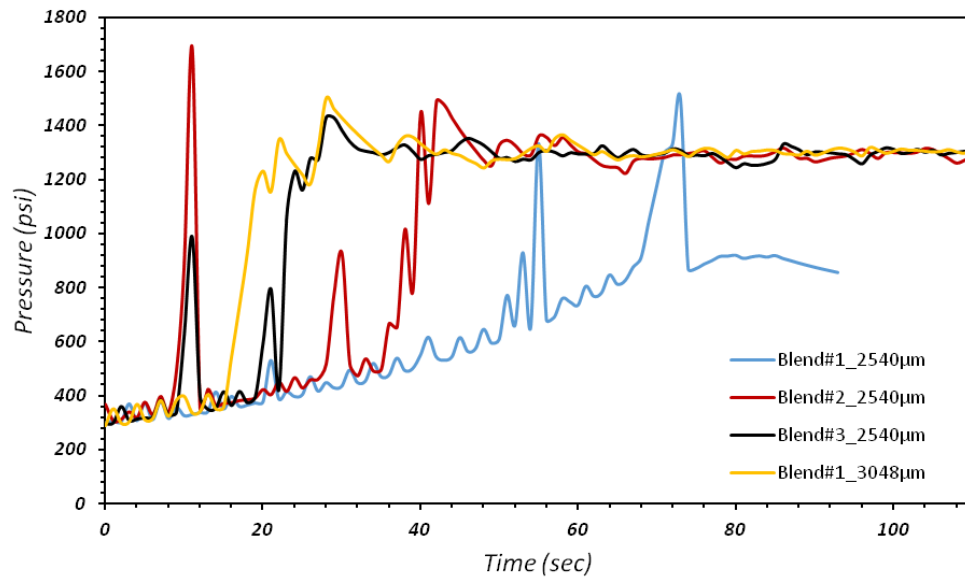


Figure 5.9 Fracture sealing time vs. pump pressure (2540, 3048 μm fracture discs)-Unimodal.

In the Appendix–C, there are individual and comparative graphs of blends obtained with unimodal particle size distribution for all discs.

5.3 Effect of Bimodal and Trimodal CaCO_3 Particle Size Distribution on Sealing Time and Fluid Loss

The efficiency of fracture plugging of bimodal and trimodal particle size distribution of CaCO_3 pills was studied to achieve more reliable and earlier plugging and plugging development time and also less amount of fluid loss. In Figure 5.10, the plugging effect of bimodal CaCO_3 particle size distribution on five slotted discs with large fracture widths is shown. Fracture plugging was started 4, 5, 8, 9 and 11 sec after the initiation of the tests for 1016, 1524, 2032, 2540 and 3048 μm fracture diameter discs, respectively. The fracture plugging time and fluid loss increases as the fracture size increases. It is found that the plug development period in 3048 μm disc was significantly reduced to at most 3 sec.

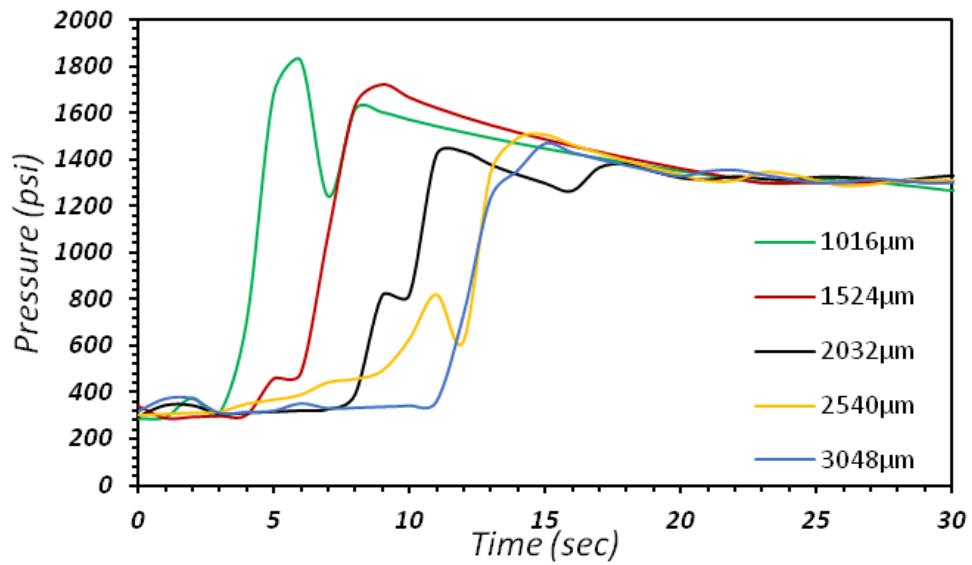


Figure 5.10 Effect of bimodal CaCO_3 particle sizes distribution on plugging evaluation parameters.

In Figure 5.11, the effect of trimodal CaCO_3 particle size distribution on fracture plugging performance is demonstrated using four discs with larger fracture widths. In 1524 and 2032 μm discs, minor differences in the plugging initiation and plugging developing time were found when the influence of the bimodal particle size distribution was examined. However, the obvious influence of the distribution of trimodal particle size was found only in 2540 and 3048 μm discs.

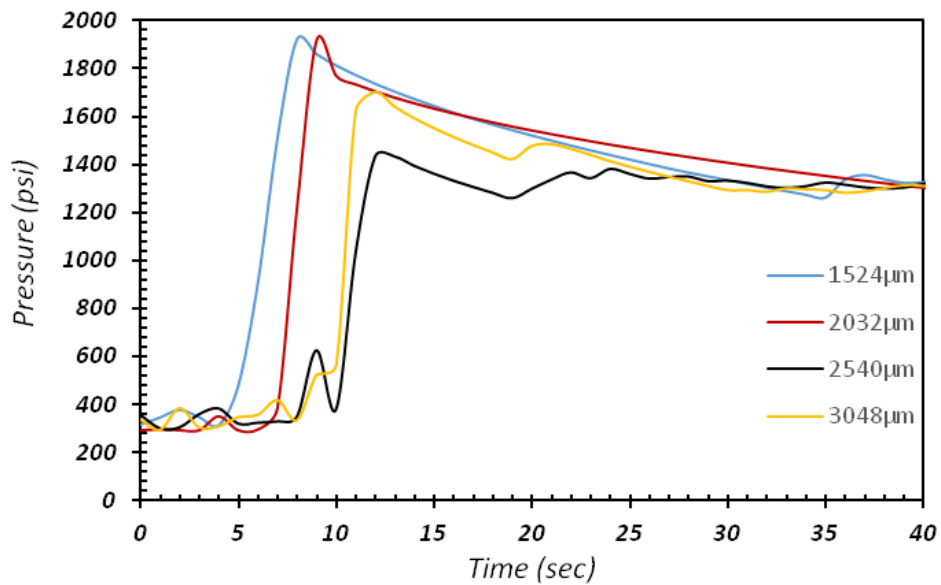


Figure 5.11 Effect of trimodal particle size distribution of CaCO_3 on fracture plugging performance.

In Figure 5.12, the effects of unimodal, bimodal and trimodal CaCO_3 particle size distribution on the measured parameters were compared. The benefit of bimodal and trimodal CaCO_3 particle size distribution is important, particularly in terms of plugging developing time in comparison with unimodal particle size distribution. Furthermore, the importance of trimodal particle size distribution was only noticed on 3048 μm discs. In comparison with the unimodal particle size distribution, the plugging developing time in the bimodal particle size distribution of 1524, 2032, 2540, 3048 μm discs decreased by 66%, 42%, 59%, and 31%, respectively. Increasing the modality of the LCM particle size distribution has proven to be an effective parameter in wide fracture plugging.

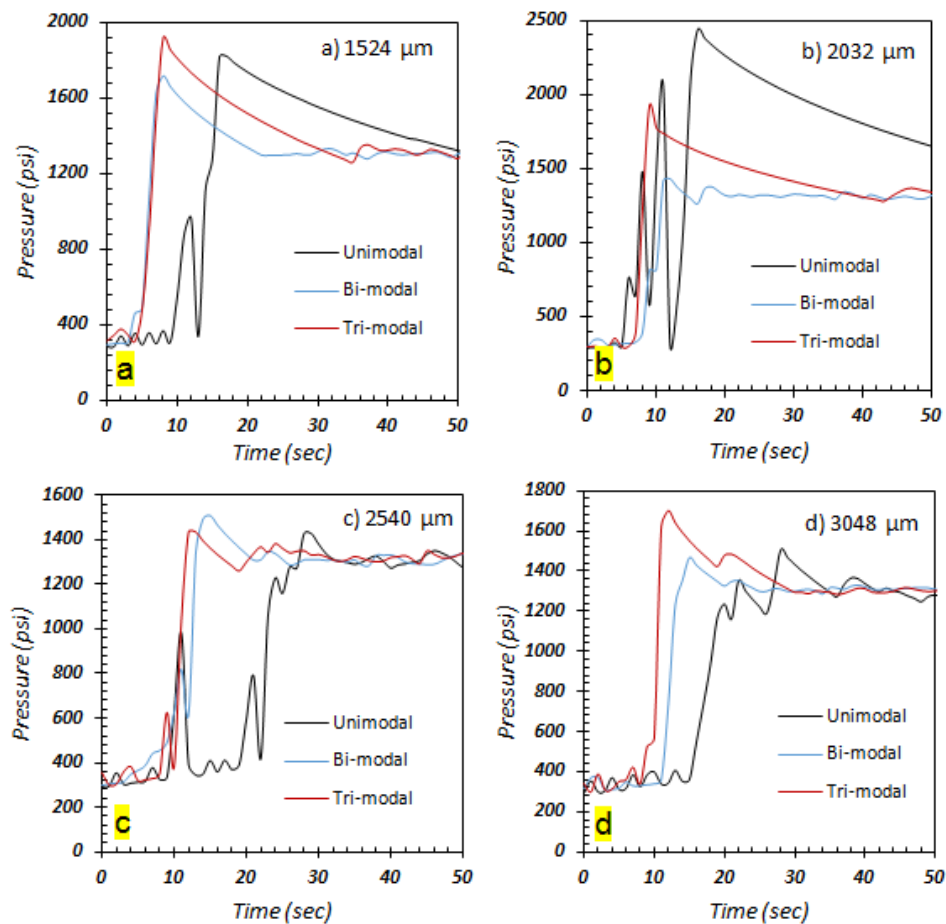


Figure 5.12 Effect of unimodal, bimodal and trimodal particle size distribution of CaCO_3 a)1524 μm , b)2032 μm , c)2540 μm d)3048 μm fractured discs.

In Appendix-D and Appendix-E, there are individual and comparative graphs of blends obtained with bimodal and trimodal particle size distribution for all discs.

5.4 Optical Microscope Analysis

5.4.1 Optical Microscope Analysis for All Discs

The fracture plugging effect was analyzed with the optical microscope using different LCM combinations for all discs.

0.12 inch (3048 μm) disc

Table 5.4 LCM size and concentration values for 3048 disc (Blend#1).

Disc Fracture Size(μm)	Blend # LCM Size(μm)	1 Total Concentration (%)
3048	3000-3360	30
	1000-1180	20
	500-600	20
	250-300	15
	75-106	15
	Total LCM	40
	30 min fluid	19

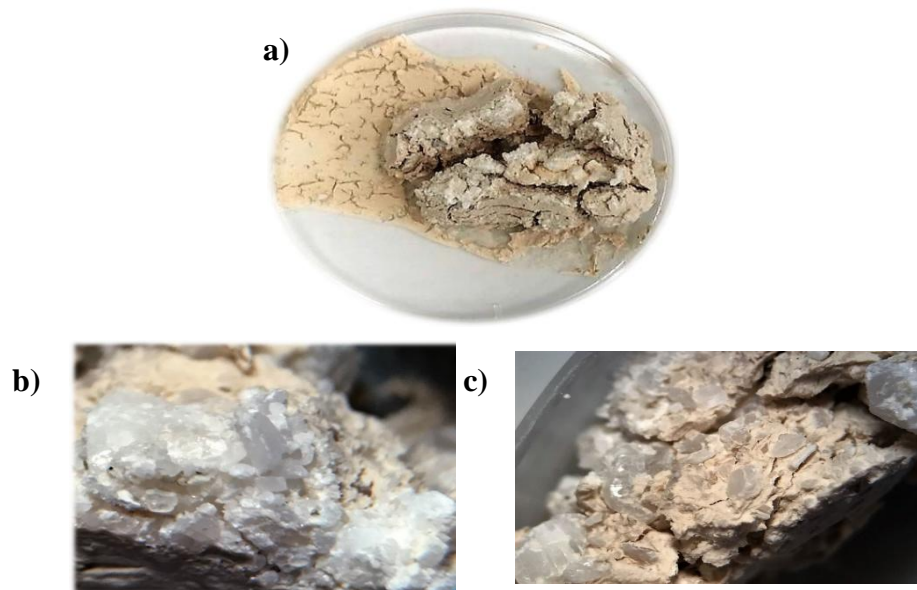


Figure 5.13 Optical Microscope Analysis for 3048 μm disc (Blend#1): a) general view, b) top view and c) side view of formed mud cake.

0.1 inch (2540 μm) disc

Table 5.5 LCM size and concentration values for 2540 disc (Blend#3).

Disc	Blend #	3
Fracture Size(μm)	LCM Size(μm)	Total Concentration (%)
2540	2500-2830	30
	1000-1180	20
	600-841	-
	500-600	20
	250-300	15
	106-150	-
	75-106	15
	Total LCM	40
30 min fluid	54	

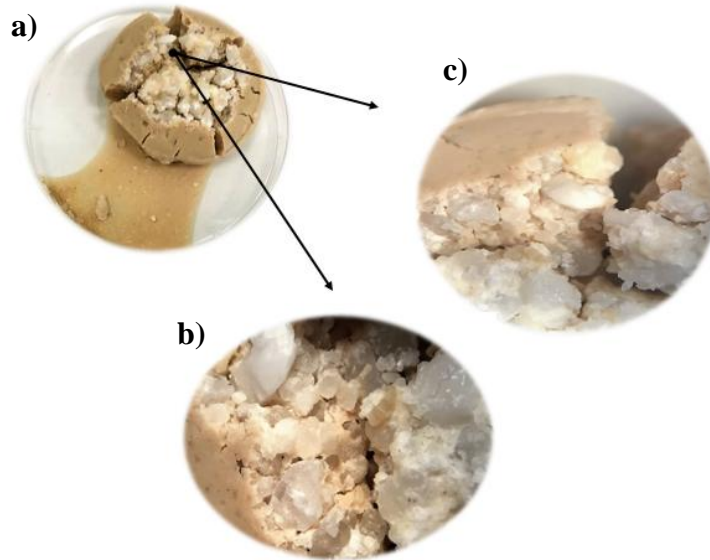


Figure 5.14 Optical Microscope Analysis for 2540μm disc (Blend#3): a) general view, b) top view and c) side view of formed mud cake.

0.08 inch (2032 μm) disc

Table 5.6 LCM size and concentration values for 2032 disc (Blend#4).

Disc	Blend #	4
Fracture Size(μm)	LCM Size(μm)	Total Concentration (%)
2032	2000-2380	30
	1000-1180	20
	841-1000	-
	600-841	-
	500-600	20
	250-300	15
	75-106	15
	Total LCM 30 min fluid	20 27

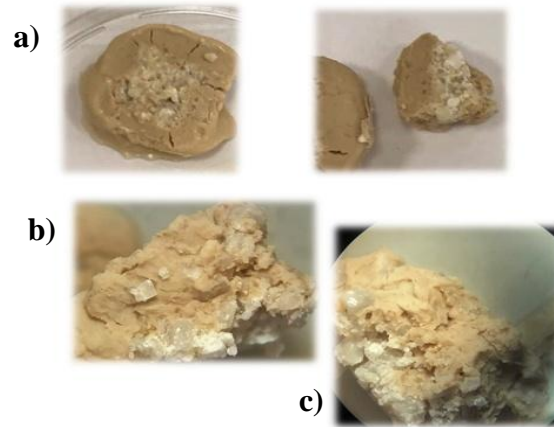


Figure 5.15 Optical Microscope Analysis for 2032 μm disc (Blend#4): a) general view, b) top view and c) side view of formed mud cake.

0.06 inch (1524 μm) disc

Table 5.7 LCM size and concentration values for 1524 disc (Blend#5).

Disc	Blend #	5
Fracture Size(μm)	LCM Size(μm)	Total Concentration (%)
1524	1410-1680	45
	500-600	25
	250-300	15
	75-106	15
	Total LCM 30 min fluid	20 24

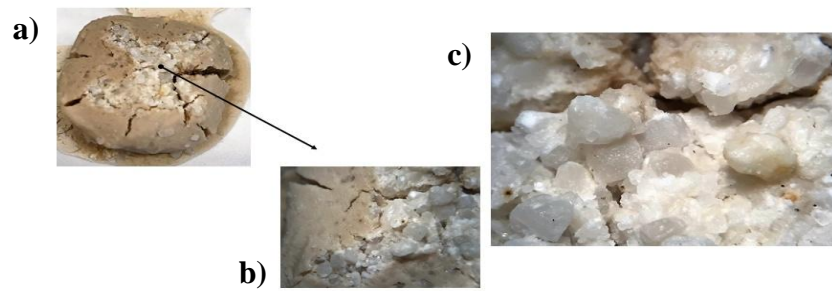


Figure 5.16 Optical Microscope Analysis for 1524 μm disc (Blend#5): a) general view and b-c) top view of formed mud cake.

0.04 inch (1016 μm) disc

Table 5.8 LCM size and concentration values for 1016 disc (Blend#6).

Disc	Blend #	6
Fracture Size(μm)	LCM Size(μm)	Total Concentration (%)
1016	1000-1180	40
	841-1000	-
	500-600	-
	355-420	-
	150-355	-
	250-300	30
	75-106	30
	0-150	-
	Total LCM 30 min fluid	20 19

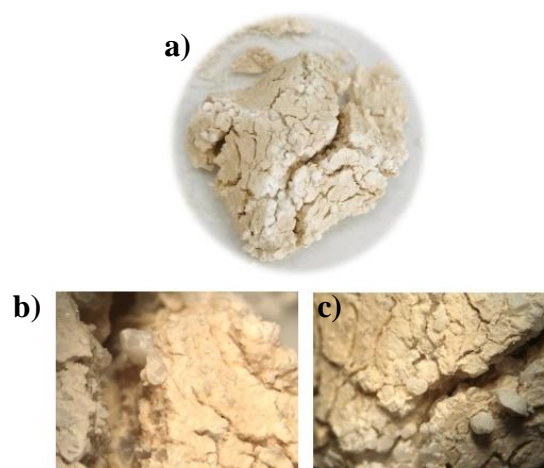


Figure 5.17 Optical Microscope Analysis for 1016 μm disc (Blend#6): a) general view and b-c) top view of formed mud cake.

5.4.2 Optical Microscope Analysis of the Effect of Unimodal, Bimodal, Trimodal Particle Size Distribution

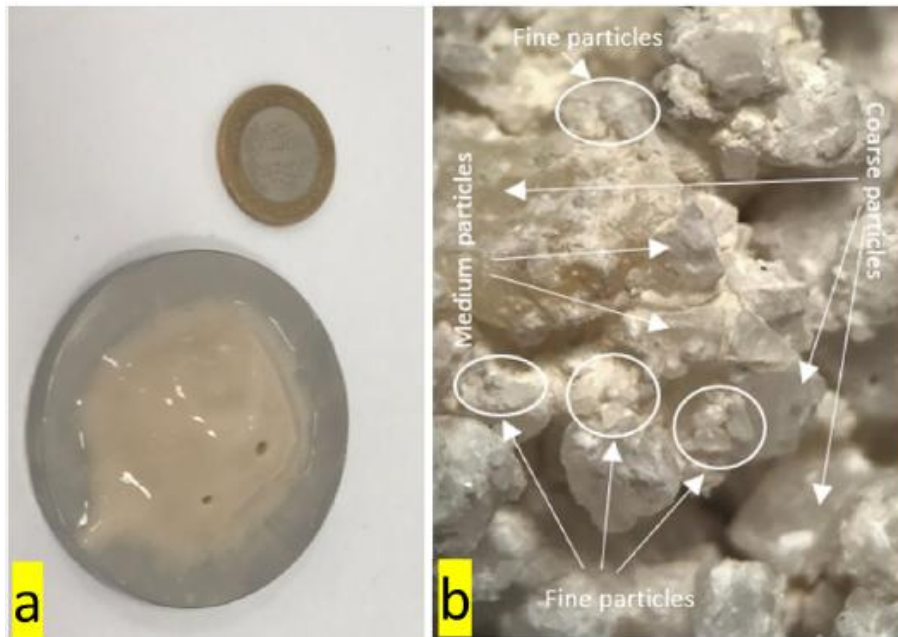


Figure 5.18 Formed seal of bimodal PSD in 2540 μm fracture: a) formed seal under fractured disc b) Optical microscopic image of formed seal.

In Figure 5.18, the plugging resulting from bimodal particle size distribution for 2540 μm disc is shown. After the high-pressure test, the mud cake was removed from the disc and left to dry for microscope analysis. Fine, medium and coarse particles are shown within a mud cake as microscope images. In Figure 5.19, the microscopic images of the mud cake formed on the 3048 μm disc are shown to compare the plugging efficiency of the unimodal, bimodal and trimodal CaCO_3 particle size distribution. The absence of medium particles in the unimodal particle size distribution caused some gaps between the particles and increased plugging time. In general, it has been observed that fine particles provide to close gaps between coarse particles. Moreover, optical microscope images showed that bimodal and trimodal distributions are more effective than unimodal distribution in wide fracture plugging. In Figure 5.19-c, trimodal particle size distribution for 3048 μm has been shown to provide effective plugging performance.

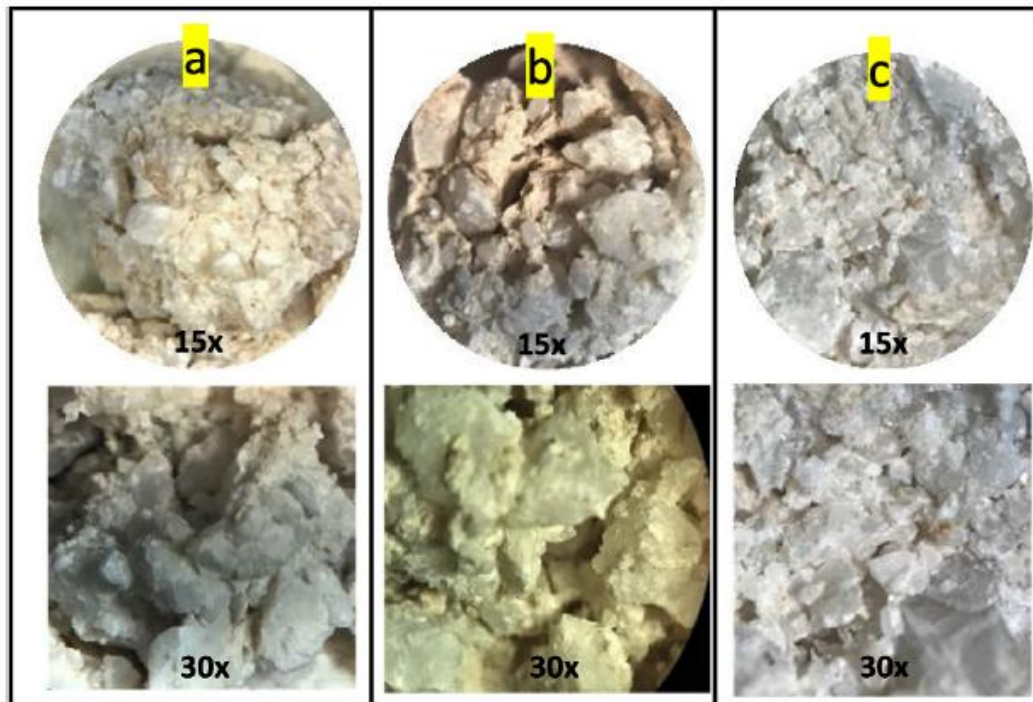


Figure 5.19 Sealing efficiency of a) unimodal, b) bimodal, and c) trimodal CaCO_3 particle sizes distribution through 3048 μm fracture disc.

5.5 Plugging Effect of LCM Geometries

5.5.1 Particle Size Distribution Analysis of LCMs-Circularity

For the size analysis of LCM particles, optical microscope images were randomly selected from each LCM size. Four images were randomly selected for each LCM size from the optical microscope images obtained and circularity values were calculated using the Image-J program. The results evaluation was conducted taking into account the average circularity values. As a result, the circularity properties of the particles decrease as the LCM particle size increases (Figure 5.20).

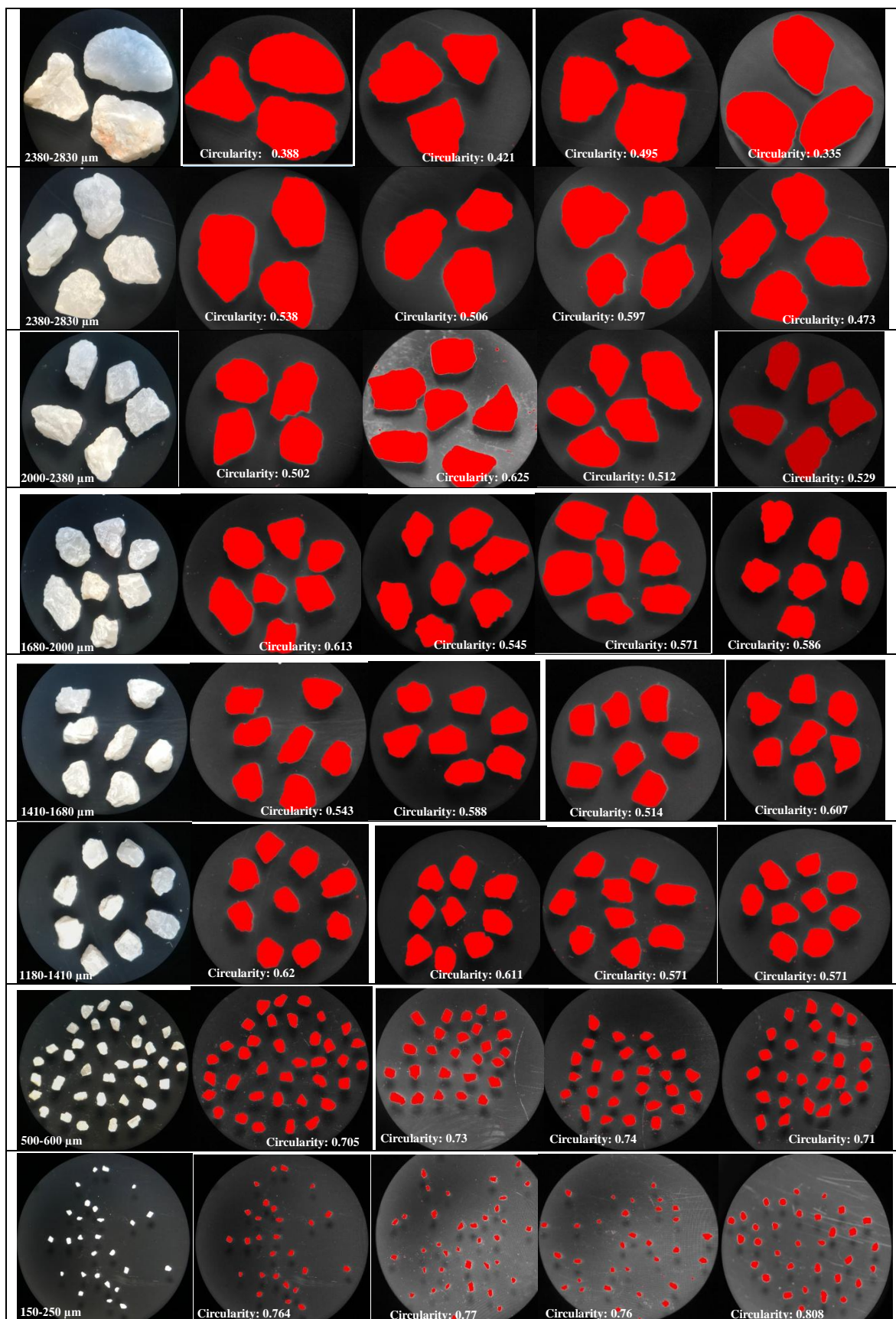


Figure 5.20 Particle Size Distribution Analysis of LCMs-Circularity using Image-J.

5.5.2 Effect of LCM Geometries (Shape)

Two different geometries of the same trimodal of LCM particles (2830-3000 μm) were chosen to investigate the plugging effect of LCM geometries on the fracture diameter of 3048 μm . Optical microscope images of these particles are shown in Figure 5.21. Optical microscopy images were analyzed using the Sphericity and Roundness Chart made by Powers (1953) (Figure 5.22). LCM particles can be classified as sub-angular with high or low sphericity (Figure 5.21). The plugging experiments were repeated 3 times on a 3048 μm disc using non-homogeneous, low spherical, and coarse LCM particles (Figure 5.21-b) under the same conditions. However, the same test was carried out using homogeneous, high spherical, and coarse LCM particles (Figure 5.21-a). The results of the measured parameters are shown in Figure 5.23. The early plugging occurred for all blends. However, the difference in plugging developing time is more noticeable when using homogeneous, high sphericity, and coarse LCM particles. The plugging developing time decreased by 81% (from 21 seconds to 4 seconds) and 66% (from 12 to 4 seconds) in the first and second trials, respectively. It has been observed that homogeneous LCM particles with higher circularity plug fracture better. The plugging effects of the homogeneous and high spherical, nonhomogeneous and low spherical and also trimodal blend containing coarse LCM particles are shown in Figure 5.24 with microscope images. Considering the microscope images, it was observed that there was more space between the particles when using nonhomogeneous, low spherical, and coarse LCM particles. Thus, the plugging efficiency of homogeneous and high spherical LCM particles has been demonstrated (Figure 5.24-b2).



Figure 5.21 Optical microscopy images of coarse CaCO_3 particles a) well sorted, high spherical b) poor sorted, low spherical.

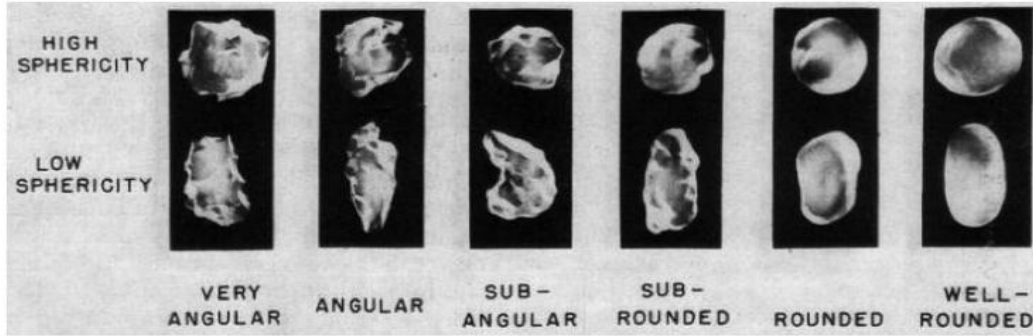


Figure 5.22 Sphericity and Roundness Chart [111].

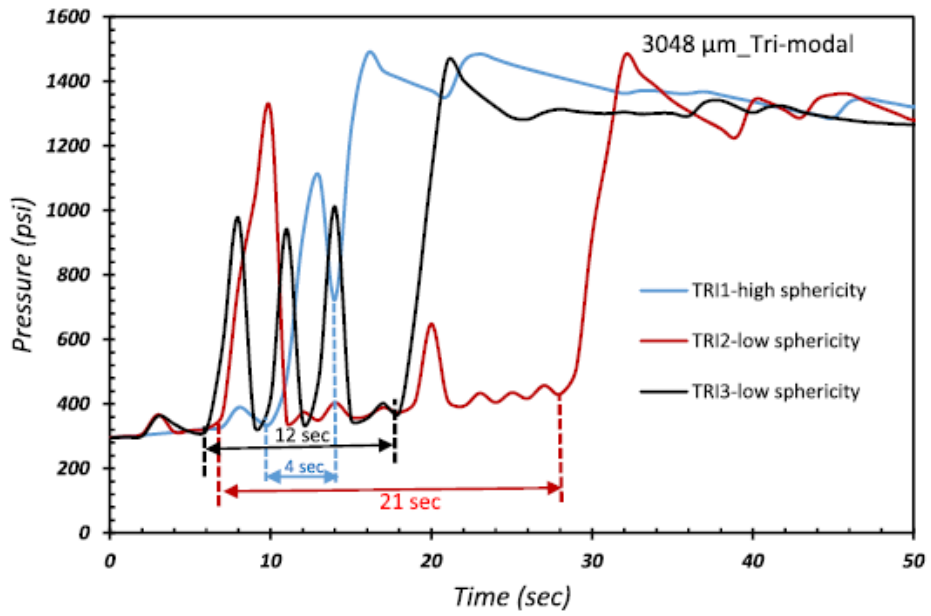


Figure 5.23 Effect of LCM Geometries on fracture sealing integrity.

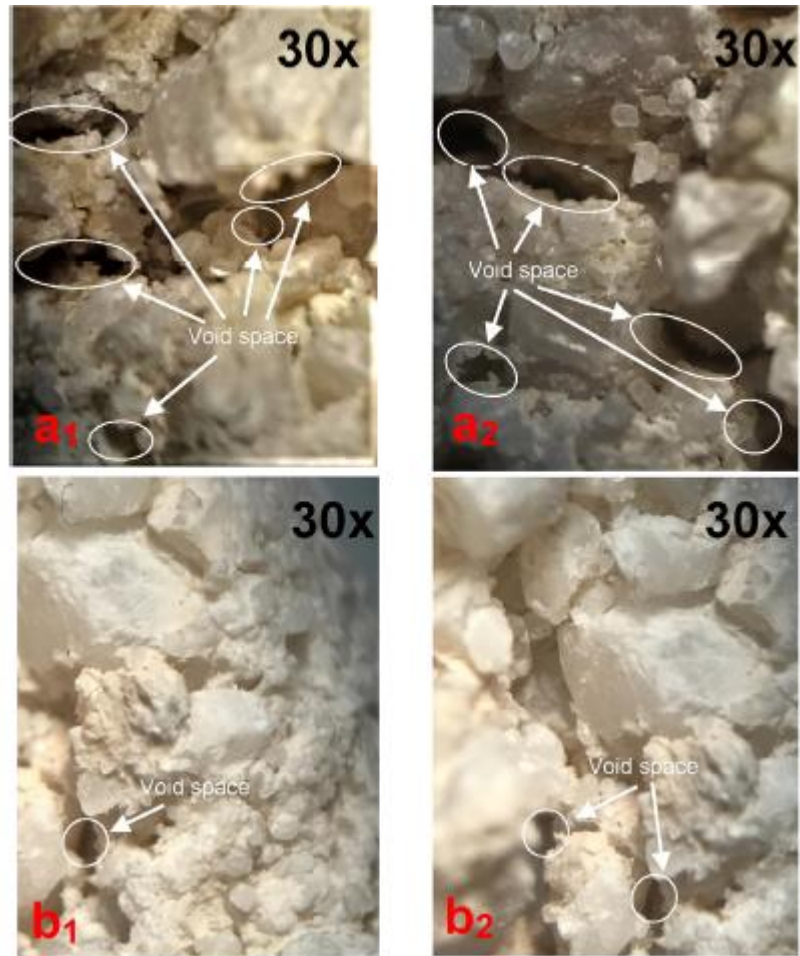


Figure 5.24 Optical microscopy images of trimodal blends seal containing a1, a2) non-homogeneous low spherical b1, b2) homogeneous high spherical coarse CaCO_3 particles.

5.5.3 LCM Particles Concentration and Its Effect on Plugging

The amount of particles effective in fracture plugging was investigated on the basis of wet sieve analysis results after the dry slurry was diluted to separate LCM from sepiolite clay. Figure 5.25 shows classified results for 2032, 2540, and 3048 μm discs. The weight percentage of the largest and remaining particles that function in fracture plugging is indicated. Also, the concentration of the largest LCM particles was observed to be much higher in all particle distributions than the rest of the other LCM particles. Therefore, the higher concentration of coarser particles has been effective in improving the plugging properties.

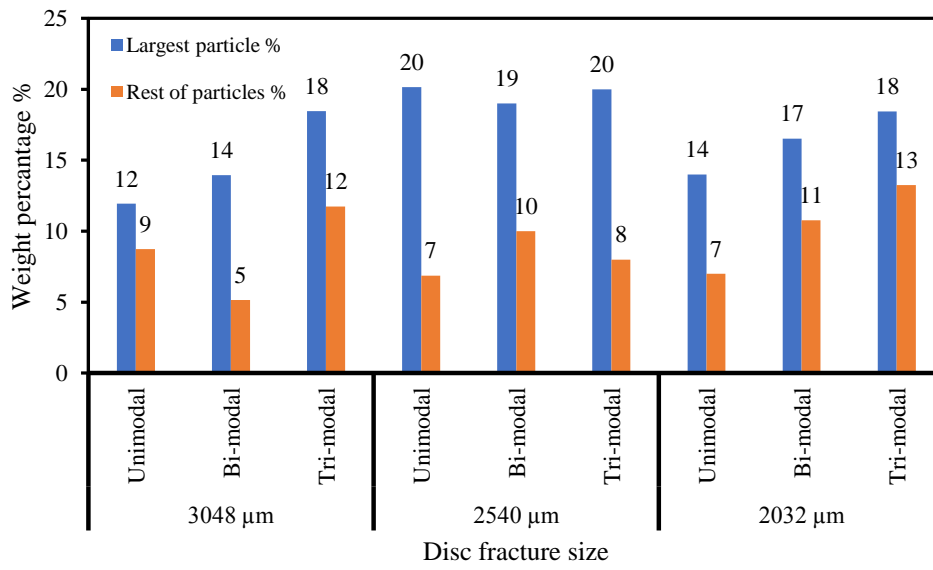


Figure 5.25 Concentration of CaCO₃ particles in formed seal.

CONCLUSIONS

This study investigated the factors affecting the efficiency of the plugging mechanism and wide fracture plugging. The results of the experiments have revealed that yield point (YP), gel strength (GS), thixotropic and rheological features of drilling mud are significant in terms of carrying LCMs. Besides, gel structure and suspension ability of sepiolite mud have been investigated by conducting steady shear flow, oscillatory dynamic shear, and thixotropic loop tests using Discovery Hybrid Rheometer (DHR-II). The experiment results indicated that a high degree of thixotropy, moderate shear thinning index, appropriate yield point, and gel strength were ensured by sepiolite mud systems.

This experimental study conducted to observe some limitations in the Pore Plugging Apparatus (PPA) which is used to characterize fracture plugging mechanisms. The modified PPA allowed larger LCM sizes to be tested and the designation of the early plugging time (plugging initiation time and development time) which is the major scope of this study. This study brings novelty to the literature by defining and measuring early plugging time in terms of plugging initiation and plugging development time. Additionally, this study has revealed that early plugging time is a critical parameter while fracture plugging analysis for the first time.

Particle Size Distribution (PSD), particle shape, and LCM concentration are major factors affecting wide fracture plugging. The modality of LCM should be increased to achieve early plugging time especially the fractures which are wider than 1 mm. Moreover, it was observed that unimodal PSD is not effective enough to plug the fractures which are wider than 500 μm . Particularly in fractures wider than 2540 μm , bimodal and trimodal PSD caused to decrease in the plugging development time compared to unimodal PSD. Well-sorted, high spherical and coarse CaCO_3 particles lead to earlier plugging time when compared to poor sorted and low spherical CaCO_3 . Also, the higher concentration of coarse particles with higher sphericity has been found more effective in plugging capabilities. Optical microscope analysis showed that bimodal and trimodal distributions are more effective than unimodal distribution in wide fracture plugging. Moreover, it has been proved that as the

fracture size increases, the amount of LCM used increases to enhance plugging efficiency. In order to ensure effective fracture plugging, coarse CaCO_3 particles should be approximately the same size as the fracture size.

Every experiment has shown that plug initiation occurred. However, it has been revealed that plugging development time is more important to ensure effective fracture plugging. The LCM concentration and particle size distribution can be optimized subject to fracture size for the purpose of minimizing plugging developing time.

RECOMMENDATIONS

In this experimental study, the valuable results were obtained using the Pore Plugging Apparatus (PPA), but there are some experimental limitations regarding the PPA. The most important of these experimental limitations is that the experiments are carried out under static conditions. In order to perform experiments in dynamic conditions, the apparatus can be developed by installing a circulation system that circulates the drilling fluids between the fractures. Additionally, different sizes of CaCO_3 were used only as lost circulation material (LCM). More research is encouraged to find more effective and early plugging conditions using new LCMs.

REFERENCES

1. Alkinani HH, Al-Hameedi AT, Flori RE, Dunn-Norman S, Hilgedick SA, Alsaba MT. Updated classification of lost circulation treatments and materials with an integrated analysis and their applications. In Society of Petroleum Engineers; 2018.
2. Howard GC, Scott Jr P. An analysis and the control of lost circulation. *J Pet Technol.* 1951;3(06):171–82.
3. Gala DM, York P, Pritchard DM, Rosenberg SM, Dodson JK, Utama B. Drilling Hazard Mitigation Technologies Key in Eliminating Non-Productive Time in Challenging Wells. In Society of Petroleum Engineers; 2010.
4. Redden J. Australia outback could Be next world-class unconventional play. *J Pet Technol.* 2009;61(12):28–30.
5. Andreasen A, Andersen J. About the relationship between density and particle spacing in products made of loose particles. *Kolloid.* 1930;50:217–8.
6. Abrams A. Mud design to minimize rock impairment due to particle invasion. *J Pet Technol.* 1977;29(05):586–92.
7. Cargnel R, Luzardo J. Particle size distribution selection of CaCO₃ in drill-in fluids: Theory and applications. In Society of Petroleum Engineers; 1999.
8. Vickers S, Cowie M, Jones T, Twynam AJ. A new methodology that surpasses current bridging theories to efficiently seal a varied pore throat distribution as found in natural reservoir formations. *Wiert Nafta Gaz.* 2006;23(1):501–15.
9. Newhouse C. Successfully drilling severely depleted sands. In Society of Petroleum Engineers; 1991.
10. Davis N, Mihalik P, Lundie P, Growcock F, Calloni G, Davidson E. New permeability plugging apparatus procedure addresses safety and technology issues. In Society of Petroleum Engineers; 1999.
11. Pilehvari AA, Nyshadham VR. Effect of material type and size distribution on performance of loss/seepage control material. In Society of Petroleum Engineers; 2002.
12. Dick M, Heinz T, Svoboda C, Aston M. Optimizing the selection of bridging particles for reservoir drilling fluids. In Society of Petroleum Engineers; 2000.
13. Gatlin C, Nemir CE. Some effects of size distribution on particle bridging in lost circulation and filtration tests. *J Pet Technol.* 1961;13(06):575–8.
14. Whitfill DL, Hemphill T. All lost-circulation materials and systems are not created equal. In Society of Petroleum Engineers; 2003.

15. Boukadi F, Yaghi B, Al-Hadrami H, Bemani A, Babadagli T, De Mestre P. A comparative study of lost circulation materials. *Energy Sources*. 2004;26(11):1043–51.
16. Collins N, Whitfill D, Kharitonov A, Miller M. Comprehensive approach to severe loss circulation problems in Russia. In *Society of Petroleum Engineers*; 2010.
17. Moazzeni A, Nabaei M, Kharrat R. A breakthrough in controlling lost circulation in a pay zone by optimizing the particle size distribution of shellfish and limestone chips. *Pet Sci Technol*. 2012;30(3):290–306.
18. Nayberg T. Laboratory study of lost circulation materials for use in both oil-based and water-based drilling muds. *SPE Drill Eng*. 1987;2(03):229–36.
19. Suyan K, Banerjee S, Dasgupta D. A practical approach for preventing lost circulation while drilling. In *Society of Petroleum Engineers*; 2007.
20. Hettama M, Horsrud P, Taugbol K, Friedheim J, Huynh H, Sanders M, et al. Development of an innovative high-pressure testing device for the evaluation of drilling fluid systems and drilling fluid additives within fractured permeable zones. In *Offshore Mediterranean Conference*; 2007.
21. Kumar A, Savari S. Lost circulation control and borehole strengthening: looking beyond particle size distribution. In 2011. p. 12–4.
22. Mostafavi Toroqi SV. *Experimental Analysis and Mechanistic Modeling of Borehole Strengthening*. 2012;
23. Alsaba M, Nygaard R, Hareland G, Contreras O. Review of lost circulation materials and treatments with an updated classification. In 2014. p. 1–9.
24. Alsaba M, Nygaard R, Saasen A, Nes O-M. Experimental investigation of fracture width limitations of granular lost circulation treatments. *J Pet Explor Prod Technol*. 2016;6(4):593–603.
25. Cecilia J, Vilarrasa-García E, Cavalcante Jr C, Azevedo D, Franco F, Rodríguez-Castellón E. Evaluation of two fibrous clay minerals (sepiolite and palygorskite) for CO₂ Capture. *J Environ Chem Eng*. 2018;6(4):4573–87.
26. Dong J, Zhang J. Biomimetic super anti-wetting coatings from natural materials: superamphiphobic coatings based on nanoclays. *Sci Rep*. 2018;8(1):1–12.
27. Murray HH. *Applied clay mineralogy: occurrences, processing and applications of kaolins, bentonites, palygorskitesepiolite, and common clays*. Elsevier; 2006.
28. Carney LL, Meyer RL. A new approach to high temperature drilling fields. In *Society of Petroleum Engineers*; 1976.

29. Carney LL, Guven N. Investigation of changes in the structure of clays during hydrothermal study of drilling fluids. *Soc Pet Eng J.* 1980;20(05):385–90.
30. Carney LL, Guven N. Investigation of high-temperature fluid loss control agents in geothermal drilling fluids. In *Society of Petroleum Engineers*; 1982.
31. Moussa M, Al-Marhoun M. Dynamic measurement of drilling fluid rheology at elevated temperature and pressure. In *Society of Petroleum Engineers*; 1985.
32. Guven N, Panfil D, Carney L. Comparative rheology of water-based drilling fluids with various clays. In *Society of Petroleum Engineers*; 1988.
33. Zilch H, Otto M, Pye D. The evolution of geothermal drilling fluid in the imperial valley. In *Society of Petroleum Engineers*; 1991.
34. Serpen U, Hacıislamoglu M, Tuna O. Use of sepiolite resources of Turkey in geothermal muds. In 1992. p. 17–21.
35. Serpen U. Use of sepiolite clay and other minerals for developing geothermal drilling fluids. *Appl Mech Eng.* 1999;4(spec.):309–13.
36. Serpen U. Investigation on geothermal drilling muds with high temperature stability. In 2000.
37. Serpen U, Hacıislamoglu M, Tuna O. Use of sepiolite resources of Turkey in geothermal muds. In 1992. p. 17–21.
38. Altun G, Serpen U. Investigating improved rheological and fluid loss performance of sepiolite muds under elevated temperatures. In 2005.
39. Altun G, Osgouei AE, Serpen U. Controlling rheological and fluid loss properties of sepiolite muds under elevated temperatures. In 2010. p. 25–9.
40. Ozyurtkan MH, Altun G, Ettehadı Osgouei A, Aydilsiz E. Dynamic filtration properties of clay based drilling muds under elevated temperatures. In *Society of Petroleum Engineers*; 2012.
41. Altun G, Osgouei AE, Ozyurtkan MH. Customization of sepiolite drilling fluids at high temperatures. In *American Rock Mechanics Association*; 2014.
42. Altun G, Osgouei AE, Ozyurtkan MH, Serpen U. Sepiolite muds as an alternate drilling fluid for hot environments. In 2015.
43. Ettehadı A, Altun G. In-situ thermal rheological properties of drilling muds. In *Society of Petroleum Engineers*; 2018.
44. Dodson J. Survey of Problem Incidents—GOM Shelf Gas Wells”. *Dodson Co.* 2004;

45. Finger J, Blankenship D. Handbook of best practices for geothermal drilling. Sandia Natl Lab Albuquerque. 2010;
46. Growcock F. How to stabilize and strengthen the borehole during drilling operations. SPE Disting Lect Program. 2010;
47. Samuel M, Marcinew R, Al-Harbi M, Samuel E, Xiao Z, Ezzat A, et al. A new solids-free non-damaging high temperature lost-circulation pill: development and first field applications. In Society of Petroleum Engineers; 2003.
48. Al Menhali S, Kashwani G, Sajwani A. Safety Engineering Controls of Lost Circulation during Cementing in Onshore Oil Construction Projects. This Paper Published Online HttpJournal Sapub Orhijme. 2015;
49. Lummus JL, Randall BV. Lost circulation material. 1968 Apr 2;
50. White RJ. Lost-circulation materials and their evaluation. In American Petroleum Institute; 1956.
51. Chilingarian GV, Vorabutr P. Drilling and drilling fluids. 1983;
52. Canson B. Lost circulation treatments for naturally fractured, vugular, or cavernous formations. In Society of Petroleum Engineers; 1985.
53. Messenger J, McNiel Jr J. Lost circulation corrective: time-setting clay cement. J Pet Technol. 1952;4(03):59–64.
54. Messenger JU. Lost circulation. 1981;
55. Morita N, Black A, Guh G. Theory of lost circulation pressure. In Society of Petroleum Engineers; 1990.
56. Fidan E, Babadagli T, Kuru E. Use of cement as lost-circulation material: best practices. In Petroleum Society of Canada; 2004.
57. Bruton JR, Ivan CD, Heinz TJ. Lost circulation control: evolving techniques and strategies to reduce downhole mud losses. In Society of Petroleum Engineers; 2001.
58. Caughron DE, Renfrow DK, Bruton JR, Ivan CD, Broussard PN, Bratton TR, et al. Unique crosslinking pill in tandem with fracture prediction model cures circulation losses in deepwater Gulf of Mexico. In Society of Petroleum Engineers; 2002.
59. Mata F, Veiga M. Crosslinked cements solve lost circulation problems. In Society of Petroleum Engineers; 2004.
60. Wang H, Sweatman RE, Engelman R, Deeg WF, Whitfill DL, Soliman MY, et al. Best practice in understanding and managing lost circulation challenges. SPE Drill Complet. 2008;23(02):168–75.

61. Lecolier E, Herzhaft B, Rousseau L, Neau L, Quillien B, Kieffer J. Development of a nanocomposite gel for lost circulation treatment. In Society of Petroleum Engineers; 2005.
62. Saasen A, Godøy R, Breivik D, Solvang S, Svindland A, Gausel E, et al. Concentrated solid suspension as an alternative to cements for temporary abandonment applications in oil wells. Pap SPE SA. 2004;34.
63. Saasen A, Wold S, Ribesen BT, Tran TN, Huse A, Rygg V, et al. Permanent abandonment of a North Sea well using unconsolidated Well-Plugging material. SPE Drill Complet. 2011;26(03):371–5.
64. Filippov A, Mack R, Cook L, York P, Ring L, McCoy T. Expandable tubular solutions. In Society of Petroleum Engineers; 1999.
65. Lohoefer CL, Mathis B, Brisco D, Waddell K, Ring L, York P. Expandable liner hanger provides cost-effective alternative solution. In Society of Petroleum Engineers; 2000.
66. Perez-Roca E, Andrews S, Keel D. Addressing Common Drilling Challenges Using Solid Expandable Tubular Technology. In Society of Petroleum Engineers; 2003.
67. Shepard S, Reiley R, Warren T. Casing drilling: An emerging technology. In Society of Petroleum Engineers; 2001.
68. Warren T, Tessari R, Houtchens B. Casing drilling with retrievable drilling assemblies. In Offshore Technology Conference; 2004.
69. Karimi M, Petrie SW, Moellendick E, Holt C. A review of casing drilling advantages to reduce lost circulation, augment borehole strengthening, improve borehole stability, and mitigate drilling-induced formation damage. In Society of Petroleum Engineers; 2011.
70. Whitfill D. Lost circulation material selection, particle size distribution and fracture modeling with fracture simulation software. In Society of Petroleum Engineers; 2008.
71. Salehi S, Nygaard R. Numerical modeling of induced fracture propagation: A novel approach for lost circulation materials (LCM) design in borehole strengthening applications of deep offshore drilling. In Society of Petroleum Engineers; 2012.
72. Van Oort E, Friedheim JE, Pierce T, Lee J. Avoiding losses in depleted and weak zones by constantly strengthening boreholes. SPE Drill Complet. 2011;26(04):519–30.
73. Mostafavi V, Hareland G, Belayneh M, Aadnoy B. Experimental and mechanistic modeling of fracture sealing resistance with respect to fluid and fracture properties. In American Rock Mechanics Association; 2011.

74. Salehi S. Numerical simulations of fracture propagation and sealing: Implications for borehole strengthening. 2012;
75. Fuh G-F, Morita N, Boyd P, McGoffin S. A new approach to preventing lost circulation while drilling. In Society of Petroleum Engineers; 1992.
76. Dupriest FE, Smith MV, Zeilinger SC, Shoykhet N. Method to eliminate lost returns and build integrity continuously with high-filtration-rate fluid. In Society of Petroleum Engineers; 2008.
77. Alberty MW, McLean MR. A physical model for stress cages. In Society of Petroleum Engineers; 2004.
78. Aadnøy BS, Belayneh M. Elasto-plastic fracturing model for borehole stability using non-penetrating fluids. *J Pet Sci Eng.* 2004;45(3–4):179–92.
79. Pilehvari AA, Nyshadham VR. Effect of material type and size distribution on performance of loss/seepage control material. In Society of Petroleum Engineers; 2002.
80. Hands N, Kowbel K, Maikranz S, Nouris R. Drill-in fluid reduces formation damage, increases production rates. *Oil Gas J.* 1998;96(28).
81. Liu D, Kang Y, Liu Q, Lei D, Zhang B. Laboratory research on fracture-supported shielding temporary plugging drill-in fluid for fractured and fracture-pore type reservoirs. *J Chem.* 2017;2017.
82. Lummus JL, Randall B. Development of drilling fluid friction additives for project MOHOLE. Pan American Petroleum Corporation Research Department; 1966.
83. Smith P, Browne S, Heinz T, Wise W. Drilling fluid design to prevent formation damage in high permeability quartz arenite sandstones. In Society of Petroleum Engineers; 1996.
84. Song JH, Rojas JC. Preventing Mud Losses by Borehole Strengthening (Russian). In Society of Petroleum Engineers; 2006.
85. Louise B, Edo B, Simon J, Tony B, Olav S, Jean-Francois A, et al. Particulate Invasion From Drilling Fluids. In 1999.
86. Borisov AS, Husein M, Hareland G. A field application of nanoparticle-based invert emulsion drilling fluids. *J Nanoparticle Res.* 2015;17(8):340.
87. KAEUFFER J, JL K. Determination de l'optimum de remplissage granulometrique et quelques proprietes s'y rattachant. 1975;
88. Lavrov A. Lost circulation: mechanisms and solutions. Gulf Professional Publishing; 2016.

89. Kageson-Loe NM, Sanders MW, Growcock F, Taugbøl K, Horsrud P, Singelstad AV, et al. Particulate-based loss-prevention material--the secrets of fracture sealing revealed! *SPE Drill Complet.* 2009;24(04):581–9.
90. Aston M, Alberty M, McLean M, De Jong H, Armagost K. Drilling fluids for borehole strengthening. In *Society of Petroleum Engineers*; 2004.
91. Aston MS, Alberty MW, Duncum SD, Bruton JR, Friedheim JE, Sanders MW. A new treatment for borehole strengthening in shale. In *Society of Petroleum Engineers*; 2007.
92. Duffadar RD, Dupriest FE, Zeilinger SC. Practical guide to lost returns treatment selection based on a holistic model of the state of the near borehole stresses. In *Society of Petroleum Engineers*; 2013.
93. Dupriest FE. Fracture closure stress (FCS) and lost returns practices. In *Society of Petroleum Engineers*; 2005.
94. Guo Q, Feng Y, Jin Z. Fracture aperture for borehole strengthening applications. In *American Rock Mechanics Association*; 2011.
95. van Oort E, Razavi OS. Borehole strengthening and casing smear: the common underlying mechanism. In *Society of Petroleum Engineers*; 2014.
96. Wang H, Towler BF, Soliman MY. Near borehole stress analysis and borehole strengthening for drilling depleted formations. In *Society of Petroleum Engineers*; 2007.
97. Wang H, Towler BF, Soliman MY. Fractured borehole stress analysis: sealing cracks to strengthen a borehole. In *Society of Petroleum Engineers*; 2007.
98. Feng Y, Gray KE. A parametric study for borehole strengthening. *J Nat Gas Sci Eng.* 2016;30:350–63.
99. Razavi O, Vajargah AK, van Oort E, Aldin M, Govindarajan S. Optimum particle size distribution design for lost circulation control and borehole strengthening. *J Nat Gas Sci Eng.* 2016;35:836–50.
100. RP A. Recommended Practice for Field Testing Water-based Drilling Fluids. 2009;
101. Assaad J, Khayat KH, Mesbah H. Variation of formwork pressure with thixotropy of self-consolidating concrete. *Mater J.* 2003;100(1):29–37.
102. <https://www.fann.com/content/dam/fann/Manuals/Permeability%20Plugging%20Apparatus.pdf>.
103. <https://www.fann.com/content/dam/fann/Manuals/Model%2035%20Viscometer.pdf>.

104. <https://www.fann.com/content/dam/fann/Manuals/High%20Temp%20Aging%20Cell.pdf>.
105. <https://www.fann.com/content/dam/fann/Brochures/Mixers2.pdf>.
106. https://www.tainstruments.com/wp-content/uploads/dhr_brochure.pdf.
107. Barnes HA. The yield stress—a review or ‘παντα ρει’—everything flows? *J Non-Newton Fluid Mech.* 1999;81(1–2):133–78.
108. Moller P, Fall A, Chikkadi V, Derks D, Bonn D. An attempt to categorize yield stress fluid behaviour. *Philos Trans R Soc Math Phys Eng Sci.* 2009;367(1909):5139–55.
109. Barnes HA. Thixotropy—a review. *J Non-Newton Fluid Mech.* 1997;70(1–2):1–33.
110. Jachnik R. Drilling fluid thixotropy & relevance. *Stress.* 2000;1500.
111. Tehrani A. Behaviour of suspensions and emulsions in drilling fluids. *Annu Trans-Nord Rheol Soc.* 2007;15:17.

APPENDIX – A: XRF AND XRD RESULTS FOR SEPIOLITE CLAY

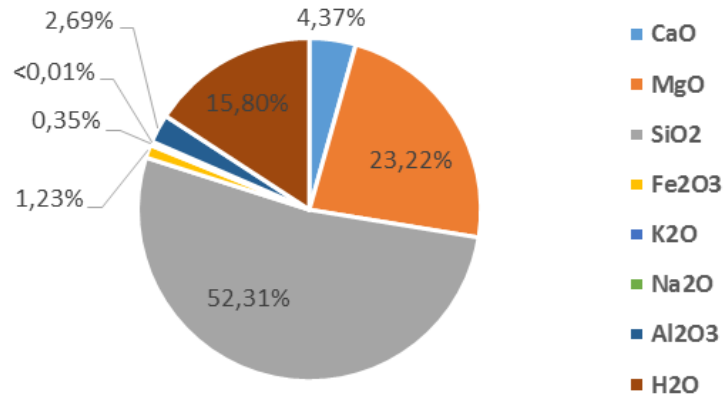


Figure A.1: Chemical analysis and mineral composition of sepiolite clay.

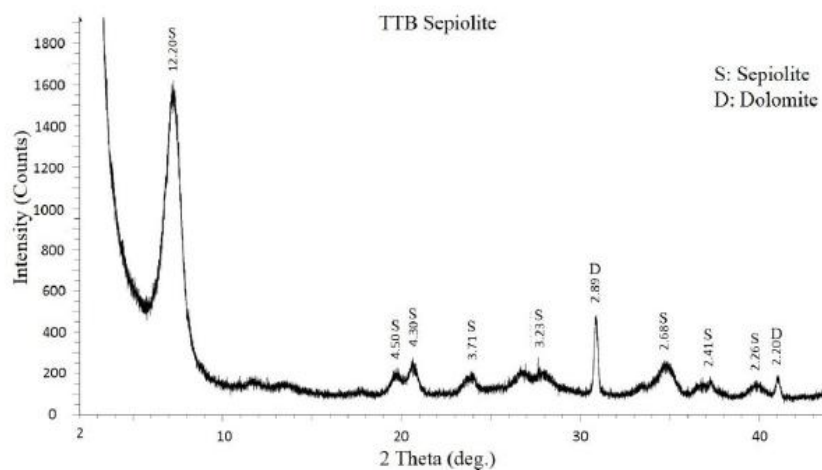


Figure A.2 XRD Analysis of Sepiolite Clay

XRF analysis which is shown in Figure A.1 was carried out by using Spectro Xepos-3. Cu was analyzed in anode tube by fusion method under the conditions of 0,9 mA ve 40 kV. Hereby, the results of XRD measurements of the sepiolite sample which is illustrated in Figure A.2 are evident of the chosen sepiolite sample is composed of 10% of dolomite and dolomite based sepiolite.

XRF results of the sepiolite sample showed that the sample includes calcium oxide (CaO) by 4.37%. Therefore, it can be concluded that the great amount of calcium oxide resulted in the existence of dolomite, ((CaMg)(CO₃)₂), which is calcium

mineral. Also, it is known that the ideal dolomite is composed of calcium oxide (CaO) by 30.41%. Although this generalization is due to free Mg and Ca from other materials, it can be assumed that the entire amount of calcium oxide (CaO) is due to dolomite. In the line with these assumptions, the maximum dolomite content of this kind of sepiolite would be as the following:

$$\text{Dolomite content} = (4.37 \times 100) / 30.41 \cong 14\%$$

As a rule of thumb, dolomite content would be assumed as 10% in the existence of free Mg and Ca.

APPENDIX – B: XRD RESULTS FOR WYOMING BENTONITE CLAY

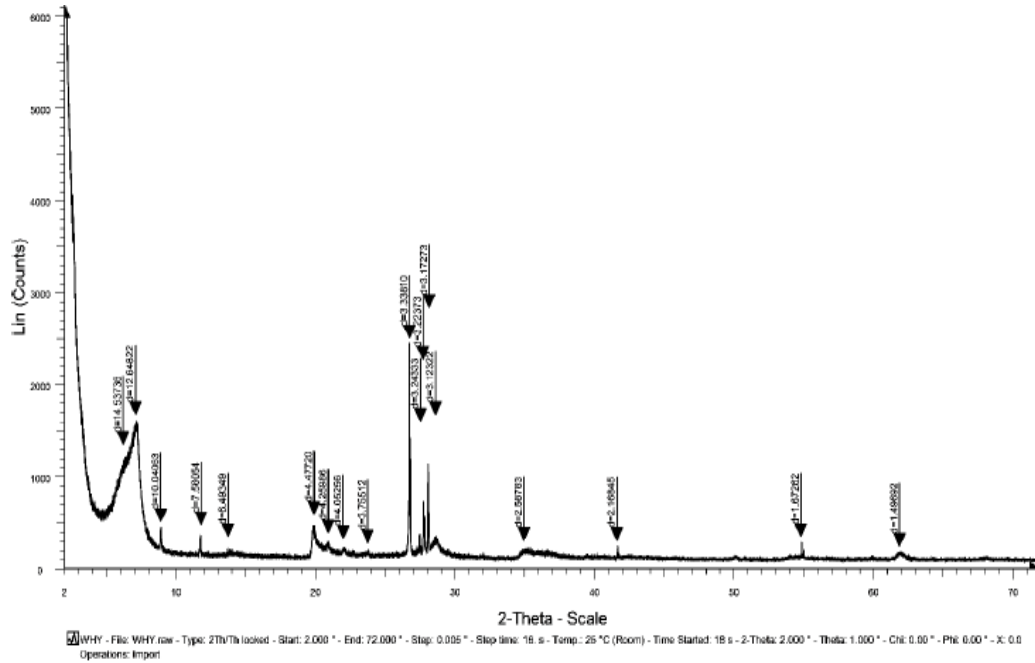


Figure B.1: XRD Analysis of Wyoming Bentonite

Wyoming bentonite contains smectite as the main mineral phase. The smectite basal peak (d001) essentially marks the distance of 12.65 Å and this main peak has a shoulder of 14.54 Å on the high 2-Theta side. Therefore, the basal peak is asymmetrical.

As well as smectite, there are other types of clay minerals and clay mica groups klorit-kaolinite and illite-mica in the sample. Excluding this clay, and clay-92 mica groups, there are quartz and feldspar minerals as non-clay minerals. In a nutshell, the approximately assumed composition of the sample is as in the followings:

“Smectite (75-80%) + Chlorite-Kaolinite/Halloysite (<5%) + Illit-Mica (<5%) + Quartz (10-15%) + Feldspat (5-10%)”

APPENDIX – C: UNIMODAL PARTICLE SIZE DISTRIBUTION FOR ALL DISCS

➤ 508 μm Disc

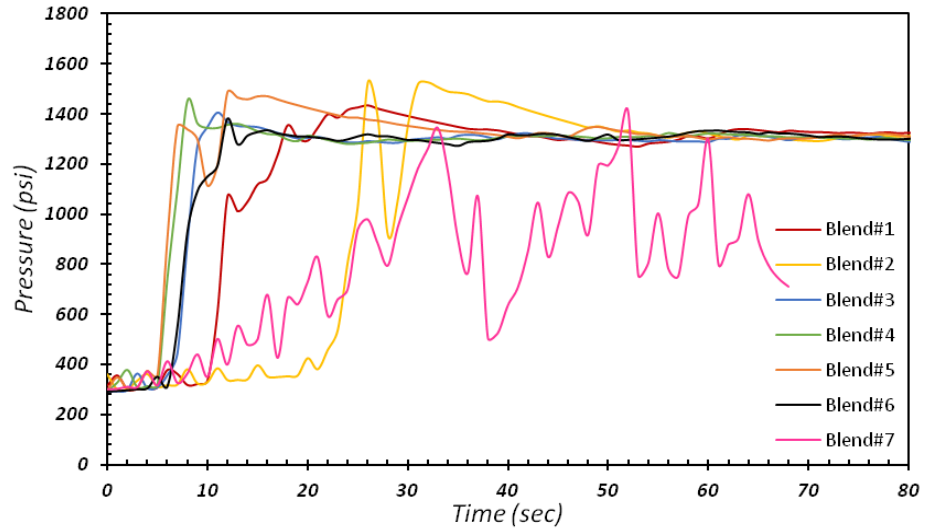


Figure C.1 Pump pressure vs. fracture sealing time of all unimodal blends for 508 μm disc.

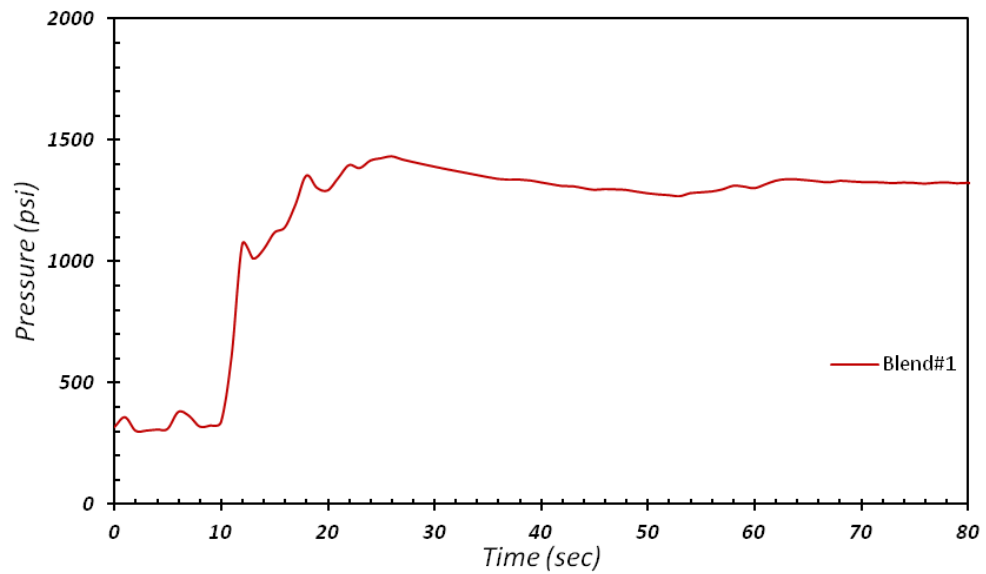


Figure C. 2 Pump pressure vs. fracture sealing time of Blend # 1 for 508 μm .

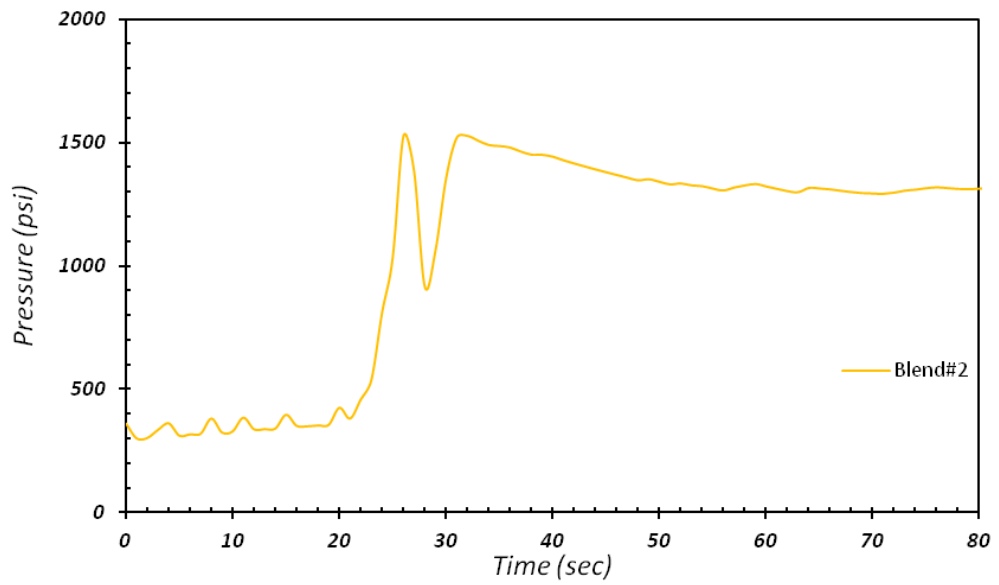


Figure C.3 Pump pressure vs. fracture sealing time of Blend # 2 for 508 μm .

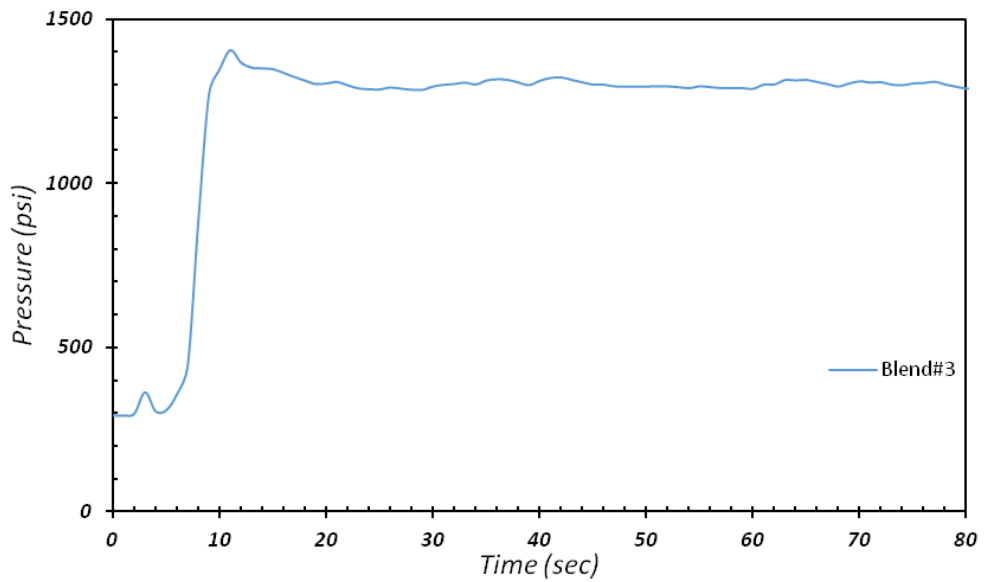


Figure C.4 Pump pressure vs. fracture sealing time of Blend # 3 for 508 μm .

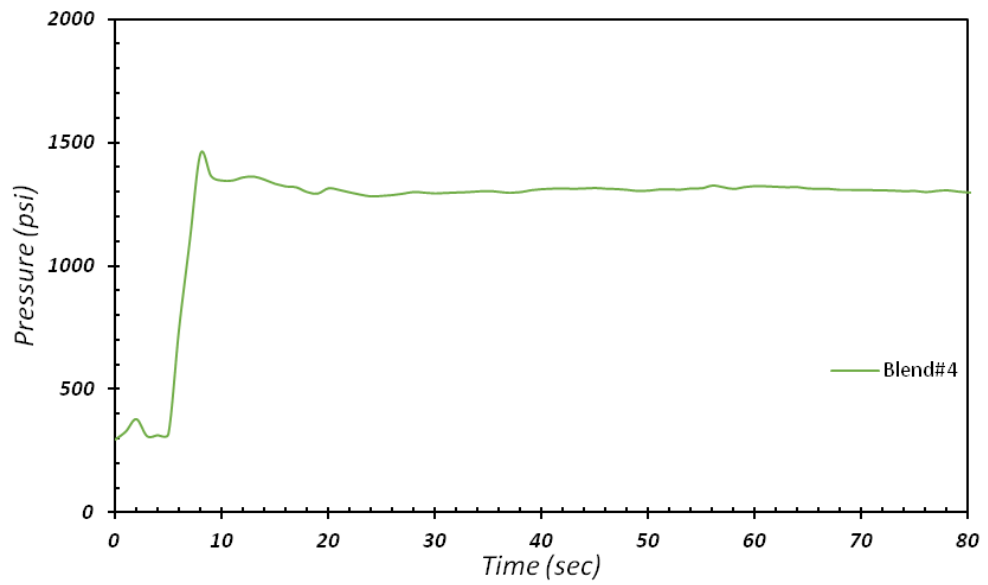


Figure C.5 Pump pressure vs. fracture sealing time of Blend # 4 for 508 μm .

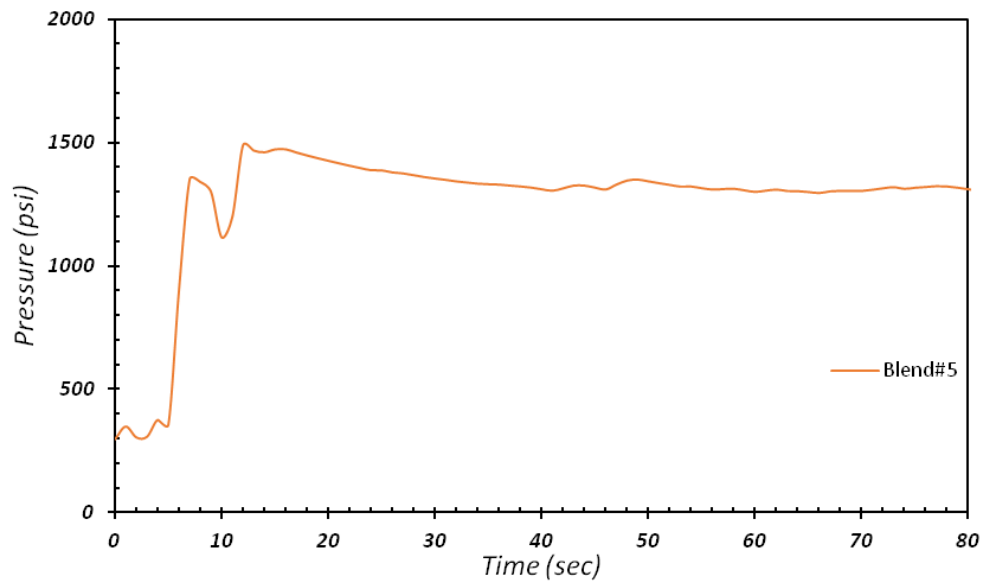


Figure C.6 Pump pressure vs. fracture sealing time of Blend # 5 for 508 μm .

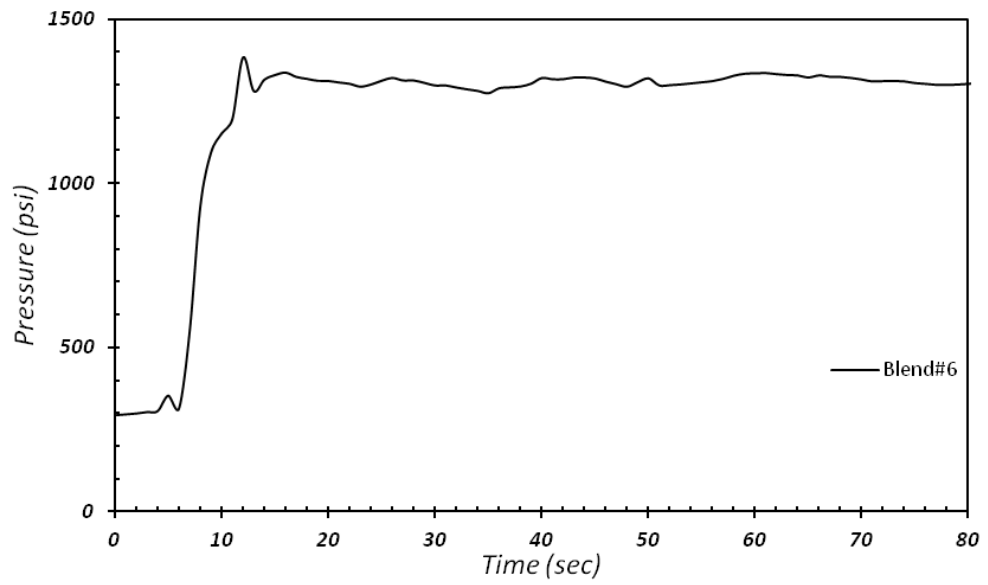


Figure C.7 Pump pressure vs. fracture sealing time of Blend # 6 for 508 μm .

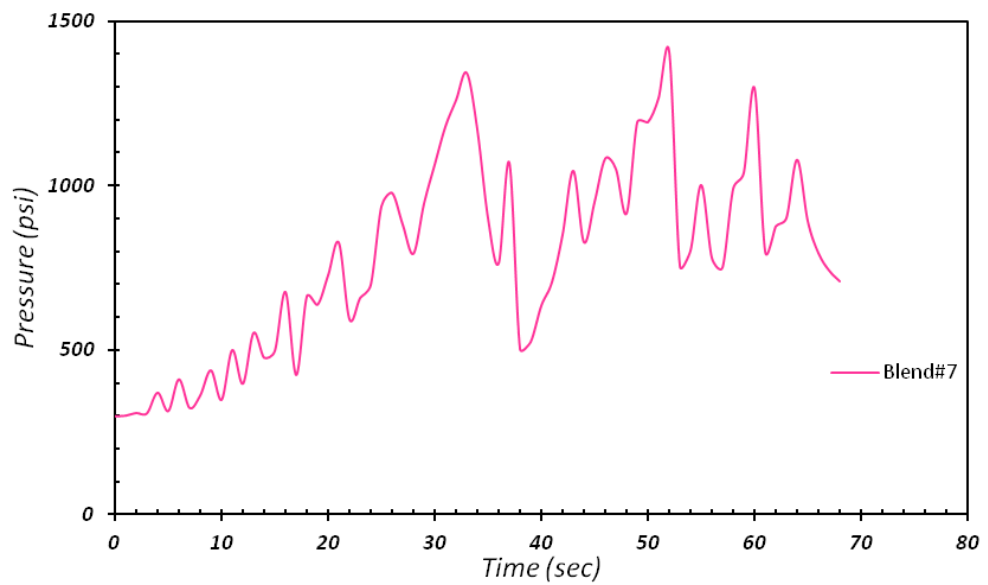


Figure C.8 Pump pressure vs. fracture sealing time of Blend # 7 for 508 μm .

➤ **1016 μm Disc**

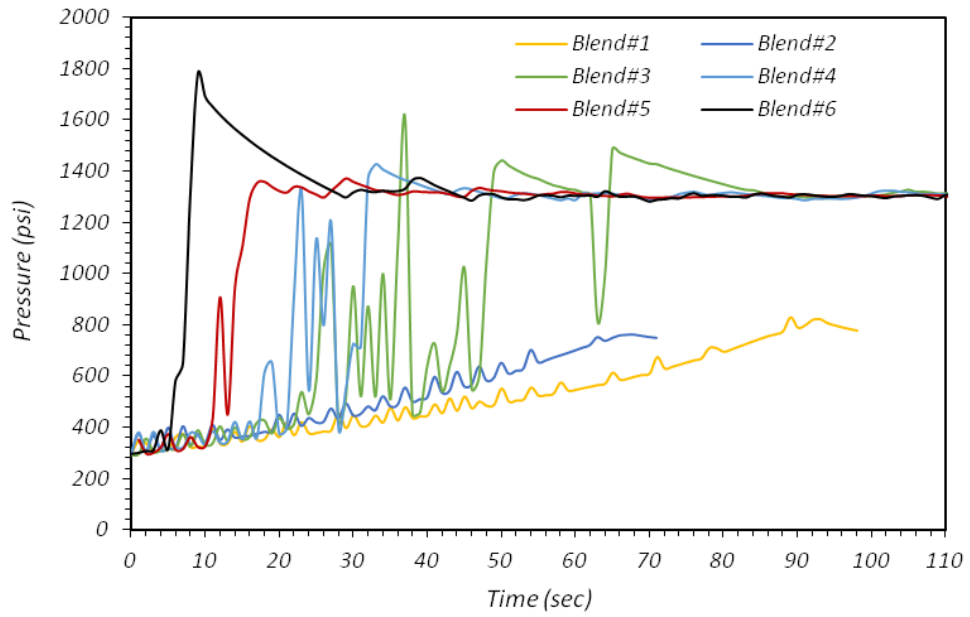


Figure C.9 Pump pressure vs. fracture sealing time of all unimodal blends for 1016 μm disc.

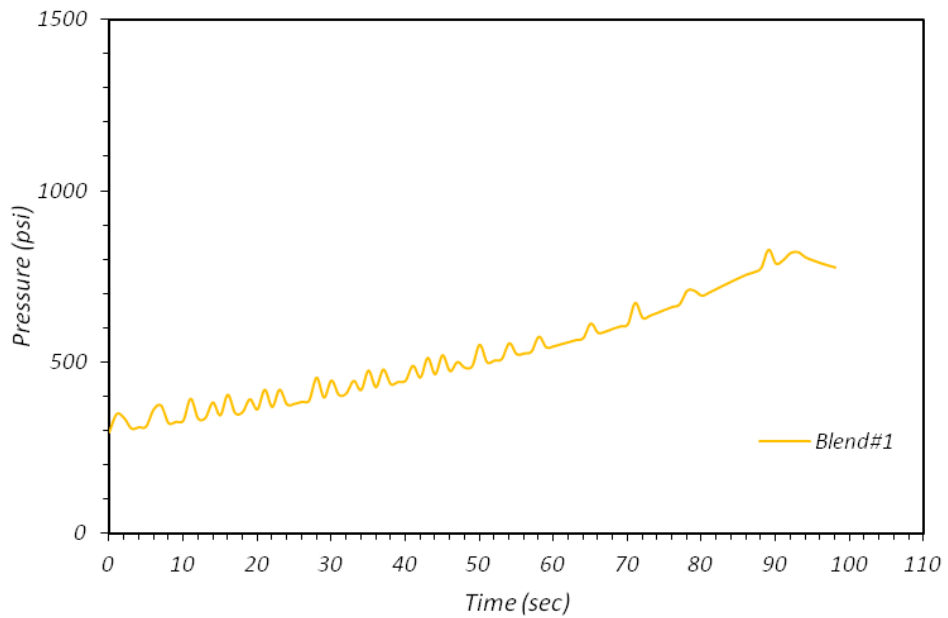


Figure C.10 Pump pressure vs. fracture sealing time of Blend # 1 for 1016 μm .

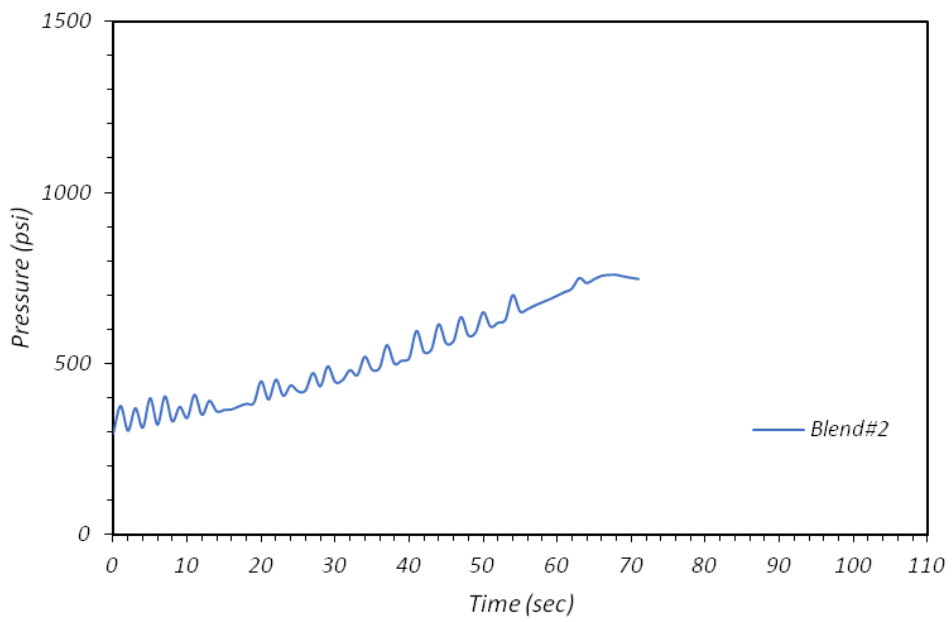


Figure C.11 Pump pressure vs. fracture sealing time of Blend # 2 for 1016 μm .

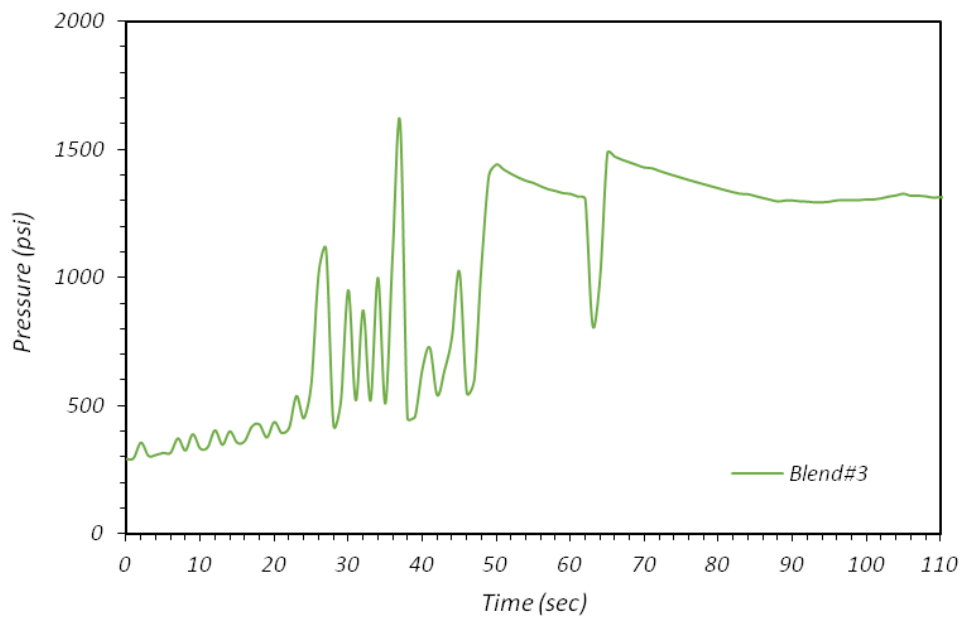


Figure C.12 Pump pressure vs. fracture sealing time of Blend #3 for 1016 μm .

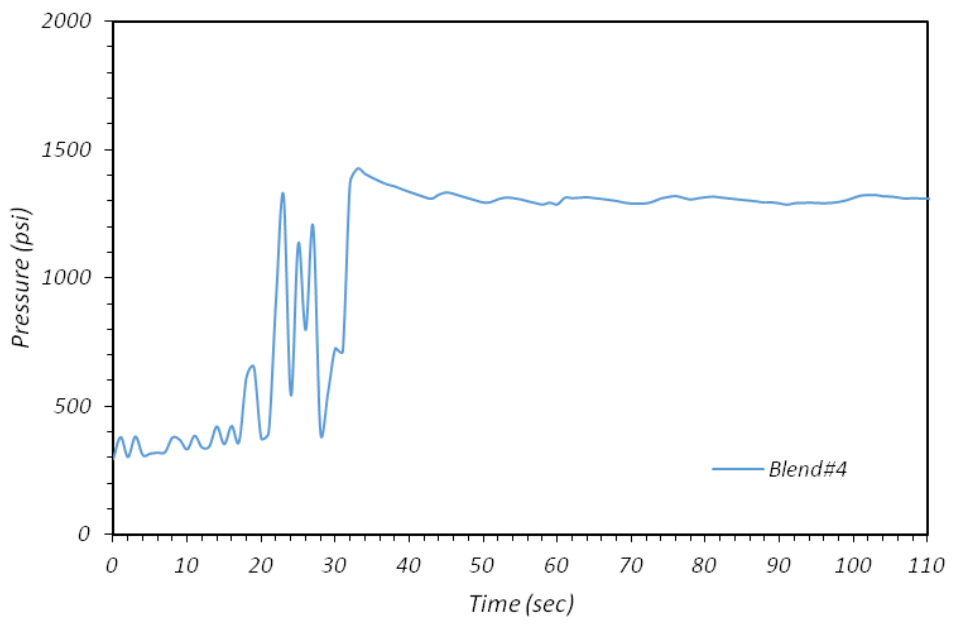


Figure C.13 Pump pressure vs. fracture sealing time of Blend #4 for 1016 μm .

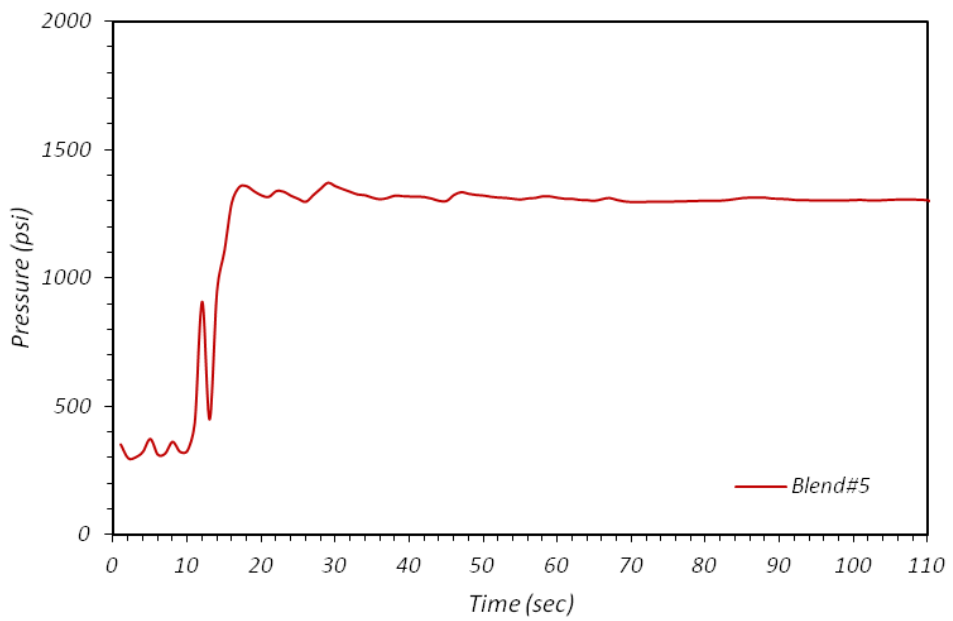


Figure C.14 Pump pressure vs. fracture sealing time of Blend #5 for 1016 μm .

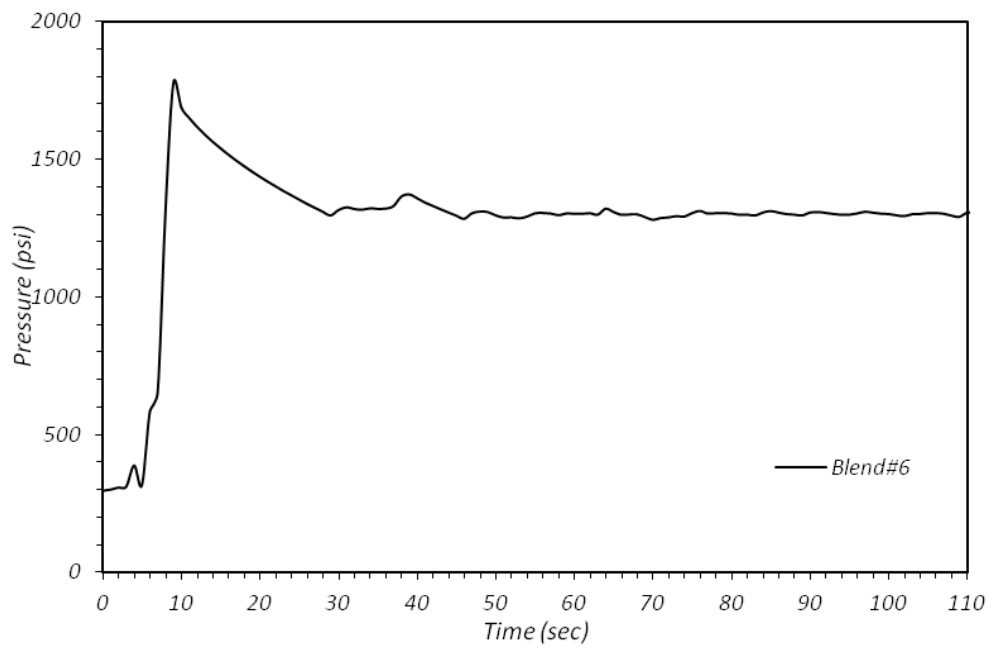


Figure C.15 Pump pressure vs. fracture sealing time of Blend #6 for 1016 μm .

➤ 1524 μm Disc

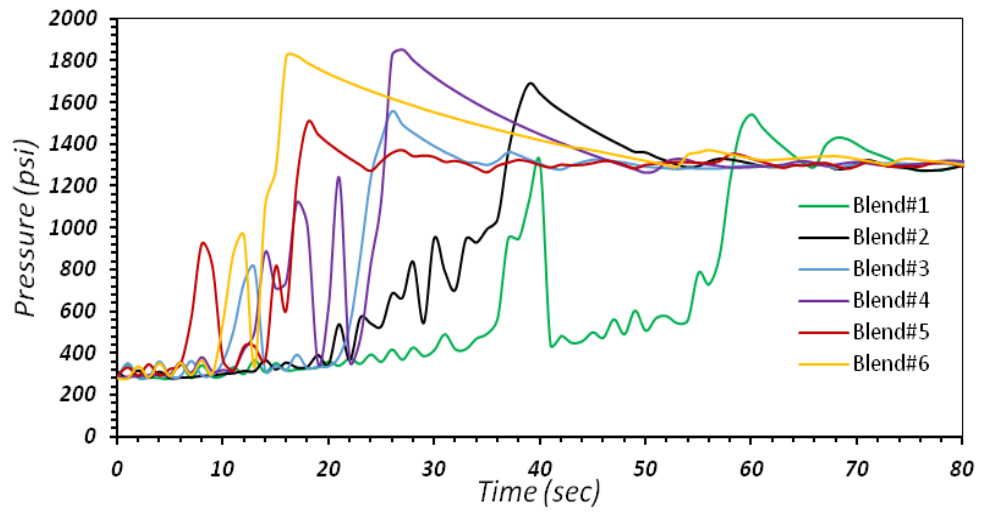


Figure C.16 Pump pressure vs. fracture sealing time of all unimodal blends for 1524 μm disc.

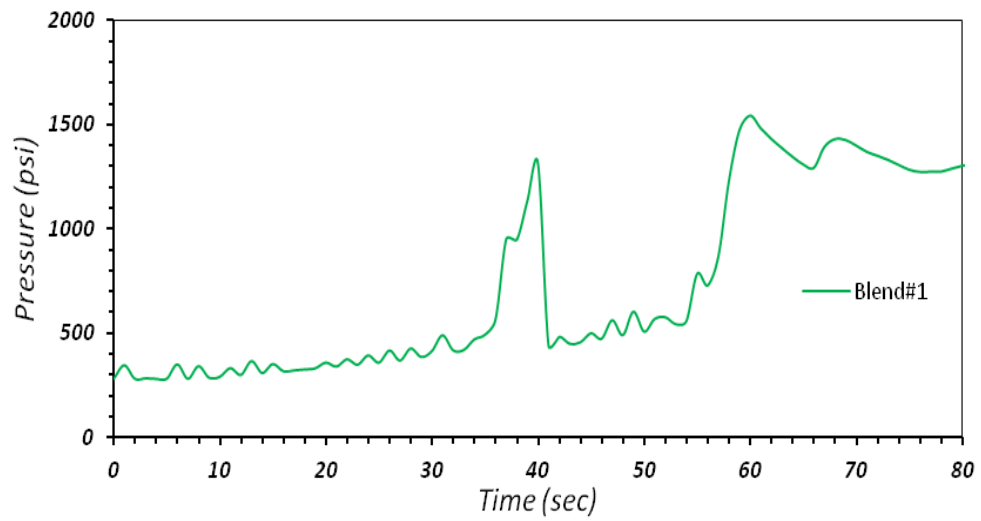


Figure C.17 Pump pressure vs. fracture sealing time of Blend #1 for 1524 μm .

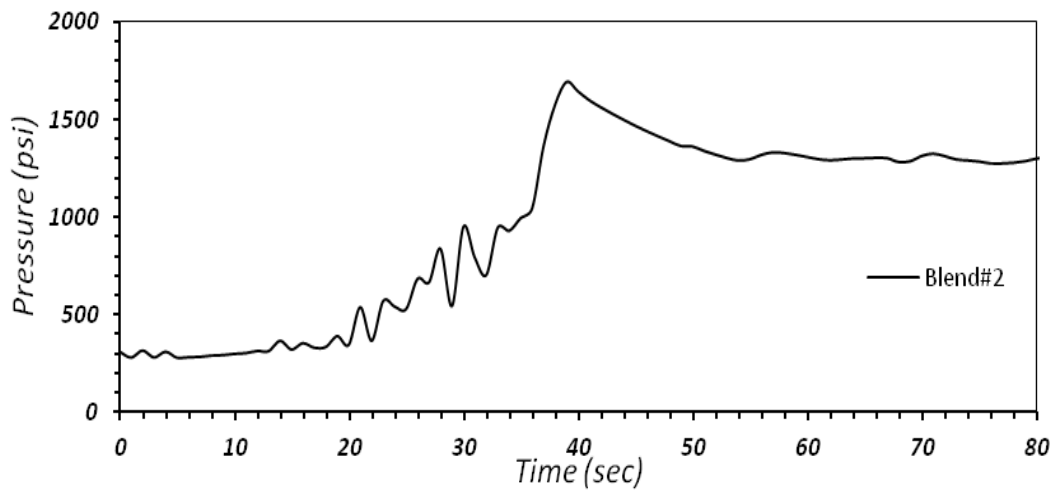


Figure C.18 Pump pressure vs. fracture sealing time of Blend #2 for 1524 μm .

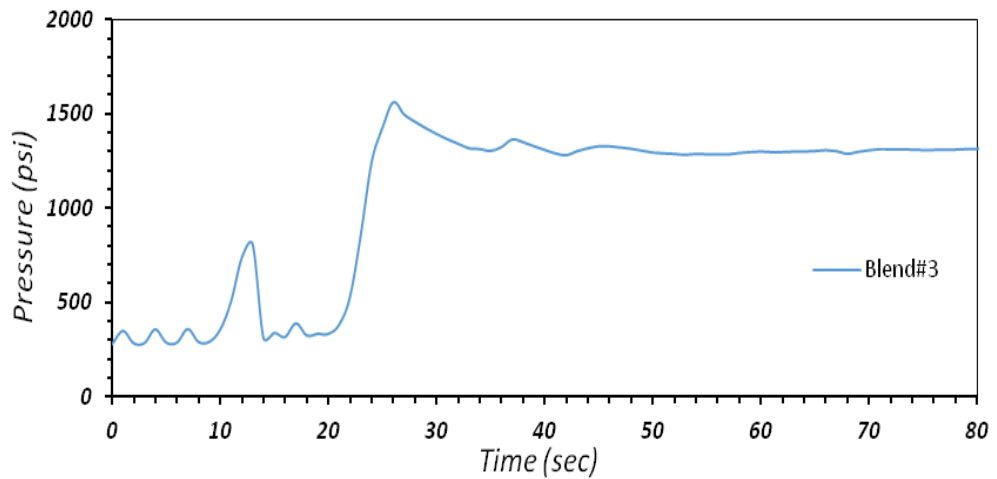


Figure C.19 Pump pressure vs. fracture sealing time of Blend #3 for 1524 μm .

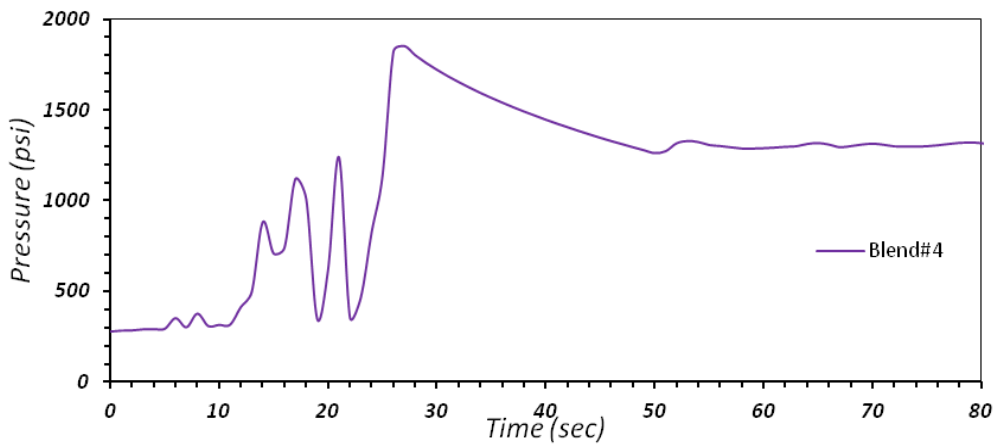


Figure C.20 Pump pressure vs. fracture sealing time of Blend #4 for 1524 μm .

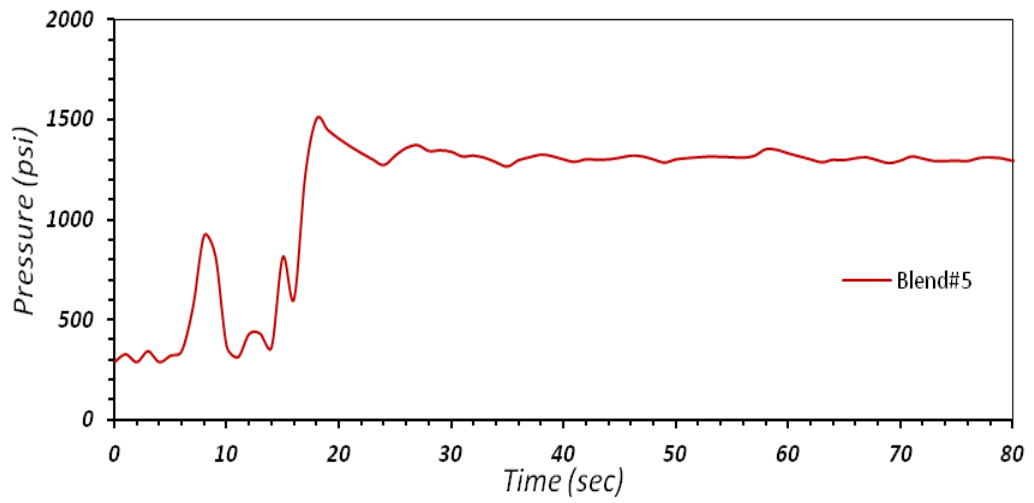


Figure C.21 Pump pressure vs. fracture sealing time of Blend #5 for 1524 μm .

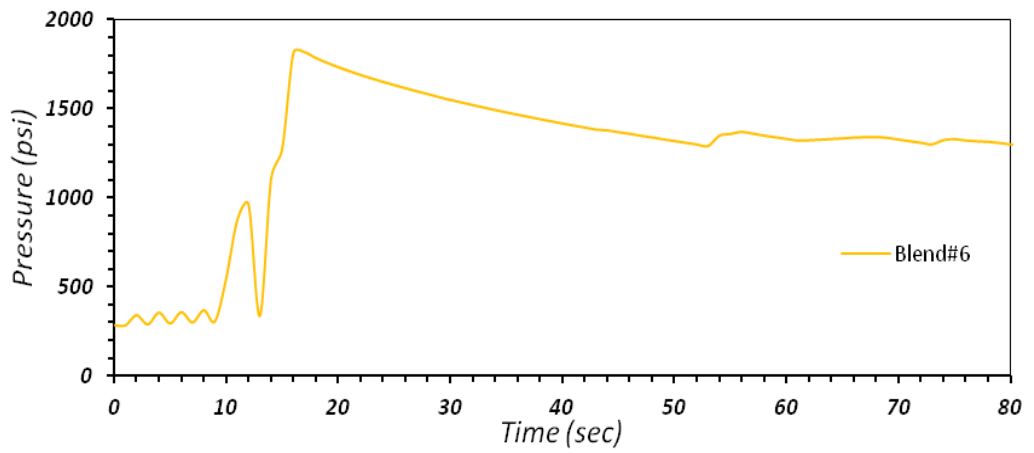


Figure C.22 Pump pressure vs. fracture sealing time of Blend #6 for 1524 μm .

➤ 2032 μm Disc

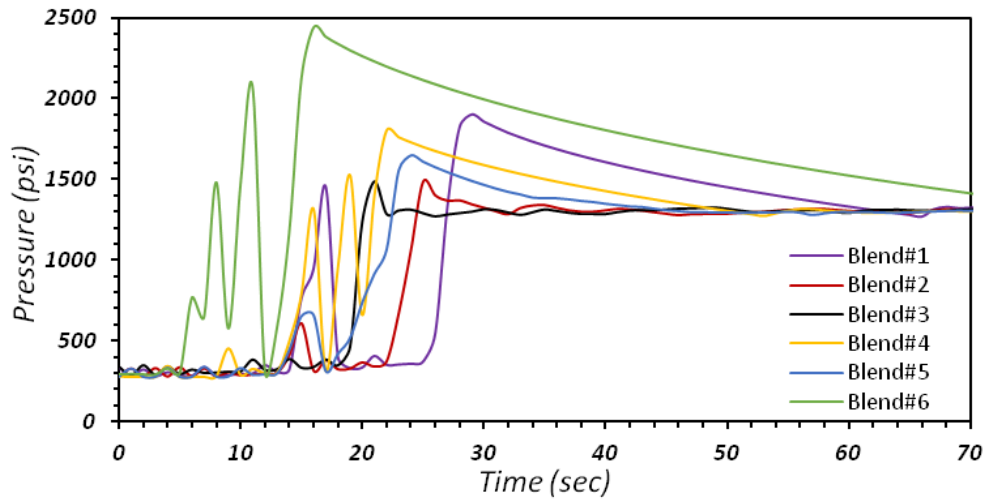


Figure C.23 Pump pressure vs. fracture sealing time of all unimodal blends for 2032 μm disc.

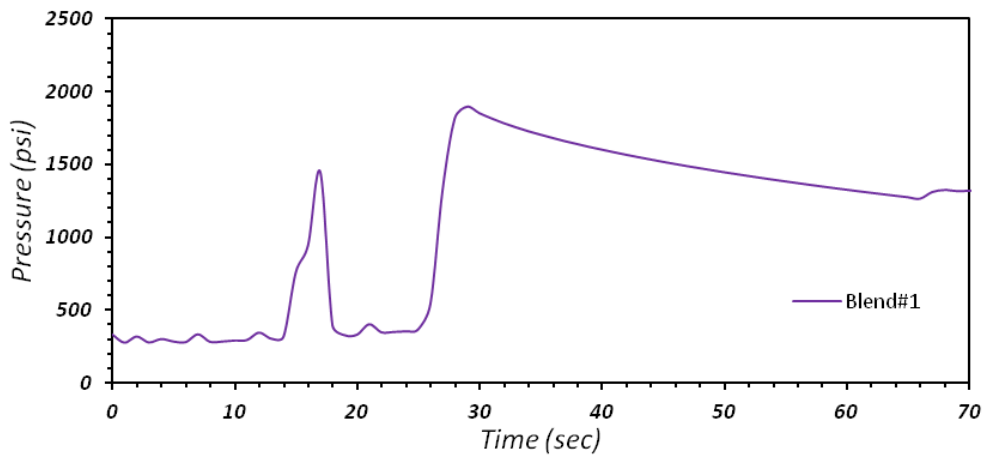


Figure C.24 Pump pressure vs. fracture sealing time of Blend #1 for 2032 μm .

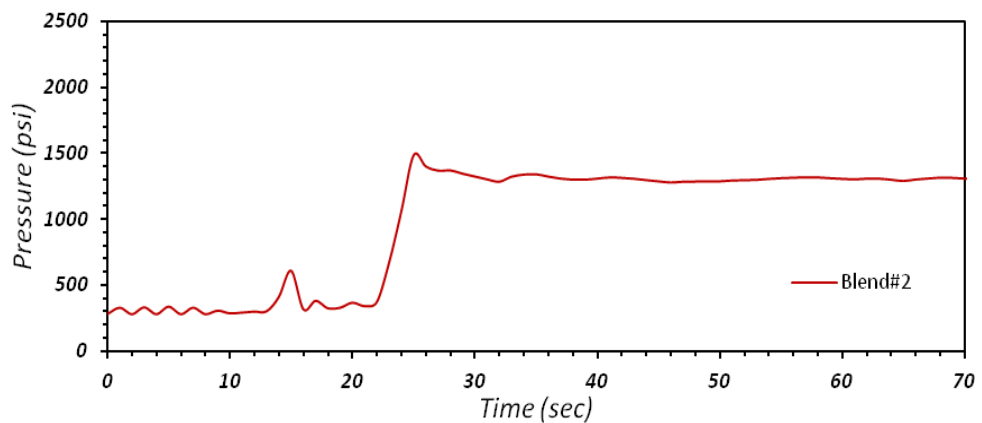


Figure C.25 Pump pressure vs. fracture sealing time of Blend #2 for 2032 μm .

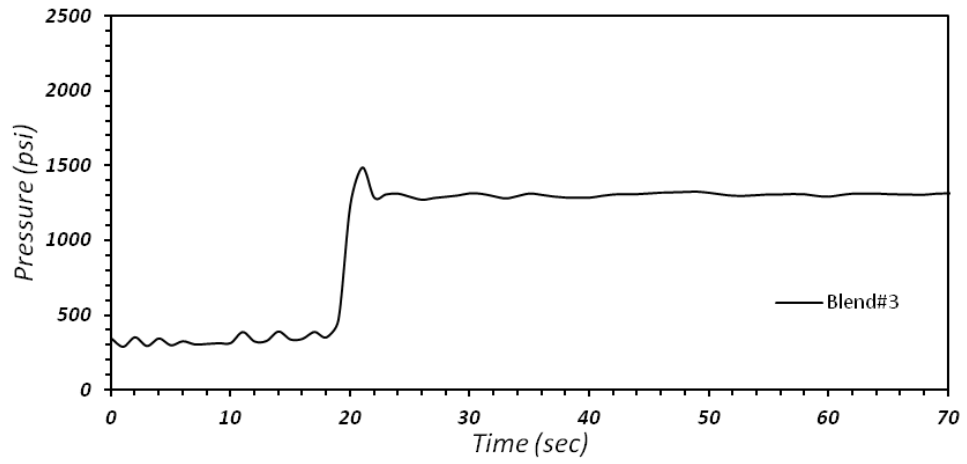


Figure C.26 Pump pressure vs. fracture sealing time of Blend #3 for 2032 μm .

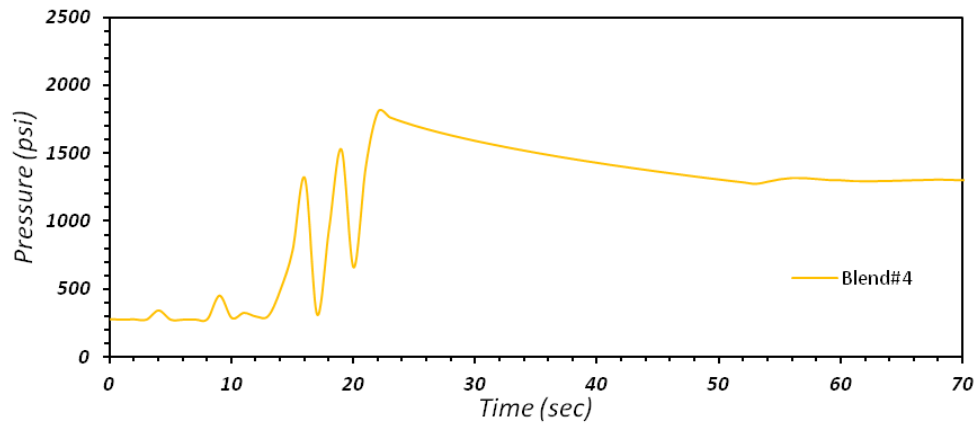


Figure C.27 Pump pressure vs. fracture sealing time of Blend #4 for 2032 μm .

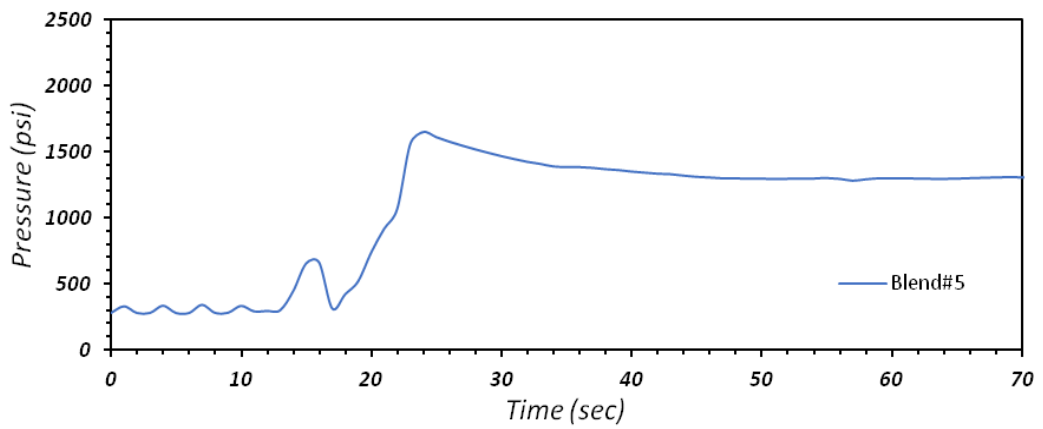


Figure C.28 Pump pressure vs. fracture sealing time of Blend #5 for 2032 μm .

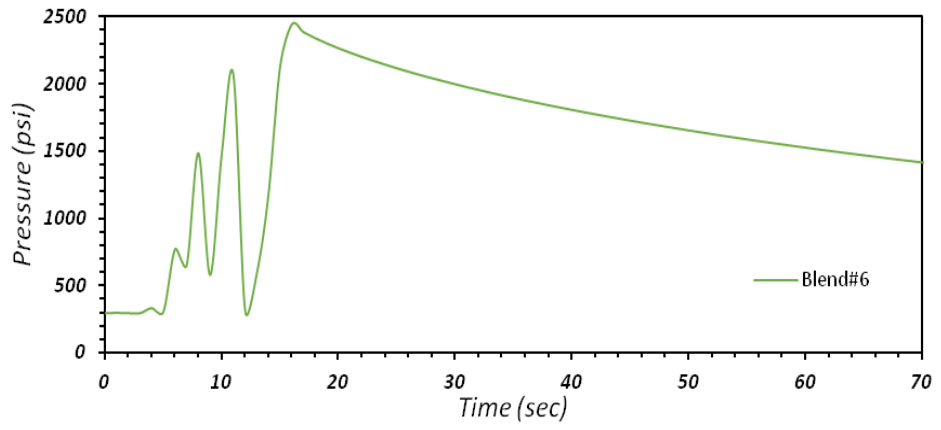


Figure C.29 Pump pressure vs. fracture sealing time of Blend #6 for 2032 μm .

➤ **2540 μm Disc**

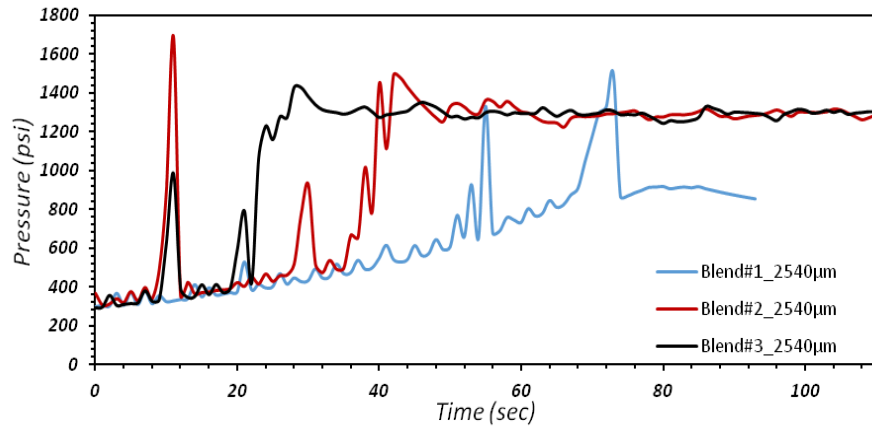


Figure C.30 Pump pressure vs. fracture sealing time of all unimodal blends for 2540 μm disc.

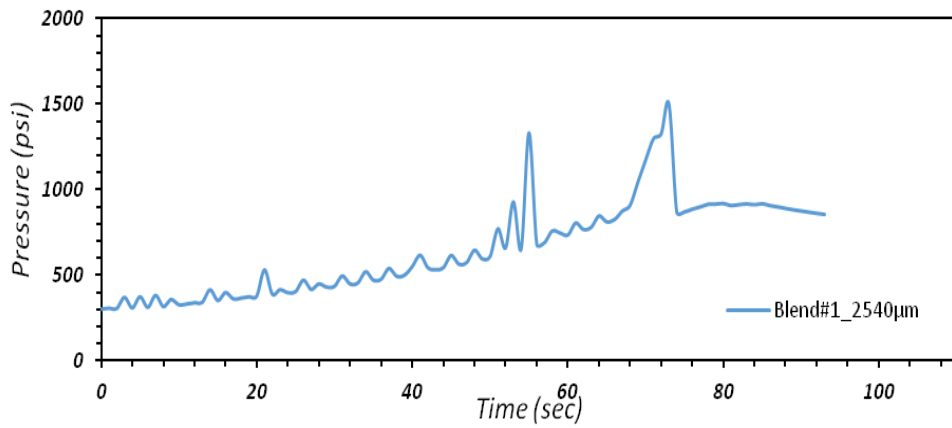


Figure C.31 Pump pressure vs. fracture sealing time of Blend #1 for 2540 μm .

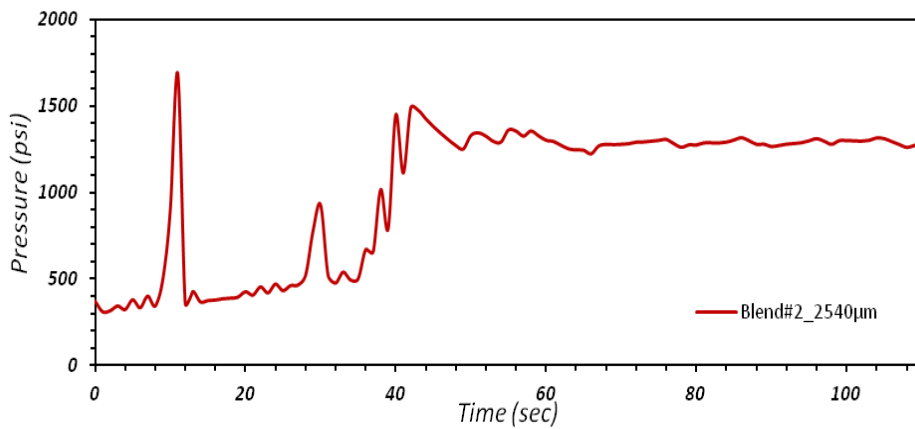


Figure C.32 Pump pressure vs. fracture sealing time of Blend #2 for 2540 μm .

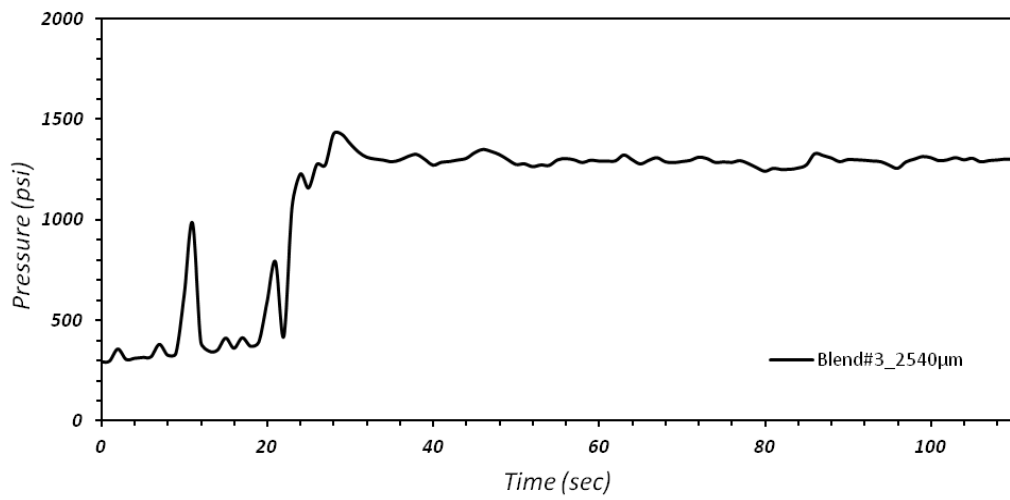


Figure C.33 Pump pressure vs. fracture sealing time of Blend #3 for 2540 μm .

➤ **3048 μm Disc**

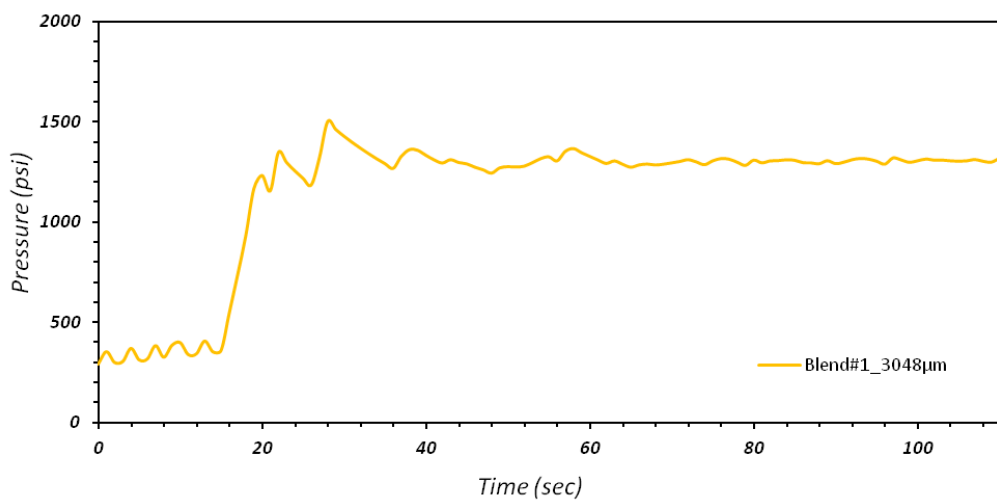


Figure C.34 Pump pressure vs. fracture sealing time of Blend #1 for 3048 μm .

APPENDIX – D: BIMODAL PARTICLE SIZE DISTRIBUTION FOR ALL DISCS

The same blend was used for each disc size, except for the largest LCM particle size.

➤ 1016 μm Disc

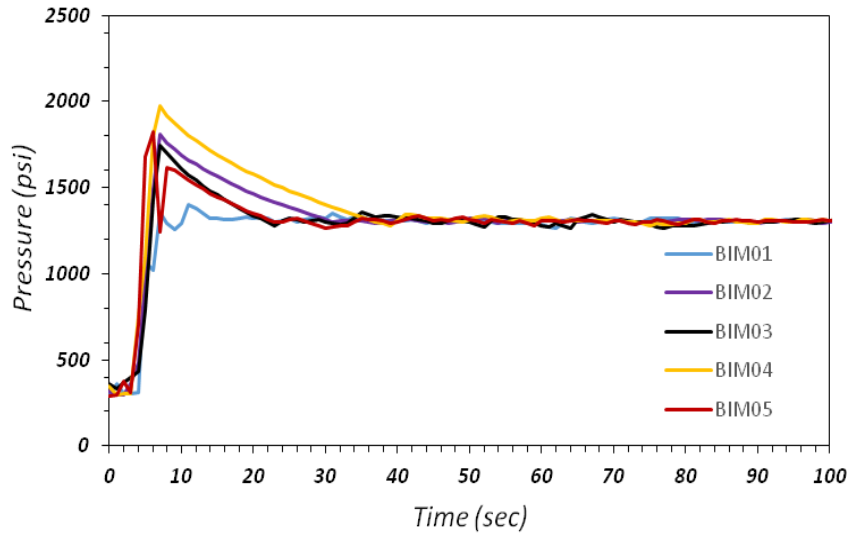


Figure D.1 Fracture sealing time vs. pump pressure consisting of 5 repetitions using the same blend (1016 μm disc).

➤ 1524 μm Disc

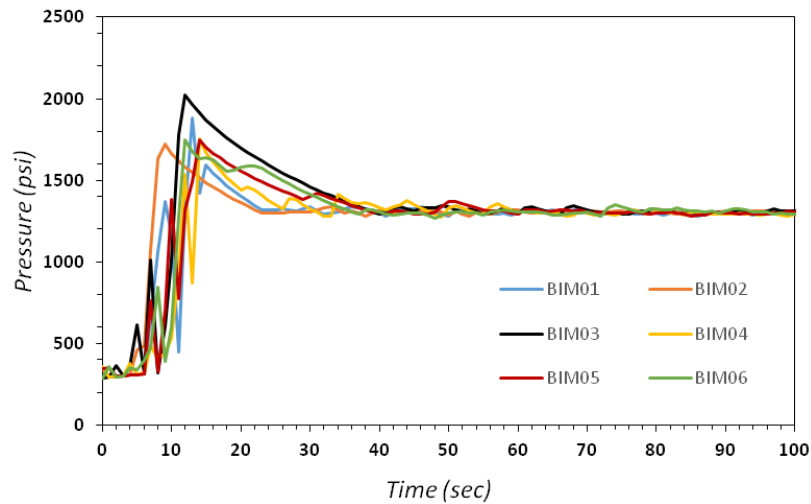


Figure D.2 Fracture sealing time vs. pump pressure consisting of 6 repetitions using the same blend (1524 μm disc)

➤ 2032 μm Disc

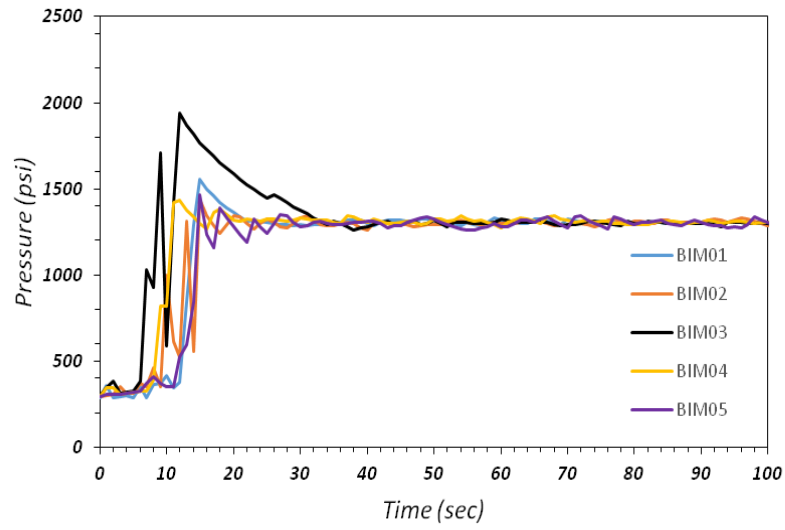


Figure D.3 Fracture sealing time vs. pump pressure consisting of 5 repetitions using the same blend (2032 μm disc).

➤ 2540 μm Disc

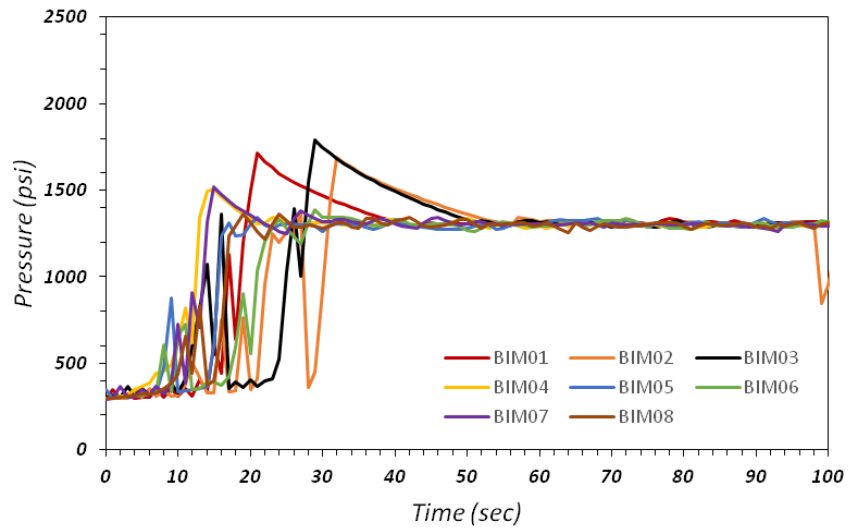


Figure D.4 Fracture sealing time vs. pump pressure consisting of 8 repetitions using the same blend (2540 μm disc).

➤ 3048 μm Disc

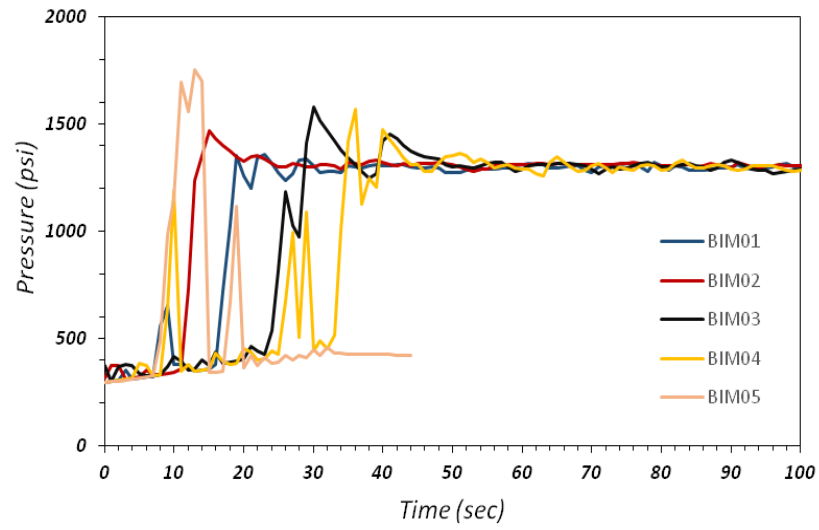


Figure D.5 Fracture sealing time vs. pump pressure consisting of 5 repetitions using the same blend (3048 μm disc).

APPENDIX – E: TRIMODAL PARTICLE SIZE DISTRIBUTION FOR ALL DISCS

The same blend was used for each disc size, except for the largest LCM particle size.

➤ 1524 μm Disc

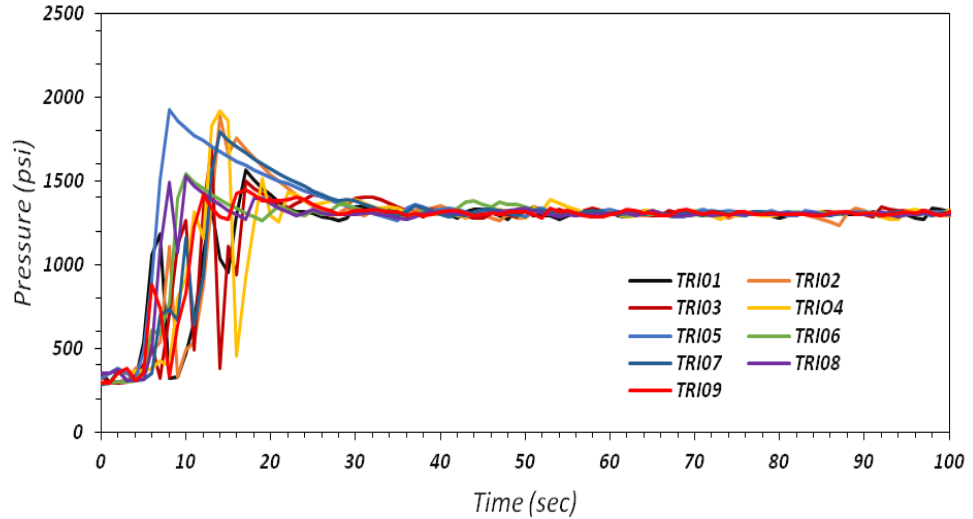


Figure E.1 Fracture sealing time vs. pump pressure consisting of 9 repetitions using the same blend (1524 μm disc).

➤ 2032 μm Disc

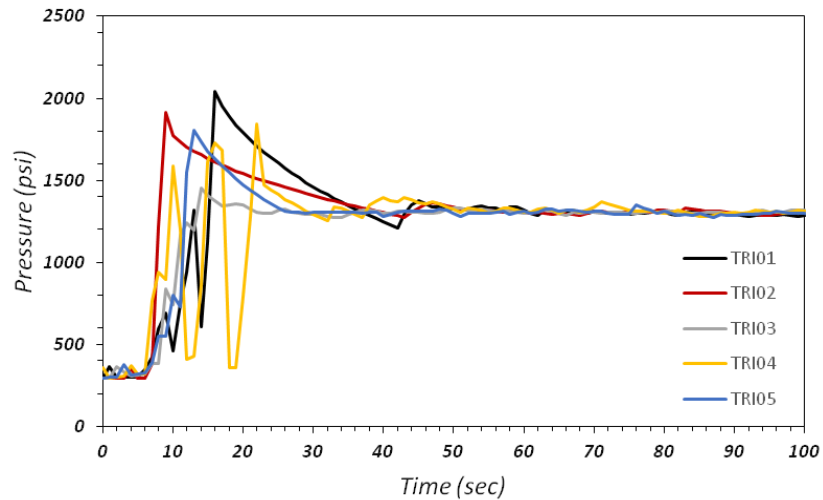


Figure E.2 Fracture sealing time vs. pump pressure consisting of 5 repetitions using the same blend (2032 μm disc).

➤ 2540 μm Disc

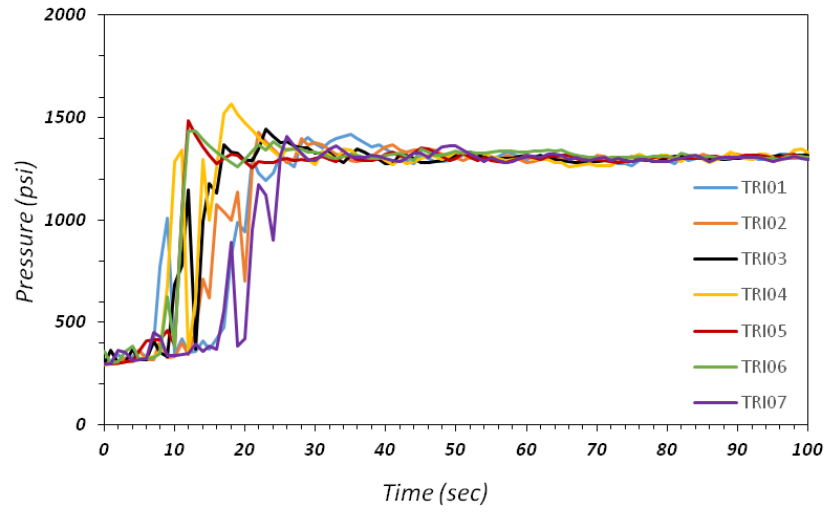


Figure E.3 Fracture sealing time vs. pump pressure consisting of 7 repetitions using the same blend (2540 μm disc).

➤ 3048 μm Disc

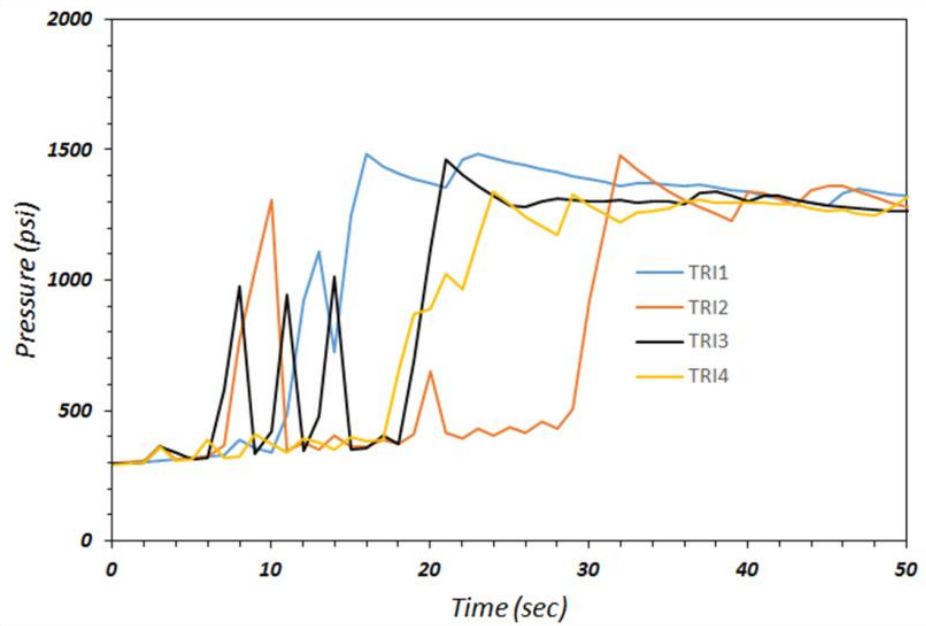


Figure E.4 Effect of low and high spherical CaCO_3 particles on fracture sealing time using the same blend for 3048 μm disc.

APPENDIX – F: PRELIMINARY EXPERIMENTS TO DETERMINE LCM OPTIMUM SIZE DISTRIBUTION

In order to determine the optimum size distribution of LCM, 20 different blends were used for all discs. Mixing results were evaluated and the most suitable unimodal, bimodal, and trimodal blends were obtained according to each disc size. Blends for each disc are expressed as D1-D20 in Table F.1 and Table F.2.

Table F.1 Preliminary experiments to determine LCM optimum size distribution
Blend# D1-D10.

Disc Fracture Size (μm)	Blend #	D1	D2	D3	D4	D5	D6	D7	D8	D9	D10	
	LCM Size (μm)	Total Concentration (%)										
1524	1680-2000	-	-	-	-	40	-	-	-	-	-	
	1410-1680	40	40	40	40	-	40	40	40	45	40	
	1180-1410	-	-	-	-	-	-	-	-	-	-	
	1000-1180	-	-	-	-	-	-	-	-	-	-	
	841-1000	-	-	-	-	-	-	-	-	-	-	
	600-841	20	-	-	-	-	-	-	15	-	-	
	500-600	-	-	20	20	20	20	-	15	20	-	
	420-500	-	20	-	-	-	-	-	-	-	-	
	300-420	-	-	-	-	-	-	-	-	-	20	
	250-300	20	-	20	20	20	-	20	15	20	20	
	150-250	-	20	-	-	-	-	-	-	-	-	
	106-150	-	-	-	-	-	-	-	-	-	-	
	75-106	20	20	20	20	20	40	40	15	15	20	
	0-150	-	-	-	-	-	-	-	-	-	-	
	Total LCM Conc. (ppb)	16	22	14	23	15	34	31	38	12	34	
30 min. Fluid loss (ml)	24	34	22	33	22	35	53	62	27	55		
2032	LCM Size (μm)	Total Concentration (%)										
	2000-2380	20	20	20	20	20	20	20	20	20	20	
	1410-1680	-	-	20	-	-	-	-	-	-	-	
	1180-1410	20	20	-	-	-	-	-	-	-	-	
	1000-1180	-	-	-	-	-	-	-	20	20	20	
	841-1000	-	-	-	20	20	20	20	-	-	-	
	600-841	-	-	-	20	-	-	-	20	-	-	
	500-600	20	20	20	-	-	-	20	-	-	-	
	420-500	-	-	-	-	20	-	-	-	20	-	
	300-420	-	-	-	-	-	20	-	-	-	20	
	250-300	20	20	20	20	20	20	-	20	20	20	
	150-250	-	-	-	-	-	-	-	-	-	-	
	106-150	-	-	-	-	-	-	20	-	-	-	
	75-106	20	20	20	20	20	20	20	20	20	20	
	Total LCM Conc. (ppb)	29,67	37	29	22	56	28	54	33	40	50	
30 min. Fluid loss (ml)	50,5	83,5	-	41	115	43	113	53	71	77		
2540	LCM Size (μm)	Total Concentration (%)										
	2500-2830	16,6	16,6	16,6	16,6	16,6	16,6	16,6	16,6	16,6	16,6	
	1410-1680	-	-	-	16,6	-	-	-	-	-	-	
	1180-1410	-	-	-	-	-	-	-	-	-	-	
	1000-1180	16,6	16,6	16,6	-	16,6	16,6	16,6	16,6	16,6	16,6	
	841-1000	-	-	-	-	-	-	-	-	-	-	
	600-841	-	-	-	-	16,6	-	-	-	-	-	
	500-600	16,6	16,6	16,6	16,6	-	-	16,6	16,6	16,6	16,6	
	420-500	-	-	-	-	-	16,6	-	-	-	-	
	300-420	16,6	16,6	16,6	16,6	16,6	16,6	-	16,6	16,6	-	
	250-300	-	-	-	-	-	-	16,6	16,6	-	-	
	150-250	16,6	16,6	16,6	16,6	16,6	16,6	16,6	-	-	16,6	
	106-150	-	-	-	-	-	-	-	-	16,6	16,6	
	75-106	16,6	16,6	16,6	16,6	16,6	16,6	16,6	16,6	16,6	16,6	
	Total LCM Conc. (ppb)	58	35	39	40	52	63	37	35	33	40	
30 min. Fluid loss (ml)	-	49	57	71	94	104	43	57	46	61		

Table F.1-cont Preliminary experiments to determine LCM optimum size distribution Blend# D1-D10.

<i>Disc Fracture Size (μm)</i>	Blend #	D1	D2	D3	D4	D5	D6	D7	D8	D9	D10
3048	LCM Size (μm)	Total Concentration (%)									
	3000-3360	25,7	25,7	25,7	25,7	14,2	16,7	25,7	25,7	30	30
	2000-2380	-	-	-	-	-	-	-	-	-	-
	1680-2000	-	-	-	-	-	-	-	-	-	-
	1410-1680	-	-	-	-	-	-	-	-	-	-
	1180-1410	17,1	14,2	8,6	17,1	14,2	16,7	17,1	14,2	-	20
	1000-1180	-	-	-	-	-	-	17,1	11,4	20	15
	841-1000	-	-	-	-	-	-	-	5,7	-	-
	600-841	17,1	14,2	8,6	17,1	14,2	16,7	-	-	-	-
	500-600	-	-	-	-	-	-	-	5,7	20	-
	420-500	17,1	11,4	11,4	11,4	14,2	16,7	-	-	-	-
	300-420	-	-	-	-	-	-	-	8,6	-	-
	250-300	-	11,4	11,4	11,4	14,2	16,7	14,2	5,7	15	15
	150-250	11,4	-	-	-	-	-	14,2	11,4	-	-
	106-150	-	11,4	17,1	8,6	14,2	16,7	-	-	-	10
	75-106	11,4	11,4	17,1	8,6	14,2	16,7	11,4	11,4	15	10
	Total LCM Conc. (ppb)	21	21	28	25	31	36	12	10	15	9
30 min. Fluid loss (ml)	38	38	52	42	40	37	27,5	25,5	48	30	

Table F.2 Preliminary experiments to determine LCM optimum size distribution Blend# D11-D20.

Disc Fracture Size(μm)	Blend #	D11	D12	D13	D14	D15	D16	D17	D18	D19	D20
	LCM Size(μm)	Total Concentration(%)									
1524	1680-2000	-	-	-	-	-	-	-	-	-	20
	1410-1680	20	43,3	20,3	43,3	40	50	50	40	40	20
	1180-1410	-	-	-	-	-	-	-	-	-	-
	1000-1180	-	-	-	-	-	-	-	15	-	-
	841-1000	-	-	-	-	-	-	-	-	-	-
	600-841	-	-	-	-	-	-	-	-	-	-
	500-600	20	23,3	20,3	23,3	20	20	16,6	15	-	20
	420-500	-	-	-	-	-	-	-	-	-	-
	300-420	-	-	-	-	-	-	-	-	-	-
	250-300	20	-	20	10	20	15	16,6	15	40	20
	150-250	-	10	-	-	-	-	-	-	-	-
	106-150	-	-	-	-	-	-	-	-	-	-
	75-106	20	-	40	-	20	15	16,6	15	20	20
	0-150	-	23,3	-	23,3	-	-	-	-	-	-
	Total LCM Conc. (ppb)	33	22	30	22	20	43	13	24	21	12
30 min. Fluid loss (ml)	40	29	43,5	31,5	26,5	-	39	48,5	47	30	
2032	LCM Size(μm)	Total Concentration(%)									
	2000-2380	20	20	20	20	20	20	30	40	40	20
	1410-1680	-	-	-	-	-	-	-	-	-	-
	1180-1410	-	-	-	-	-	-	-	-	-	-
	1000-1180	-	-	20	20	20	20	20	20	10	15
	841-1000	20	20	-	-	-	-	-	-	-	-
	600-841	-	-	-	-	-	-	-	-	-	-
	500-600	20	20	20	20	20	20	20	20	10	15
	420-500	-	-	-	-	-	-	-	-	-	-
	300-420	-	-	-	-	-	-	-	-	-	-
	250-300	20	20	-	-	20	20	15	10	20	25
	150-250	-	20	20	-	-	20	-	-	-	-
	106-150	20	-	-	20	20	-	-	-	-	-
	75-106	-	-	20	20	-	-	15	10	20	25
	Total LCM Conc.(ppb)	24	50	29	32	22	35	22	23	55	59
30 min. Fluid loss (ml)	41,5	70	60	46	35	54	35	40	101	94	
2540	LCM Size(μm)	Total Concentration(%)									
	2500-2830	33,3	26,6	30	30	26,6	26,6	30	30	30	30
	1410-1680	-	-	-	-	-	-	-	-	-	-
	1180-1410	-	-	-	-	13,3	13,3	20	15	15	15
	1000-1180	13,3	16,6	20	20	13,3	10	15	10	10	10
	841-1000	-	-	-	-	10	10	-	10	5	-
	600-841	-	-	-	-	-	-	-	-	-	-
	500-600	13,3	16,6	20	15	10	6,6	-	10	5	-
	420-500	-	-	-	-	-	-	-	-	-	-
	300-420	13,3	13,3	10	15	6,6	6,6	-	10	5	-
	250-300	-	-	-	-	6,6	6,6	15	5	10	15
	150-250	-	-	-	-	-	-	-	-	-	-
	106-150	13,3	13,3	10	10	6,6	10	10	5	10	15
	75-106	13,3	13,3	10	10	6,6	10	10	5	10	15
	Total LCM Conc.(ppb)	44	21	35	30	32	32	15	-	13	13
30 min. Fluid loss (ml)	66	27	60	53	60	60	38	-	33	35	

Table F.2-cont Preliminary experiments to determine LCM optimum size distribution
Blend# D11-D20.

<i>Disc Fracture Size (μm)</i>	Blend #	D1	D12	D13	D14	D15	D16	D17	D18	D19	D20
		1									
	LCM Size (μm)	Total Concentration (%)									
	3000-3360	30	30	30	30	75	25	30	-	-	-
	2000-2380	-	-	-	-	-	7,5	-	-	-	-
	1680-2000	-	-	-	-	-	7,5	-	-	-	-
	1410-1680	-	-	-	-	-	7,5	-	-	-	-
	1180-1410	15	15	15	15	5	7,5	-	-	-	-
	1000-1180	10	10	10	10	5	10	15	-	-	-
	841-1000	10	2,5	5	5	-	-	10	-	-	-
	600-841	-	-	-	-	-	-	10	-	-	-
	500-600	10	2,5	5	5	-	-	-	-	-	-
	420-500	-	-	-	-	-	-	-	-	-	-
	300-420	10	5	5	5	-	-	-	-	-	-
	250-300	5	10	10	10	5	15	15	-	-	-
	150-250	-	-	10	10	-	20	-	-	-	-
	106-150	5	5	-	-	5	10	10	-	-	-
	75-106	5	5	10	10	5	10	10	-	-	-
	Total LCM Conc. (ppb)	17	20	24	10	-	18	22	-	-	-
	30 min. Fluid loss (ml)	50	41	-	29	-	48	58	-	-	-

3048

Figures F.1-F.15 are plotted to compare the fracture time values of the blends obtained for each disc. The results are provided for each disc separately.

0.06 inch (1524 μ m) disc

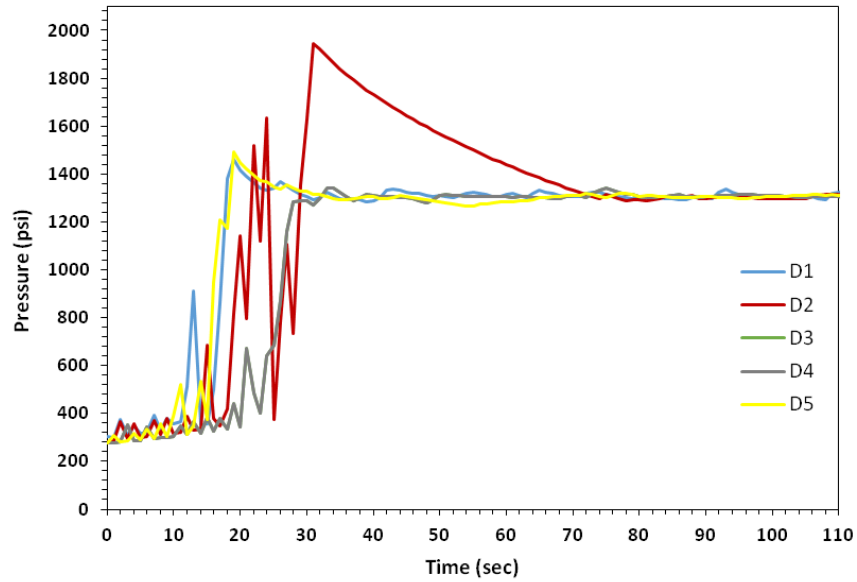


Figure F.1 Fracture sealing time vs. pump pressure (1524 μ m disc)-Blend# D1-D5

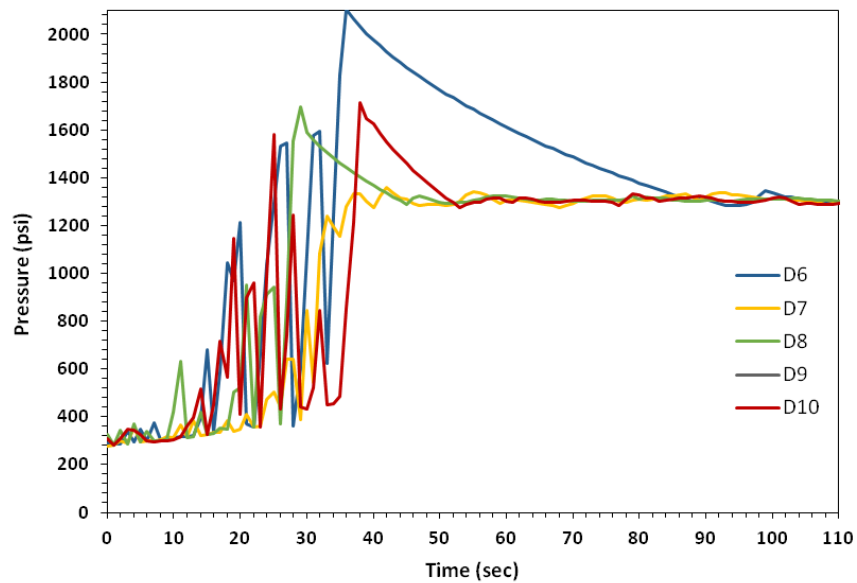


Figure F.2 Fracture sealing time vs. pump pressure (1524 μ m disc)-Blend# D6-D10.

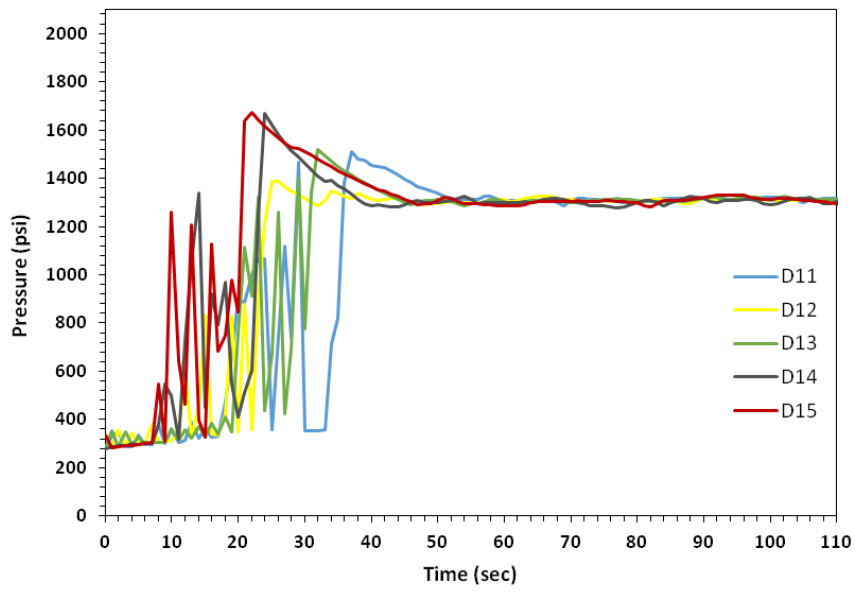


Figure F.3 Fracture sealing time vs. pump pressure (1524 μm disc)-Blend# D11-D15.

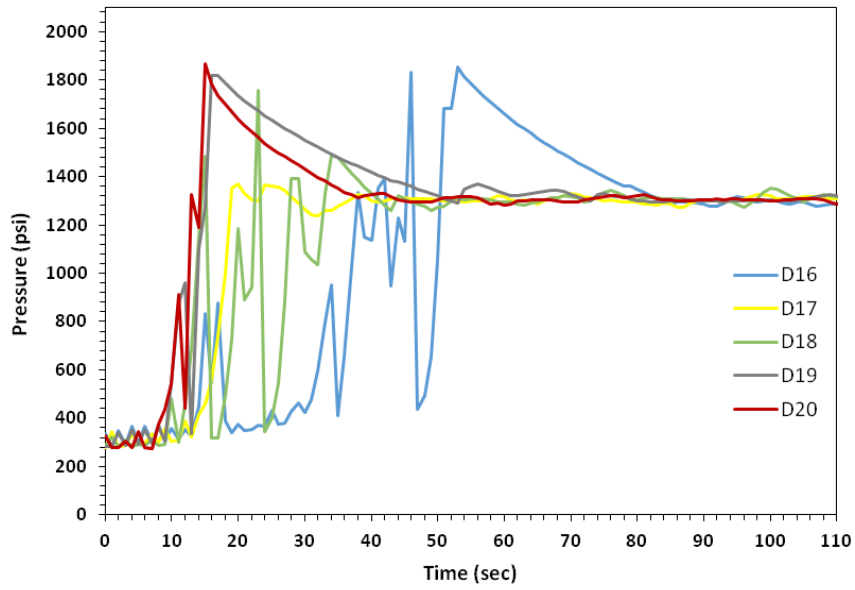


Figure F.4 Fracture sealing time vs. pump pressure (1524 μm disc)-Blend# D16-D20.

0.08 inch (2032 μm) disc

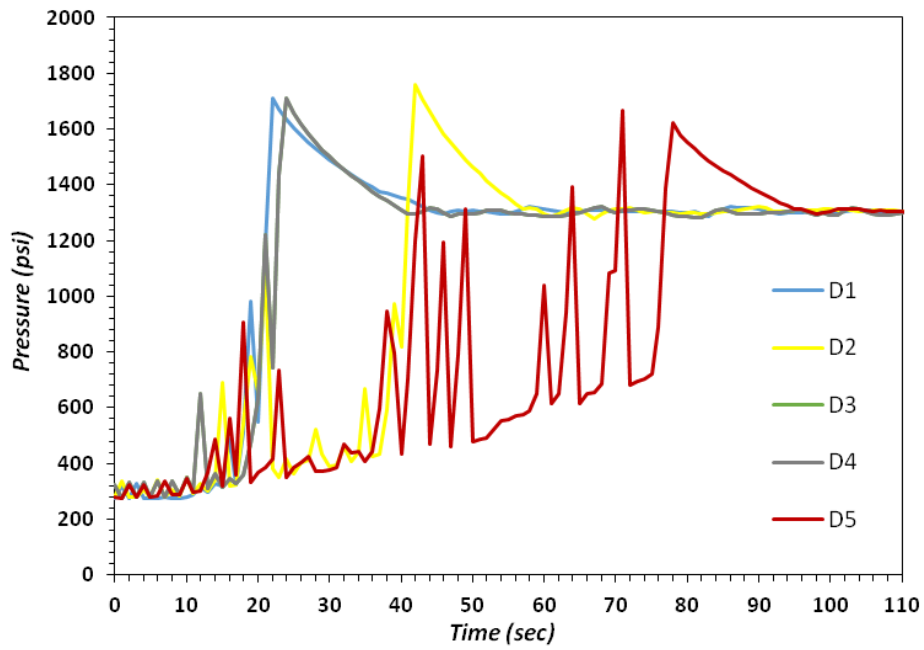


Figure F.5 Fracture sealing time vs. pump pressure (2032 μm disc)-Blend# D1-D5.

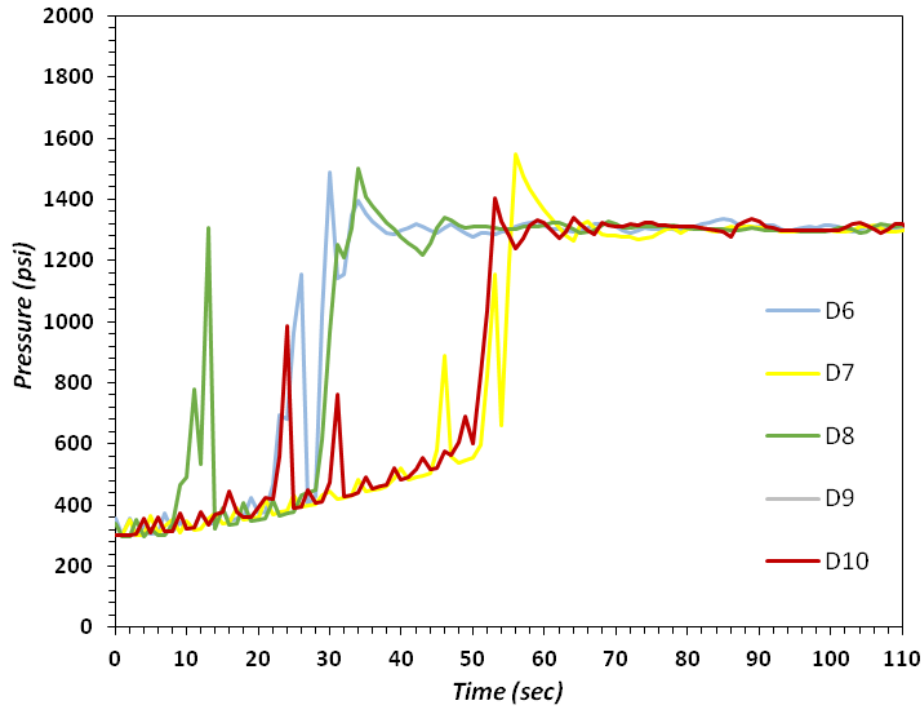


Figure F.6 Fracture sealing time vs. pump pressure (2032 μm disc)-Blend# D6-D10.

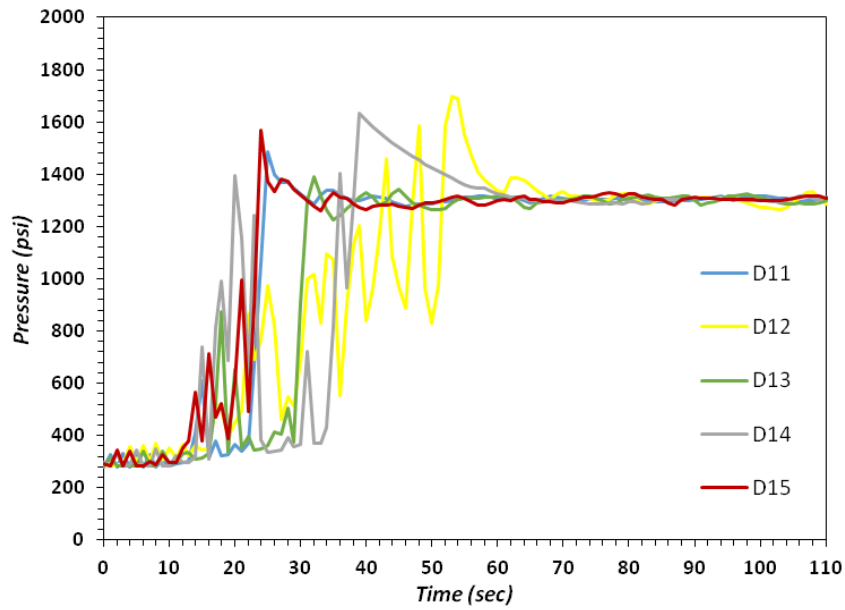


Figure F.7 Fracture sealing time vs. pump pressure (2032 μm disc)-Blend# D11-D15.

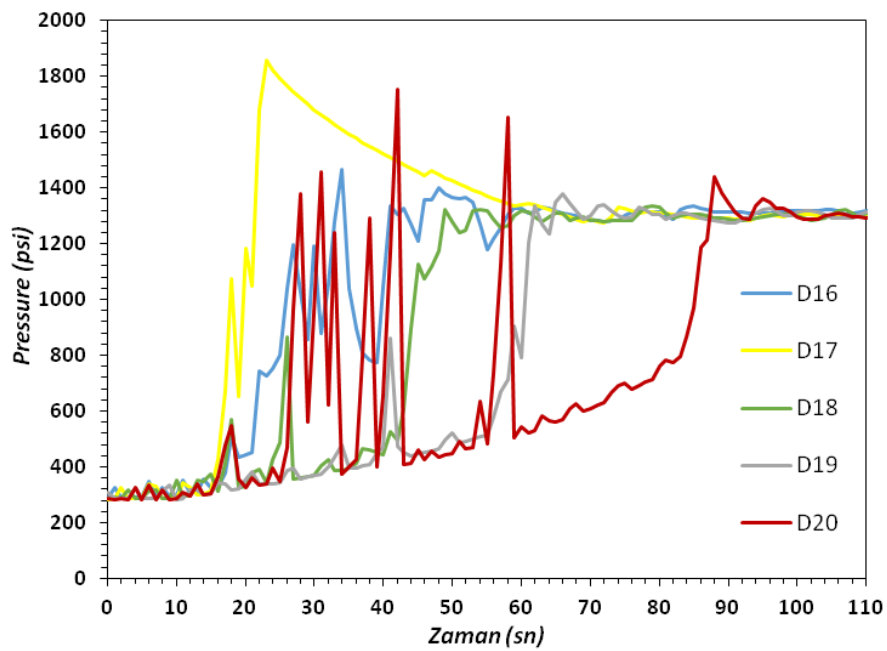


Figure F.8 Fracture sealing time vs. pump pressure (2032 μm disc)-Blend# D16-D20.

0.1inch (2540 μm) disc

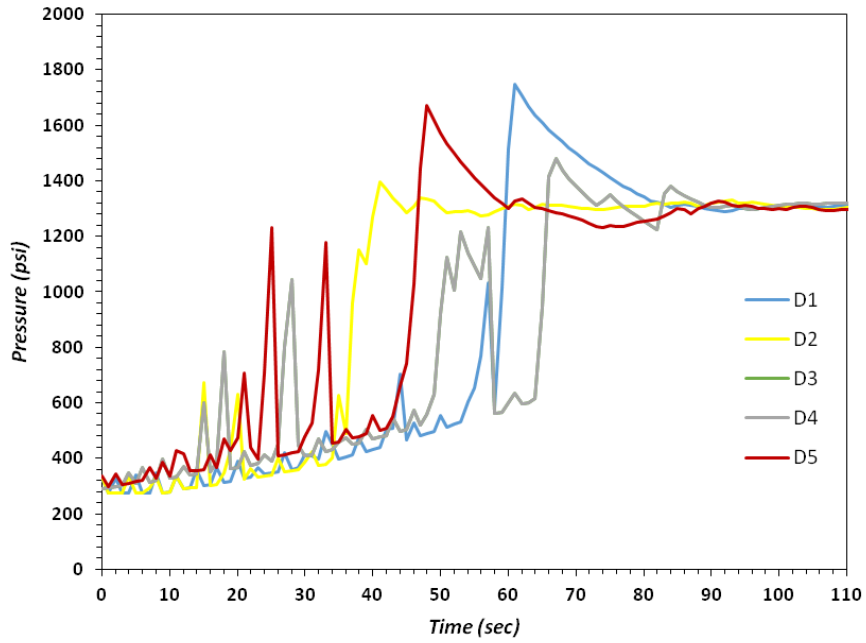


Figure F.9 Fracture sealing time vs. pump pressure (2540 μm disc)-Blend# D1-D5.

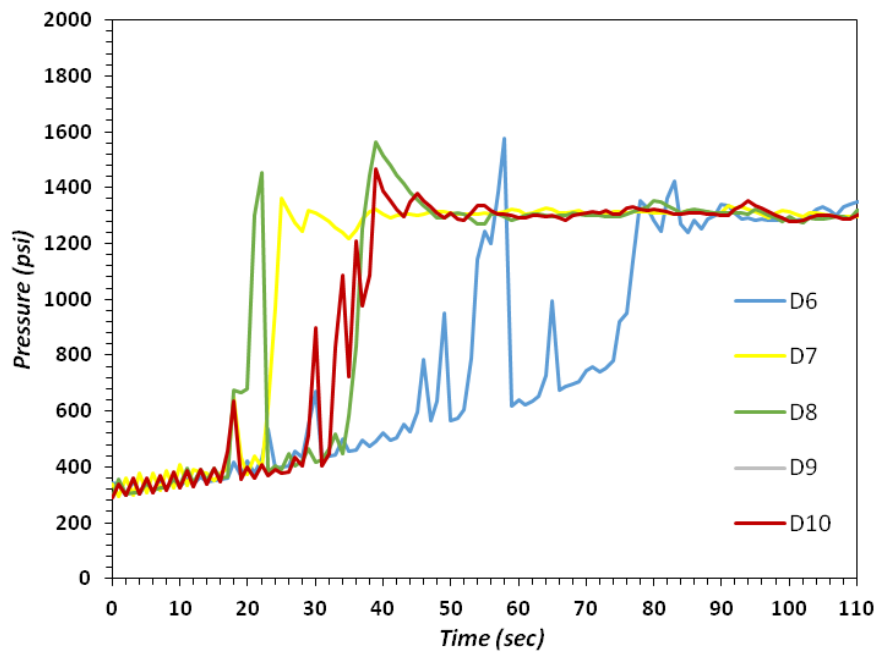


Figure F.10 Fracture sealing time vs. pump pressure (2540 μm disc)-Blend# D6-D10.

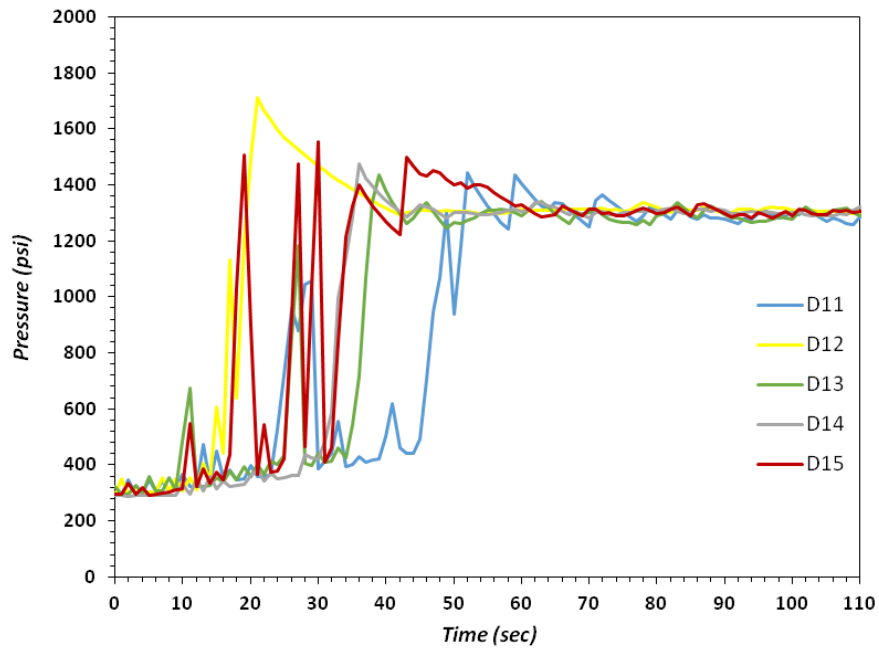


Figure F.11 Fracture sealing time vs. pump pressure (2540 μm disc)-Blend# D11-D15.

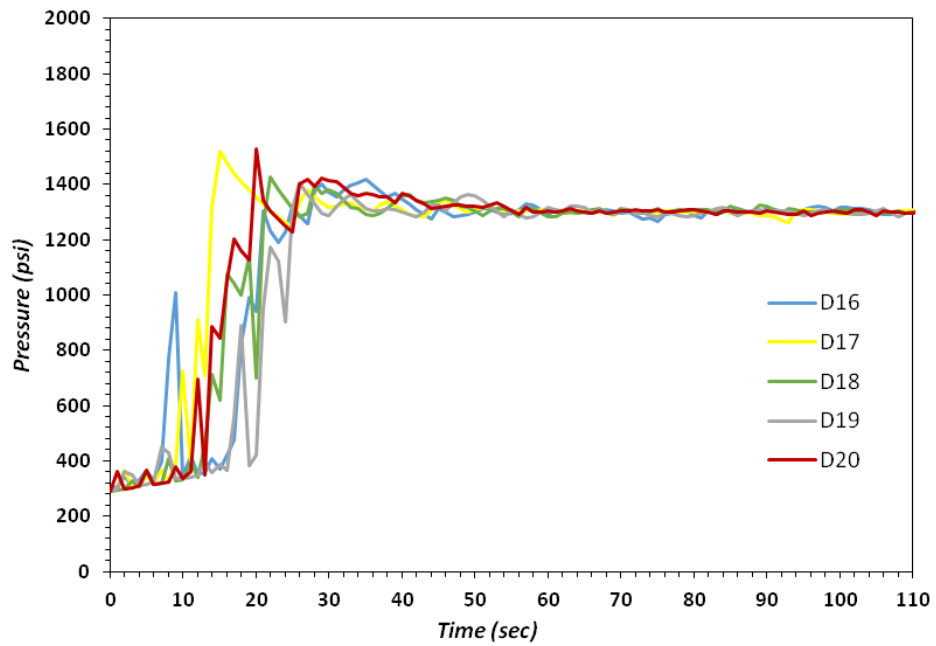


Figure F.12 Fracture sealing time vs. pump pressure (2540 μm disc)-Blend# D16-D20.

0.12inch (3048 μ m) disc

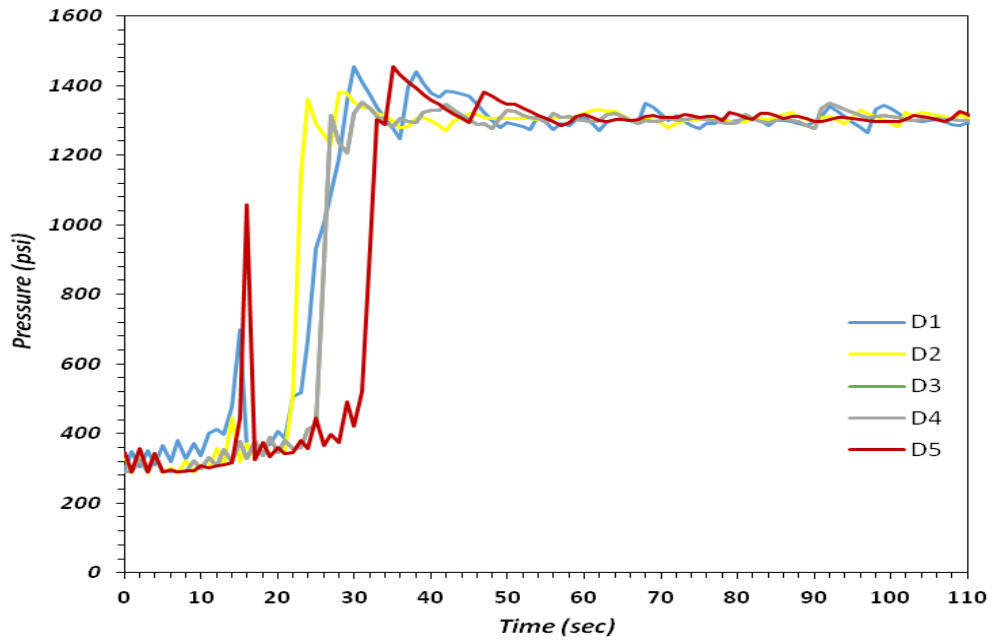


Figure F.13 Fracture sealing time vs. pump pressure (3048 μ m disc)-Blend# D1-D5.

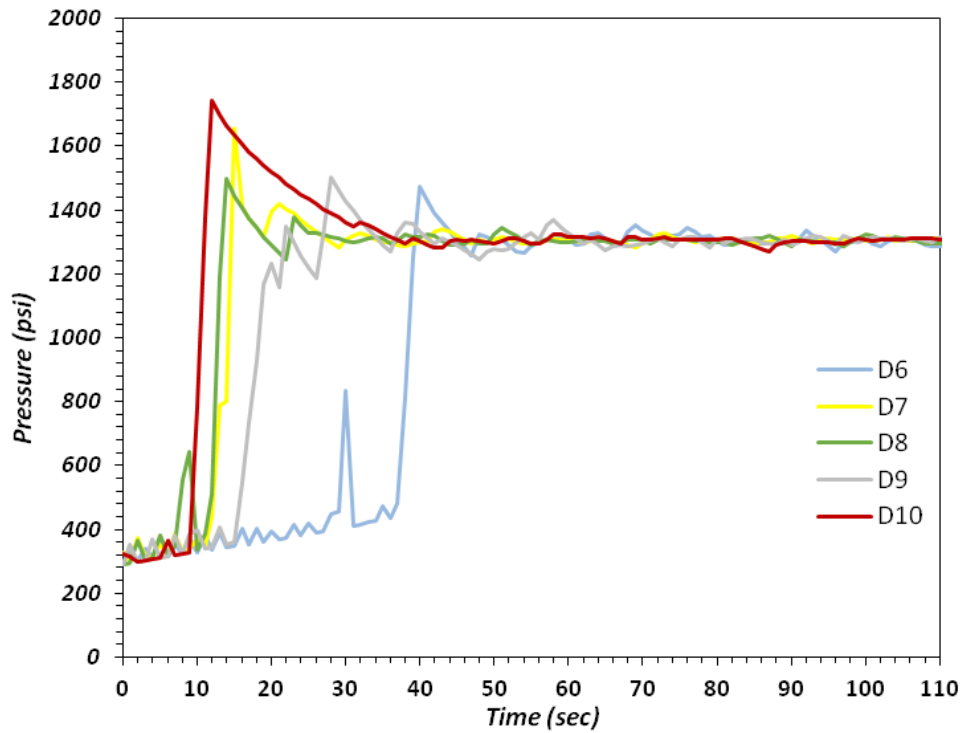


Figure F.14 Fracture sealing time vs. pump pressure (3048 μ m disc)-Blend# D6-D10.

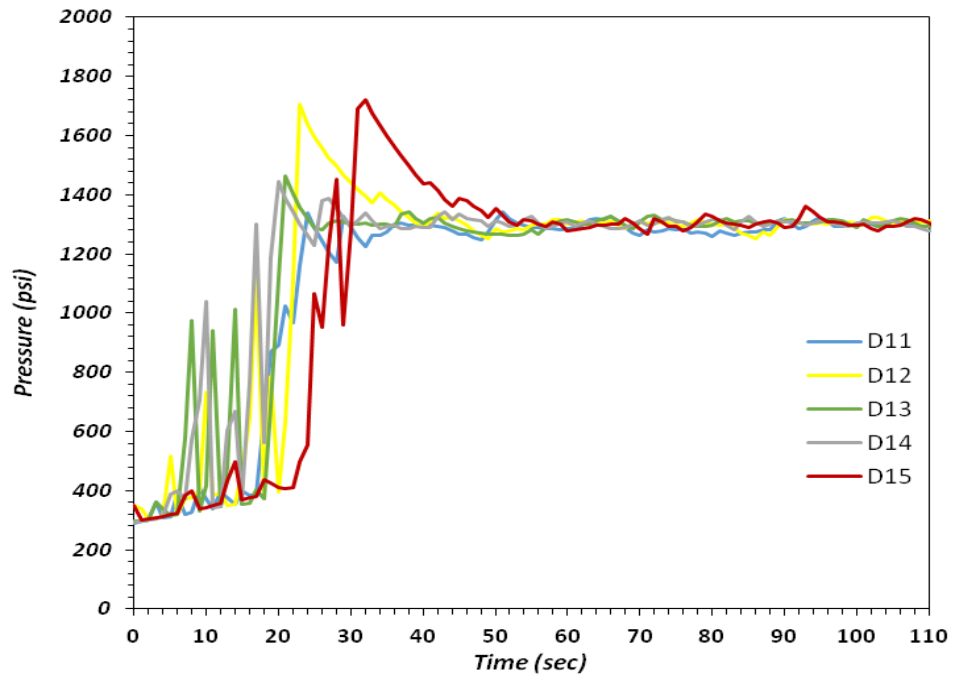


Figure F.15 Fracture sealing time vs. pump pressure (3048 μm disc)-Blend# D11-D15.

APPENDIX – G: EFFECT OF BENTONITE CLAY ON FRACTURE PLUGGING

0.06 inch (1524 μm) disc

Table G.1 LCM size and concentration values for 1524 μm disc-1

Disc Fracture Size (μm)	LCM Size (μm)	Total Concentration (%)
1524	1410-1680	30
	1180-1410	15
	1000-1180	10
	841-1000	10
	500-600	10
	300-420	10
	250-300	5
	106-150	5
	75-106	5
	Total LCM Conc.	
30 min fluid loss (ml)		24

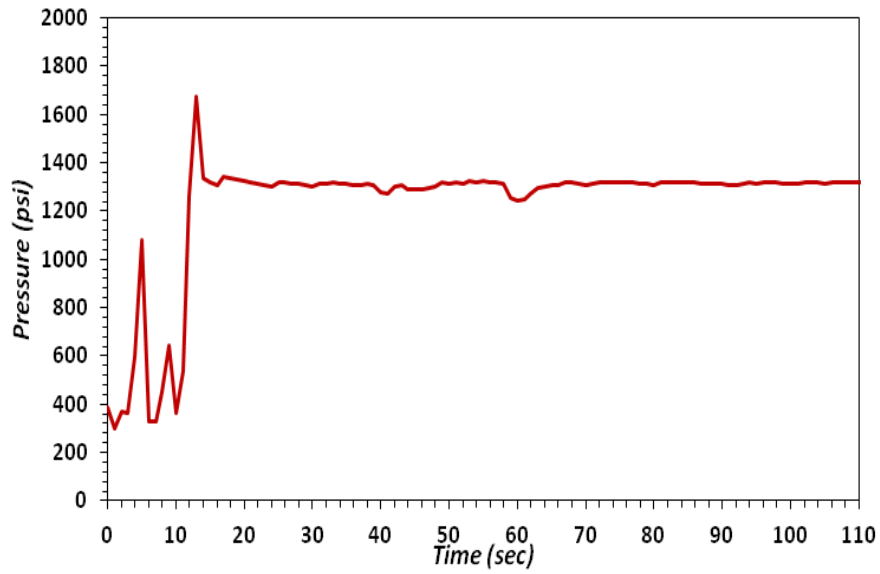


Figure G.1 Fracture sealing time vs. pump pressure of Bentonite Clay (1524μm disc) Blend#1

Table G.2 LCM size and concentration values for 1524 μm disc-2.

Disc Fracture Size (μm)	LCM Size(μm)	Total Concentration (%)
1524	1410-1680	30
	1180-1410	20
	1000-1180	15
	250-300	15
	106-150	10
	75-106	10
	Total LCM Conc.	40
30 min fluid loss (ml)	20	

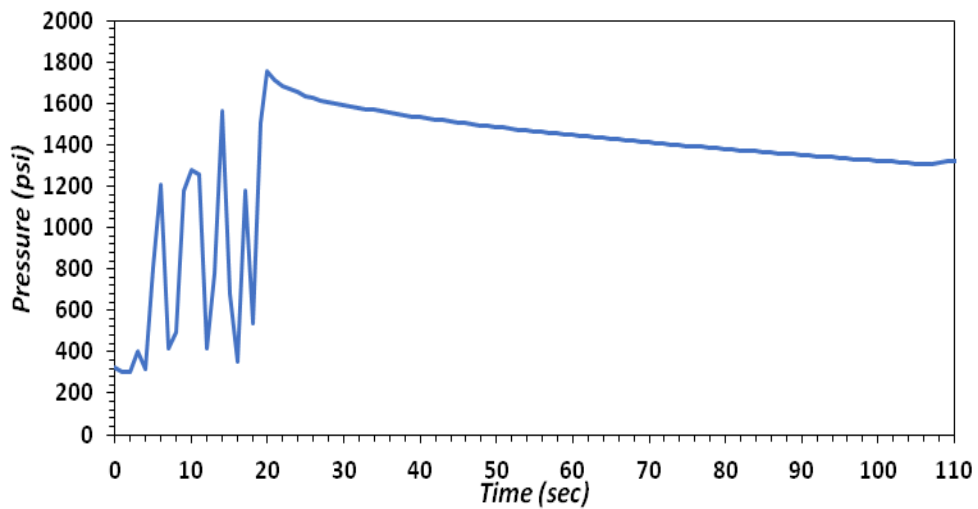


Figure G.2 Fracture sealing time vs. pump pressure of Bentonite Clay (1524 μm disc)-Blend#2.

0.08 inch (2032 μm) disc

Table G.3 LCM size and concentration values for 2032 μm disc-1

Disc Fracture Size (μm)	LCM Size(μm)	Total Concentration (%)
2032	2000-2380	30
	1180-1410	15
	1000-1180	10
	841-1000	10
	500-600	10
	300-420	10
	250-300	5
	106-150	5
	75-106	5
	Total LCM Conc.	40
30 min fluid loss (ml)	8	

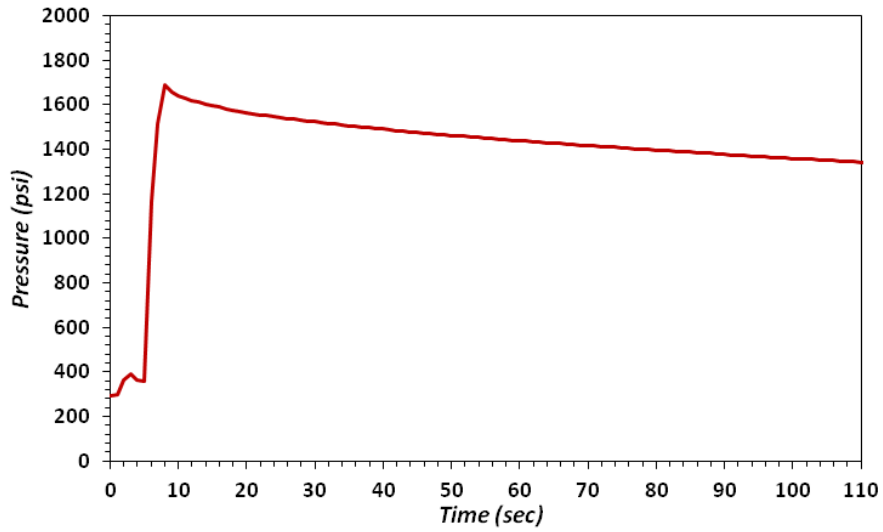


Figure G.3 Fracture sealing time vs. pump pressure of Bentonite Clay (2032 μm disc)-Blend#1.

Table G.4 LCM size and concentration values for 2032 μm disc-2

Disc Fracture Size (μm)	LCM Size(μm)	Total Concentration (%)
2032	2000-2380	30
	1180-1410	20
	1000-1180	15
	250-300	15
	106-150	10
	75-106	10
Total LCM Conc.		40
30 min fluid loss (ml)		15

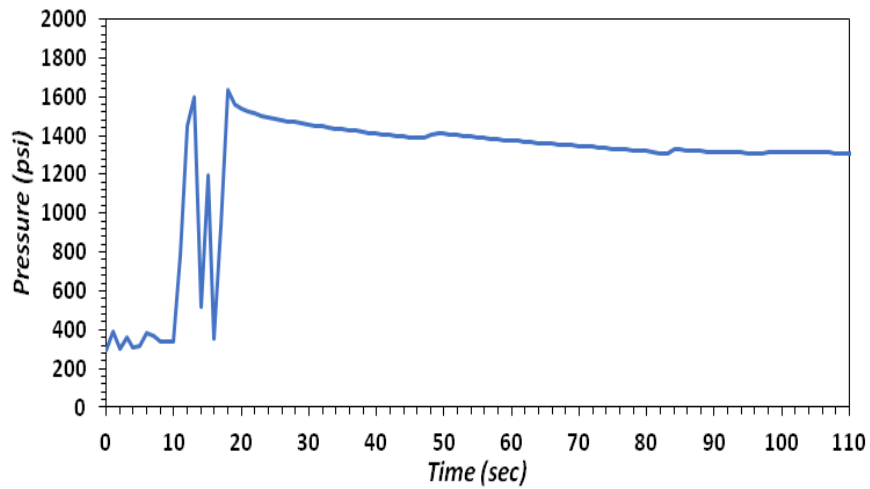


Figure G.4 Fracture sealing time vs. pump pressure of Bentonite Clay (2032 μm disc)-Blend#2.

0.1inch (2540 μm) disc

Table G.5 LCM size and concentration values for 2540 μm disc-1

Disc Fracture Size (μm)	LCM Size(μm)	Total Concentration (%)
2540	2500-2830	30
	1180-1410	15
	1000-1180	10
	841-1000	10
	500-600	10
	300-420	10
	250-300	5
	106-150	5
	75-106	5
Total LCM Conc.		40
30 min fluid loss (ml)		17

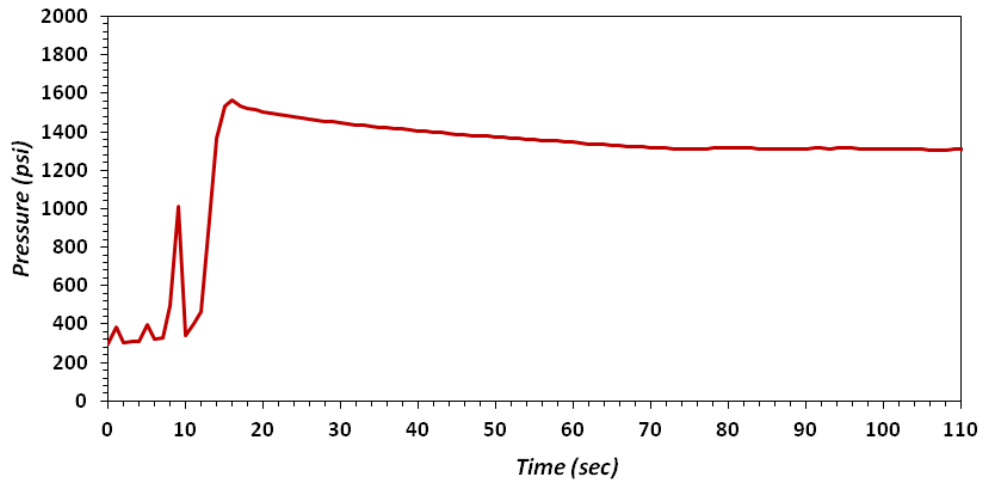


Figure G.5 Fracture sealing time vs. pump pressure of Bentonite Clay (2540 μm disc)-Blend#1.

Table G.6 LCM size and concentration values for 2540 μm disc-2

Disc Fracture Size (μm)	LCM Size(μm)	Total Concentration (%)
2540	2500-2830	30
	1180-1410	20
	1000-1180	15
	250-300	15
	106-150	10
	75-106	10
Total LCM Conc.		40
30 min fluid loss (ml)		31

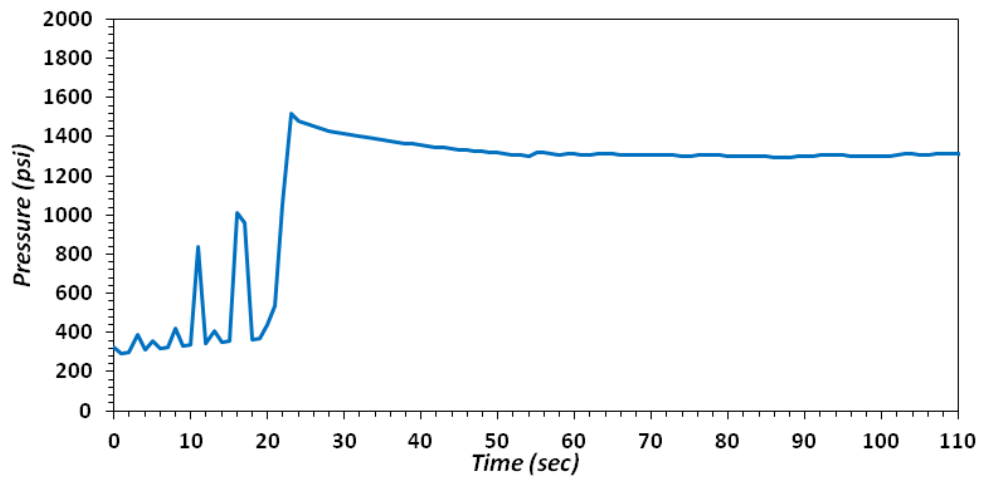


Figure 12 Fracture sealing time vs. pump pressure of Bentonite Clay (2540 μm disc)-Blend#2.

APPENDIX – H: EFFECT OF SEPIOLITE AND BENTONITE CLAY BLEND ON FRACTURE PLUGGING

Sepiolite and Bentonite clay blend consist of 13 g Sepiolite and 4.5 g Bentonite clay.

0.1inch (2540 μm) disc

Table H.1 LCM size and concentration values for 2540 μm disc

Disc Fracture Size (μm)	Repetition #	1	2	3
	LCM Size(μm)	Total Concentration (%)		
2540	2500-2830	30	30	30
	1180-1410	15	15	15
	1000-1180	10	10	10
	841-1000	10	10	10
	500-600	10	10	10
	300-420	10	10	10
	250-300	5	5	5
	106-150	5	5	5
	75-106	5	5	5
	Total LCM Conc.	40	40	40
30 min fluid loss	8	14	13	

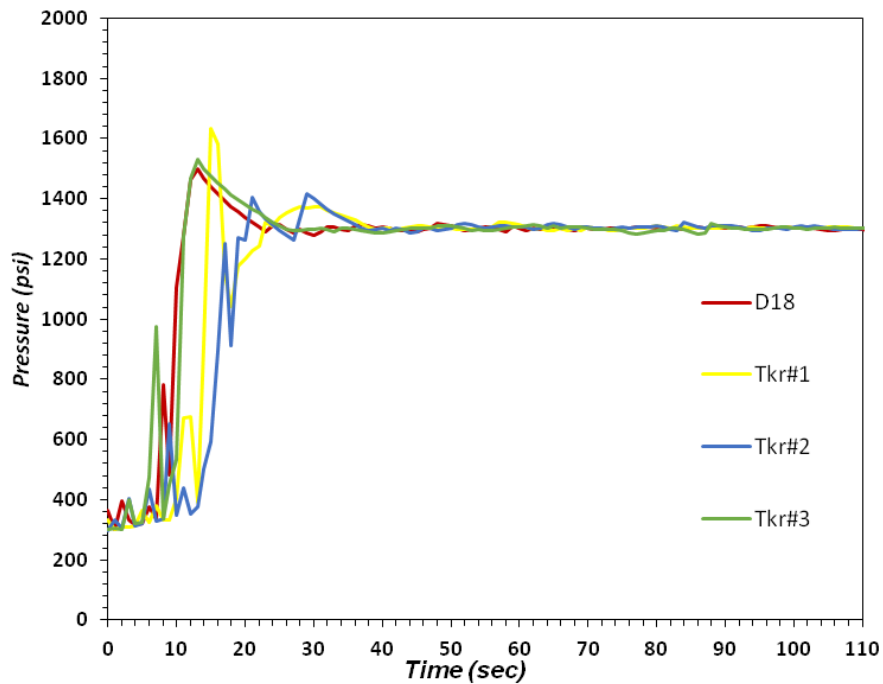


Figure H. 1 Fracture sealing time vs. pump pressure consisting of 3 repetitions using the same blend (2540 μm disc)-Bentonite & Sepiyolite Blend.

Table H.2 Effect of clay type on fracture sealing time and fluid loss

<i>Clay Type</i>	<i>Fracture sealing time (sec)</i>	<i>30 min fluid loss (ml)</i>
<i>Bentonite</i>	11	17
<i>Sepiyolite</i>	13	35
<i>Bentonite & Sepiyolite Mix.</i>	12	13

In bentonite, sepiolite, and bentonite + sepiolite clay experiments using the same blend, the structural difference of bentonite and sepiolite clay affected the plugging time and fluid loss values. Due to its layered structure, the less fluid loss was observed when bentonite clay was used. In addition, when a blend of bentonite and sepiolite was used, there was a crucial change in plugging time, and the fluid loss was significantly reduced.

CURRICULUM VITAE

She was born in Soma on June 24, 1994. She has received his BSc. degree from Petroleum & Natural Gas Engineering Department of Middle East Technical University, in Ankara as a petroleum and natural gas engineer in 2017. In addition, she is a master student in the Department of Energy Engineering in Izmir Katip Celebi University from 2018. Her research interests are in drilling fluids and their rheological applications. Currently, she is a research assistant in the Department of Petroleum & Natural Gas Engineering at Izmir Katip Celebi University.

PUBLICATIONS

Journal Papers

Ettehad, A., **Tezcan, M.**, & Altun, G. (2019). A comparative study on essential parameters to minimize sealing time in wide fractures. *Journal of Petroleum Science and Engineering*, 183, 106422.

<https://doi.org/10.1016/j.petrol.2019.106422>

Ettehad, A., **Tezcan, M.**, & Altun, G. (2020). Rheological Behavior of Water-Clay Suspensions under Large Amplitude Oscillatory Shear. *Journal of Rheologica Acta*.

DOI:10.1007/s00397-020-01221-9

Conference Papers

Ettehad, A., **Tezcan, M.**, & Altun, G. 2019 “Rheological Properties of Bentonite Based Drilling Fluid under the Small and Large Amplitude Oscillatory Shear” Conference paper accepted at 4th International Conference on Rheology and Modelling of Materials, Miskolc-Lillafüred, Hungary, 7-11 October, 2019.

Ettehad, A., **Tezcan, M.**, & Altun, G. (2020) “Loss Circulation through Wide Fractured Formation: Review on Concept Theories and Recent Studies” Conference paper accepted at IV. Scientific and Technical Petroleum Congress, METU Petroleum and Natural Gas Engineering Department, Ankara, 26-28 October, 2020.